

Southern Illinois University Carbondale

OpenSIUC

---

Dissertations

Theses and Dissertations

---

6-1-2021

## REAL-TIME CONGESTION MANAGEMENT IN MODERN DISTRIBUTION SYSTEMS

Meisam Ansari

*Southern Illinois University Carbondale*, [ansari.meisam@gmail.com](mailto:ansari.meisam@gmail.com)

Follow this and additional works at: <https://opensiuc.lib.siu.edu/dissertations>

---

### Recommended Citation

Ansari, Meisam, "REAL-TIME CONGESTION MANAGEMENT IN MODERN DISTRIBUTION SYSTEMS" (2021). *Dissertations*. 1904.

<https://opensiuc.lib.siu.edu/dissertations/1904>

This Open Access Dissertation is brought to you for free and open access by the Theses and Dissertations at OpenSIUC. It has been accepted for inclusion in Dissertations by an authorized administrator of OpenSIUC. For more information, please contact [opensiuc@lib.siu.edu](mailto:opensiuc@lib.siu.edu).

REAL-TIME CONGESTION MANAGEMENT IN MODERN DISTRIBUTION SYSTEMS

by

Meisam Ansari

B.S., Shahid Bahonar University, Kerman, Iran, 2008

M.S., Power And Water University Of Technology, Tehran, Iran, 2010

A Dissertation

Submitted in Partial Fulfillment of the Requirements for the  
Doctor of Philosophy Degree

School of Electrical, Computer, and Biomedical Engineering  
in the Graduate School  
Southern Illinois University Carbondale  
May 2021

DISSERTATION APPROVAL

REAL-TIME CONGESTION MANAGEMENT IN MODERN DISTRIBUTION SYSTEMS

by

Meisam Ansari

A Dissertation Submitted in Partial

Fulfillment of the Requirements

for the Degree of

Doctor of Philosophy

in the field of Electrical and Computer Engineering

Approved by:

Dr. Arash Asrari, Chair

Dr. Constantine Hatziadoniu

Dr. Mohammad Sayeh

Dr. Dimitrios Kagaris

Dr. Arash Komaee

Dr. Dashun Xu

Graduate School  
Southern Illinois University Carbondale  
January 22, 2021

## AN ABSTRACT OF THE DISSERTATION OF

Meisam Ansari, for the Doctor of Philosophy degree in Electrical Power Engineering, presented on January 22, 2021, at Southern Illinois University Carbondale.

TITLE: REAL-TIME CONGESTION MANAGEMENT IN MODERN DISTRIBUTION SYSTEMS

MAJOR PROFESSOR: Dr. Arash Asrari

In this research, the problem of real-time congestion management in a modern distribution system with massive active elements such as electric vehicles (EVs), distributed energy resources (DERs), and demand response (DR) is investigated. A novel hierarchical operation and management framework is proposed that can take advantage of the demand side contribution to manage the real-time congestion. There are five main steps in this framework as 1) the aggregators send their demand to the microgrid operators (MGOs), 2) the MGOs send their demand to the distribution system operator (DSO), 3) the DSO detects the congestions and calls the engaged MGOs to reduce their demand, 4) the MGOs update the electricity price to motivate the aggregators to reduce the overall demand, and 5) the DSO dispatches the system according to the finalized demand. The proposed framework is validated on two modified IEEE unbalanced test systems. The results illustrate two congestion cases at  $t=8:45$  am and  $t=9:30$  am in the modified IEEE 13-bus test system, which needs 363kW and 286 kW load reductions, respectively, to be fully addressed. MG#1 and MG#2 are engaged to maintain the 363 kW reduction at  $t=8:45$ , and MG#3 and MG#4 are called to reduce their demands by 386 kW at  $t=9:30$  am. The overall interactions can relieve the congested branches. The DSO's calculations show three congestions at  $t=1$  pm,  $t=3$  pm, and  $t=9$  pm on the IEEE 123-bus test system. These congestion cases can be alleviated by reducing 809 kW, 1177 kW, and 497 kW from the corresponding MGs at  $t=1$  pm,  $t=3$  pm, and  $t=9$  pm, respectively. The second part of the

simulation results demonstrates that the proposed real-time data estimator (RDE) can reduce the DSO's miss-detected congestion cases due to the uncertain data. There are two miss-detected congestions in the IEEE 13-bus test system at  $t=1:15$  pm and  $t=1:30$  pm that can be filtered for  $t=1:15$  pm and minored for  $t=1:30$  pm using the RDE. The proposed RDE can also reduce the miss-detected congestions from 18 cases to four cases in the IEEE 123-bus test system. As a result, the RDE can minimize the extra costs due to the uncertain data. The overall results validate that the proposed framework can adaptively manage real-time congestions in distribution systems.

## TABLE OF CONTENTS

<u>CHAPTER</u>	<u>PAGE</u>
ABSTRACT.....	i
LIST OF TABLES .....	vi
LIST OF FIGURES .....	vii
LIST OF ABBREVIATIONS.....	x
CHAPTERS	
CHAPTER 1 - INTRODUCTION AND LITERATURE REVIEW .....	1
1.1.Introduction.....	1
1.1.1.History of power systems.....	1
1.1.2.The first round of restructuring: deregulated power systems .....	5
1.1.3.The second round of restructuring: modern distribution systems.	12
1.2. Research motivation.....	15
1.3.Literature review .....	17
1.4.Main research contributions.....	24
CHAPTER 2 - PROPOSED METHODOLOGY .....	26
2.1.Introduction.....	26
2.2.Problem definition .....	26
2.2.1.The management platform .....	26
2.2.2.Entities definition.....	29
2.3.Mathematical modeling for aggregators .....	31
2.3.1.EVAG optimization model .....	32
2.3.2.DGAG optimization problem .....	33

2.3.3.DRAG optimal bidding.....	34
2.4.Cartesian unbalanced load flow equations.....	35
2.5.MGO optimization formulation.....	40
2.6.Proposed real-time CM framework.....	44
2.6.1.The proposed real-time market framework.....	44
2.6.2.The DSO decision making.....	47
2.6.3.Real-time data estimating (RDE) system.....	47
2.7.DLMP revisiting mechanism.....	49
2.8.Distributed ULF calculation process.....	51
CHAPTER 3 - GAMS-MATLAB CONFIGURATIONS.....	55
3.1.Software tools.....	55
3.2.Steps to solve an optimization problem using GAMS-MATLAB.....	56
3.2.1.Define GAMS in MATLAB’s path library.....	56
3.2.2.Generate input parameters in “gdx” format.....	57
3.2.3.Saving the output GAMS results in gdx format.....	59
3.2.4.Executing a GAMS model from MATLAB.....	59
3.2.5.Extracting results form generated gdx files.....	60
3.3.An example of unbalanced load flow GAMS-MATLAB programming.....	60
CHAPTER 4 - CASE STUDIES AND INPUT DATA.....	64
4.1.Input data.....	64
4.2.DER, EV, and DR designations.....	66
4.3.IEEE case studies.....	69
4.3.1.Modified IEEE 13-bus unbalanced test system.....	69

4.3.2.Modified IEEE 123-bus unbalanced test system .....	72
CHAPTER 5 - NUMERICAL RESULTS .....	79
5.1.Introduction.....	79
5.2.Case study #1: IEEE 13-bus .....	79
5.2.1.Real-time simulation without considering uncertainty .....	80
5.2.2.Considering uncertainty in transferred data.....	87
5.3.Case study #2: IEEE 123-bus .....	88
5.3.1.Real-time simulation without considering uncertainty .....	88
5.3.2.Considering uncertainty in transferred data.....	96
CHAPTER 6 - CONCLUSION AND FUTURE WORK .....	100
6.1.Conclusion .....	100
6.2. Future studies .....	101
REFERENCES .....	104
VITA.....	108

## LIST OF TABLES

<u>TABLE</u>	<u>PAGE</u>
Table 1- 1: The market output for 2-bus system.....	12
Table 4- 1: Types of Modeled EVs .....	68
Table 4- 2: Demand Response contracts.....	69
Table 4- 3: Shiftable DR contracts.....	69
Table 4- 4: Spot load Data associated with IEEE 13-bus test system [43].....	70
Table 4- 5: MGs components in the modified case .....	72
Table 4- 6: Spot load Data associated with IEEE 123-bus test system [43].....	73
Table 4- 7: MGs' components in the modified 123-bus test system .....	77
Table 5- 1: The MGOs response to the DSO's demand reduction orders .....	83
Table 5- 2: The managed congestions during 24 hours of real-time operation .....	91
Table 5- 3: Total detected congestions .....	98
Table 6- 1: The overall needed load reduction and the maintained load reduction .....	101

## LIST OF FIGURES

<u>FIGURE</u>	<u>PAGE</u>
Figure 1- 1: A typical power system structure.....	2
Figure 1- 2: A steam generator [5].....	3
Figure 1- 3: A typical transmission system.....	4
Figure 1- 4: A typical electrical distribution system [6].....	5
Figure 1- 5: The vertical structure of the power system.....	6
Figure 1- 6: The restructured form of the electrical industry.....	7
Figure 1- 7: The uniform pricing mechanism.....	8
Figure 1- 8: The uniform pricing mechanism.....	10
Figure 1- 9: A typical LMP mechanism.....	11
Figure 1- 10: A typical modern distribution system with active components [10].....	13
Figure 1- 11: A modern distribution system with massive active customers [11].....	14
Figure 1- 12: A modern distribution system with different control levels [12].....	15
Figure 2- 1: A two-layer management platform.....	27
Figure 2- 2: A two-layer management platform.....	28
Figure 2- 3: A three-layer management platform.....	29
Figure 2- 4: Different entities and layers in the proposed platform.....	31
Figure 2- 5: A typical bus n of a system with the input, output power/currents.....	36
Figure 2- 6: A typical branch and its end nodes.....	37
Figure 2- 7: A typical two bus with four wires and local loads.....	38
Figure 2- 8: Conversion from phasor to x-y domain.....	40
Figure 2- 9: The proposed real-time market operation framework.....	46

Figure 2- 10: The error estimation modeling system.....	48
Figure 2- 11: A discrete Kalman filtering block [40] .....	49
Figure 2- 12: Electricity rate calculation process .....	50
Figure 2- 13: Cash flow process .....	50
Figure 2- 14: A typical distribution system .....	52
Figure 2- 15: Dividing a distribution system into several low-voltage and a high-voltage part ..	54
Figure 3- 1: The interaction between MATLAB and GAMS.....	55
Figure 3- 2: Adding GAMS directory to the MATLAB paths list .....	57
Figure 3- 3: A two-bus unbalanced test system.....	60
Figure 4- 1: (a)-Daily solar radiation, (b)-wind velocity, (c)-ambient temperature [44].....	64
Figure 4- 2: Hourly load pattern .....	65
Figure 4- 3: The wholesale electricity price [46].....	66
Figure 4- 4: Modified IEEE 13-bus test system.....	71
Figure 4- 5: The single diagram for the IEEE 123-bus test system.....	76
Figure 5- 1: GAMS solvers configuration .....	80
Figure 5- 2: The congestions in the system .....	82
Figure 5- 3: The congested branches and down MGs.....	83
Figure 5- 4: MGs power purchased from the grid during time.....	84
Figure 5- 5: MGs Currency components for the whole interval.....	85
Figure 5- 6: Wholesale price and updated MG price .....	86
Figure 5- 7: DLMP in MGs at the detected congestion times .....	87
Figure 5- 8: (a)-Loading for branch B1-B6, (b)- loading for branch B1-B2 in 3 scenarios .....	88
Figure 5- 9: Congested branches with called MGs.....	90

Figure 5- 10: Total purchasing power before and after real-time congestion management .....	92
Figure 5- 11: The MG#10 (a) DGAGs production, (b) aggregated load, (c) overall demand .....	94
Figure 5- 12: Average electricity price of the system.....	95
Figure 5- 13: All congested branches along with three wrong detections .....	97
Figure 5- 14: Loading of branch 21-23.....	99
Figure 6- 1: The main scheme of hacking the data.....	102

## LIST OF ABBREVIATIONS

<u>ITEM</u>	<u>ABBREVIATION</u>
Aggregator	AGG
Congestion Management	CM
Data Traffic Operator	DTO
Demand Response	DR
Demand Response Aggregator	DRAG
Distributed generation aggregators	DGAG
Distributed Energy Resource	DER
Distribution System Operator	DSO
Distribution System	DS
Dynamic Tariff	DT
Electric Vehicle	EV
Full Cell	FC
Independent System Operator	ISO
Kalman Filtering	KF
Locational Marginal Price	LMP
Market Clearing Price	MCP
Micro-Grid	MG
Micro-Grid Operator	MGO
Micro-Grid Financial Center	MGFC
Mixed-Integer Linear Programming	MILP
Pay As Bid	PAB

Photovoltaic	PV
Real-time Data Estimating	RDE
Smart-Grid	SG
Smart Home	SH
Unbalanced Load Flow	ULF
Vehicle to Grid	V2G
Wind Turbine	WT

# CHAPTER 1

## INTRODUCTION AND LITERATURE REVIEW

### 1.1. Introduction

#### 1.1.1. History of power systems

Electricity has become an inseparable part of people's life in this century. The initial steps of electrical science were taken by several scientists such as Michael Faraday<sup>1</sup>, Georg Ohm<sup>2</sup>, and James Clerk Maxwell<sup>3</sup> in the 18<sup>th</sup> century [1],[2]. While steam power was affecting the world rapidly, it was hard to imagine that electricity would take the first place of energy shapes in the near future. Electricity was not well-developed until the early 19<sup>th</sup> century, where electrical science started to progress rapidly, and the late 19<sup>th</sup> century was the landmark point for electrical energy. Several scientists such as Alexander Graham Bell, Thomas Edison, Nikola Tesla, George Westinghouse, etc., had a significant role in making electricity usable in human's life. Electricity is a clean energy type that can be moved from place to place very fast using transmission lines. Today, electrical science is very vast, and thousands of researchers, craftsmen, and investors are engaged with electricity worldwide.

While the use of electricity has been growing, the challenges have been revealed accordingly. One of the concerns that showed up during increasing electricity usage was providing adequate and reliable energy for the customers in an extensive system. While electrical systems were becoming larger, control and management also became more problematic for the operators. As a solution, the electrical systems are divided into three main parts: generation, transmission, and distribution [3]. Figure 1-1 illustrates a typical diagram for a power system with all major

---

<sup>1</sup> invented the electric motor in 1821

<sup>2</sup> mathematically analyzed the electrical circuit in 1827

<sup>3</sup> Electricity and magnetism (and light) were definitively linked in 1862

features. Each part of this structure has a different role as follows:

- **Generation:**

The generators are used to convert the primary energy source (natural gas, coal, diesel, wind, solar, etc.) to electricity. For the electric power industry's utilities, this step is known as the first step and prior to delivery to the transmission system. Figure 1-2 shows a typical steam generator where water is heated by coal and converted to steam [5]. Then, the superheat steam can spin the turbines and produce electrical energy. Initially, the ownership of the power plants belonged to the governments. But after a while, when the management became costly and started bothering the governments, the investors found this industry beneficial, and the private power plants started growing. Today, many of the power plants are owned by private generation companies.

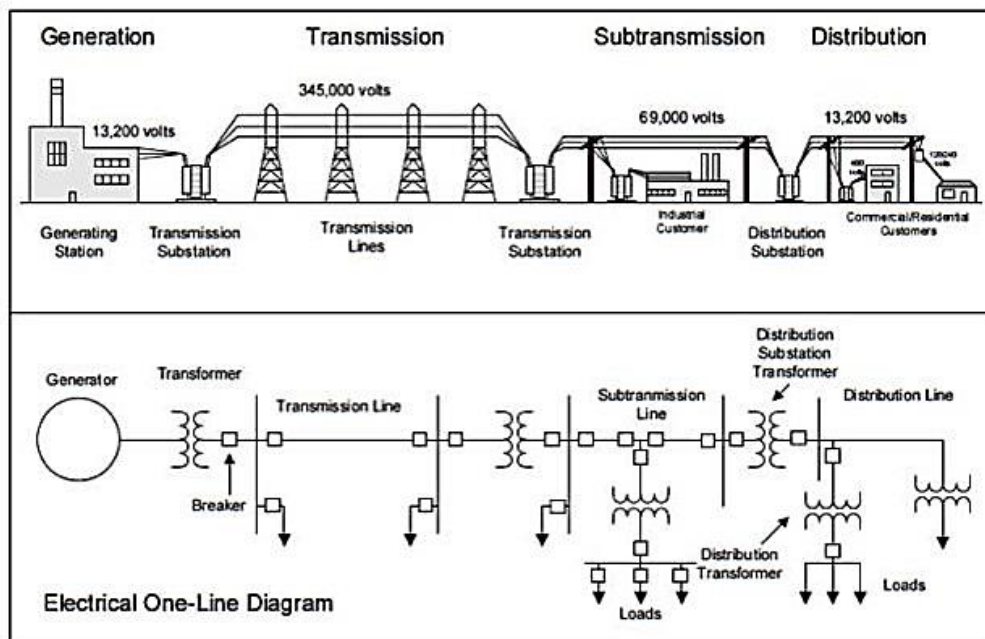


Figure 1-1: A typical power system structure



Figure 1-2: A steam generator [5]

- **Transmission system:**

This system takes the electrical energy from the generating site, such as a power plant, and delivers it to the next level. The interconnected lines which make this movement possible are known as a *transmission network*. Usually, the transmission systems' last chain is a step-down substation, which reduces the voltage to facilitate the delivery to the customers. Figure 1-3 shows a typical transmission system. As is shown in this figure, large towers are used to hold the transmission wires. Due to the higher voltage level in the transmission systems; long distance should be maintained among different phases and the ground. Thus, the giant towers are used in the transmission lines' construction.



Figure 1-3: A typical transmission system

- **Distribution system:**

After the step-down substation, the electricity is carried using the distribution lines with a medium voltage (e.g., 12.4 kV, 24.8 kV). Generally, an electrical distribution system is a combination of different equipment such as distribution lines, voltage regulators, distribution transformers, breakers, capacitors, etc., needed to make the end-users' delivery possible. Figures 1-4 show a whole power system with all major entities. There are several differences between the transmission and distribution lines. The distribution lines are shorter than transmission lines because they are supposed to spread in a neighborhood. Also, the voltage is lower in the distribution compared to the transmission. The network structure is radial in the distribution systems, and it is ring in the transmission systems. Each distribution line, which is started from a substation and ended to the customers, is called a feeder. Although the feeders are radially

shaped in the distribution systems, there are several points that a feeder can be connected to the other neighbor feeders. These points are equipped with disconnectors/switches and used when a reconfiguration is needed, while at the end of the day, the system should operate in a radial shape. As a result, the distribution systems are more flexible than transmission, and changing the topology of the system causes fewer issues.

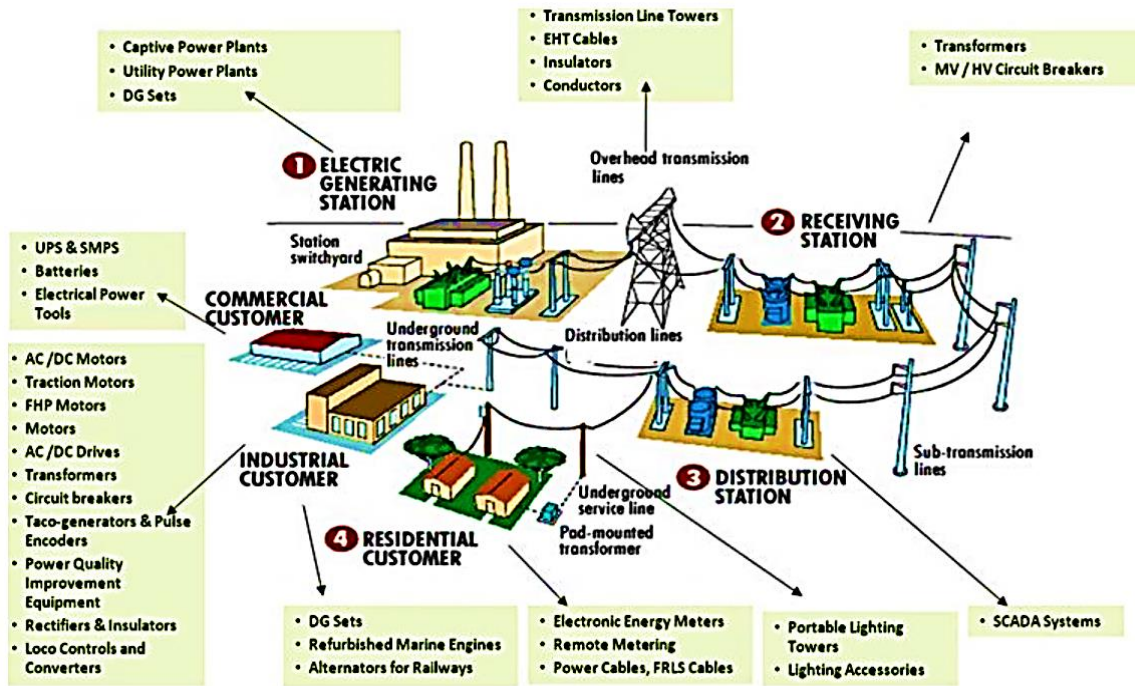


Figure 1-4: A typical electrical distribution system [6]

### 1.1.2. The first round of restructuring: deregulated power systems

Since the birth of electricity, many challenges have been addressed by engineers and scientists in the electrical industry. Sometimes the solution for a challenge was a small modification in the system, and sometimes it caused a more profound revision in fundamentals. After a while, when electricity industry evolved in most countries around the world, the pioneer countries faced a new challenge. By growing the electricity demand, the electrical industry started to cause challenges for the governments. The need for further investment, lack of efficiency, problems to

set a price for this service, and many other concerns sent this signal to the governments that the electrical industry cannot keep going by the current layout. Figure 1-5 illustrates a vertical structure for the electrical industry where the government or its agency can simultaneously control generation, transmission, and distribution. As is evident, managing such an extensive system is very challenging for the governments, and the customers do not have a clear vision of the pricing process. The deregulation in the power industry started from the 1970's decade in the US and a decade after that in Europe. This restructuring was supposed to change the electricity from a service to a product with a transparent pricing process and make the power industry competitive and productive. During that period, the generation and transmission sections profoundly changed. The result of that revolution was the deregulation of energy markets and private companies that own different industrial energy parts.

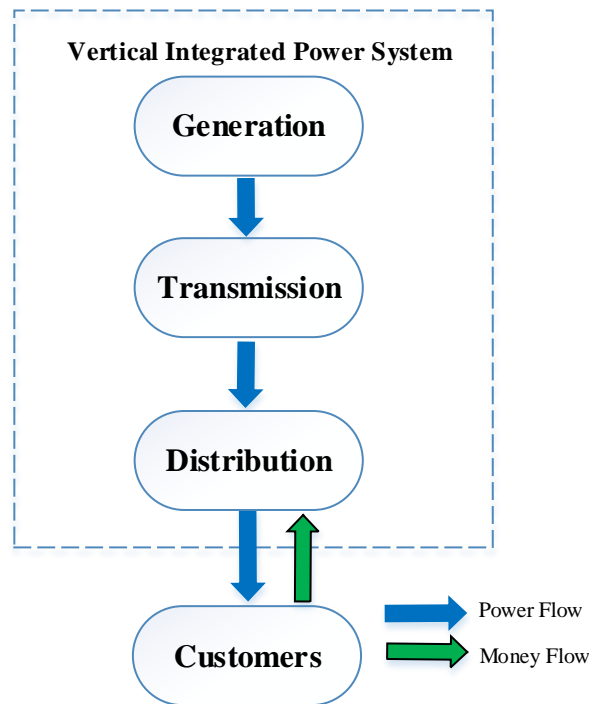


Figure 1-5: The vertical structure of the power system

Figure 1-6 shows the new structure after the first round of restructuring in the power industry.

The generation, transmission, and distribution parts are owned by private companies in this

structure. Also, an independent system operator (ISO) is responsible for the system's operation and management. The ISO should perform all technical/commercial required coordination among the entities in this structure. The electricity is traded within a wholesale market or PX. The generators are the sellers, and the distribution companies and larger customers are the buyers in this market. This structure is fully deregulated on the generation and transmission side. But on the distribution side, there is limited flexibility where the retailers or service providers can directly trade with the customers. The sellers and buyers in this structure can also make a bilateral contract directly and bypass the ISO. This is a reasonable choice for larger customers (e.g., large factories) who do not want to be negatively affected by electricity price variation.

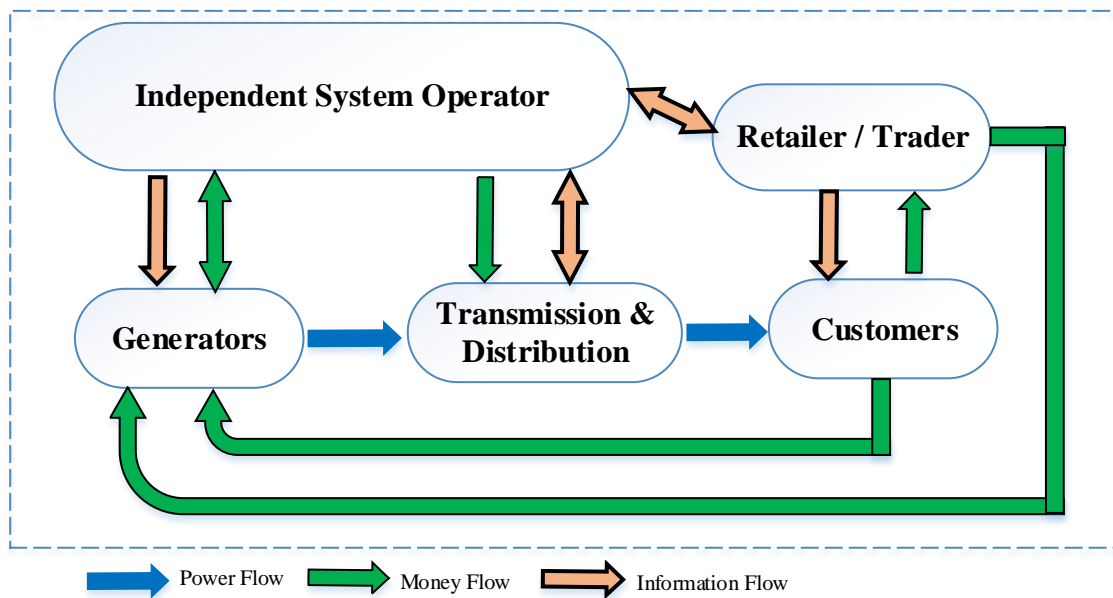


Figure 1-6: The restructured form of the electrical industry

A wholesale market is a place that the sellers submit their bids to sell the electricity, and the buyers also submit their offers to buy the electricity. The ISO uses this information and runs the market under the technical constraints on the generation and transmission side. The result would

show which group of the sellers have won in the market. According to the market's time horizon, the market can be day-ahead, hour-ahead, or spot (real-time). In the real world, the major part of the energy is traded through bilateral contracts, then the day-ahead market, and finally, the spot market. In fact, a spot market is a platform that gives a chance to the market participants to update their bids/offers according to the last changes in their schedule.

There are three different pricing models in the wholesale energy markets as follows:

- **Uniform pricing**

Figure 1-7 shows the uniform pricing mechanism. In this mechanism, all offers from the demand side are aggregated descending (from high to low), and all bids from the sellers are aggregated ascending (from low to high) according to the price. The intersection between the two curves shows the market-clearing point. The electricity price associated with this point is the market-clearing price (MCP). All the sellers will be paid with the MCP rate; all the buyers will be charged with the MCP rate, similarly. Due to simplicity, uniform pricing is a common pricing method in the European power markets such as Nordic, Nordpool. [8].

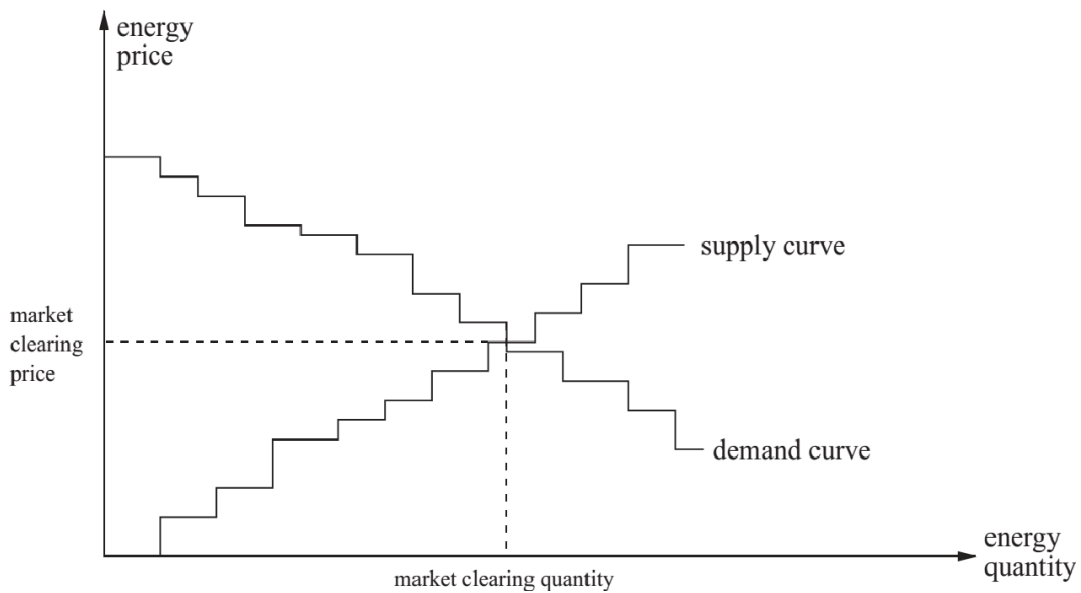


Figure 1-7: The uniform pricing mechanism

- **Pay as bid pricing**

Another way to settle a wholesale market is via using the pay as a bid (PAB) mechanism. After the ISO determines the market winners in this method, the sellers will be paid with their submitted bids, and the buyers will be charged with their proposed offer. Figure 1-8 demonstrates the PAB pricing method. As is shown, there is not a fixed rate for electricity in this market, and the sellers and buyers experience different prices. Also, there is residual money since the ISO's received money from the buyers is more than the payment to the sellers. In Figure 1-8, the surplus money is filled with green and named "B." As is shown, the buyers pay an "A+B" amount of money while the sellers only receive an "A" amount. According to each markets' policy, this surplus is spent in different ways, such as using to upgrade the system, compensate for power loss, make the price smoother, etc. A few countries, such as Chile [9], use PAB mechanisms in their power market. Due to the different rates that sellers and buyers are faced in the market, providing a fixed price for the end-users is challenging, and it is one of the disadvantages regarding this method.

On the other hand, this structure is more competitive than the uniform pricing because the players will be paid/charged by their submitted price. In contrast, since the price is fixed for all players in the uniform mechanism, the only matter is to win in the market. Hence, it persuades the sellers and buyers to submit promising rates (i.e., not necessarily actual rates) to only stay in the winner group.

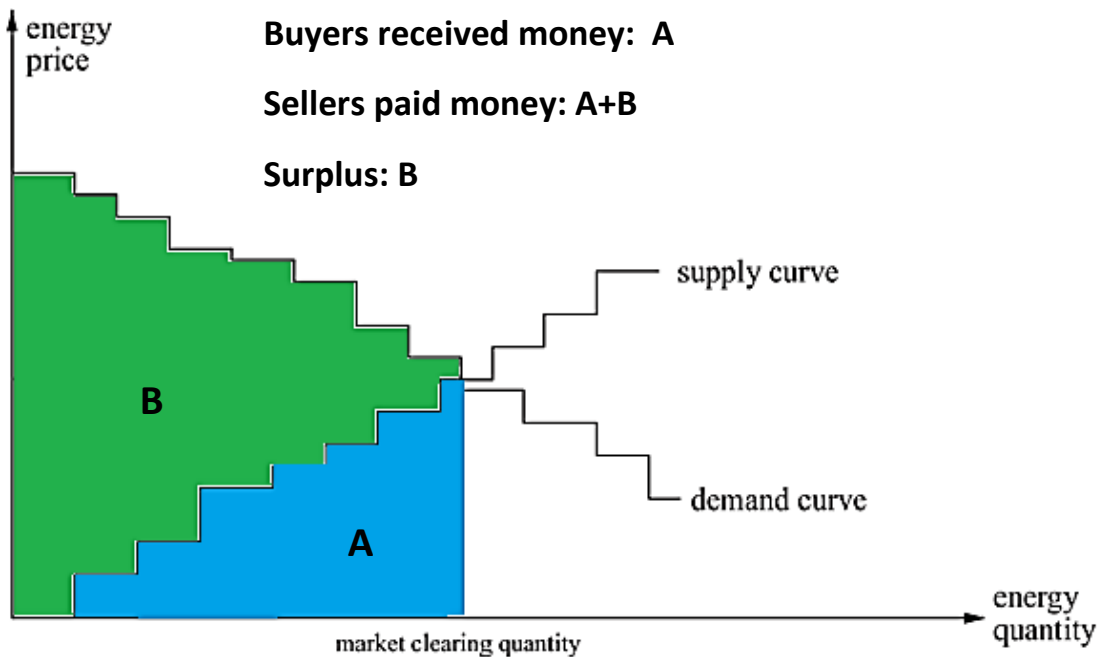
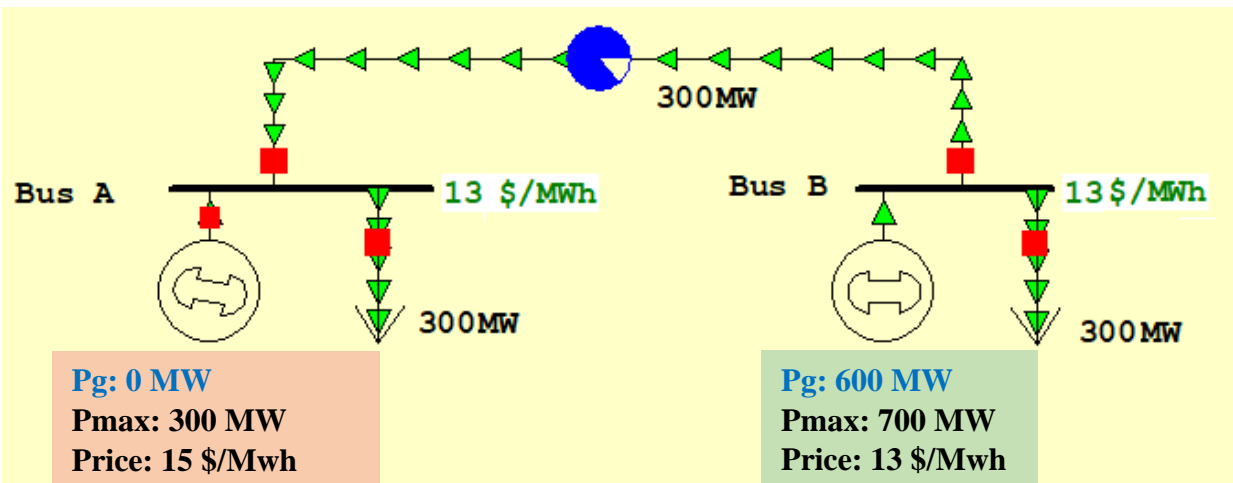


Figure 1-8: The uniform pricing mechanism

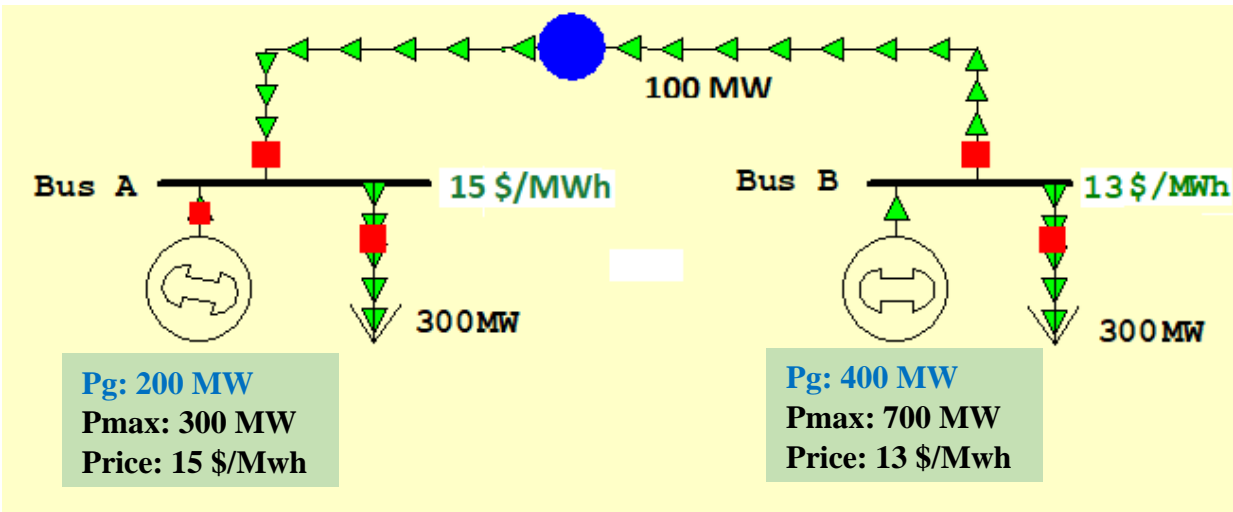
- **Locational marginal pricing**

Although the uniform and PAB pricing mechanisms are easy to be utilized in the power markets, these methods do not consider the grid structure's effect on the electricity price. It means all the customers in the same power market territory experience a similar wholesale electricity rate. This is why some of the consumers cause technical troubles to the system. As a result, the locational marginal pricing (LMP) method is used in some countries like the US to identify electricity prices per customers' locations. The LMP is the cost of electricity for the next MW demand on each part of the system. To calculate the LMPs in a power system, the ISO runs a market like PAB pricing to identify the winners. All technical constraints are considered at this point. In the next step, ISO calculates the cost of adding one more MW power at each bus. This cost is the LMP at the corresponding location. Figure 1-9 illustrates a 2-bus system with two generators and two loads. The generator at bus A offers 200 MW with a price of \$15/MWh, and

the generator at bus B offers 600 MW at \$13/MWh. As shown in Figure 1-6 (a), if the transmission line can carry 300 MW, the generator at bus B should generate 600MW and supply both the loads since this generator offers a cheaper price (\$13/MWh vs. \$15/MWh). Suppose one MW load is added to bus B ( $PL_B=301$  MW), then generator B can supply it because its maximum capacity is 700 MW while it is producing 600 MW currently. Therefore, LMP at this bus is 13 \$/MWh. Also, for the same reason, an extra MW at bus A can be supplied by generator B at the price of 13 \$/MWh. Therefore, the electricity price for buses A and B is \$13/MWh.



(a)



(b)

Figure 1-9: A typical LMP mechanism

In another case, if the transmission line can only pass 100 MW, the output of the market will be as Figure 1-9 (b). As is shown, generator B supplies all load at bus B, and 100 MW from the demand at bus A. Generator A supplies the rest of the load at bus A. Although generator A is more expensive than B, the ISO has to engage generator A due to the transmission line constraint. In this structure, the next MW load at bus A cannot be supplied by generator B. Therefore, generator A determines the LMP at bus A which is \$15/MWh. Also, the LMP at bus A is \$13/MWh. Table 1-1 shows a summary of the results.

Table 1-1: The market output for 2-bus system

	Line Capacity (MW)	$PG_A$ (MW)	$LMP_A$ (\$/MWh)	$PG_B$ (MW)	$LMP_B$ (\$/MWh)
Case1	500	0	13	600	13
Case2	100	200	15	400	13

### 1.1.3. The second round of restructuring: modern distribution systems

It can be inferred from Figure 1-6 that the end users are not engaged in the market process, directly. In fact, the structure is still vertical on the distribution side, which means the customers have limited options to buy the electricity, and there is no apparent collaboration among customers and distribution companies or energy retailers at this level. As a result, this distribution system structure will face challenges when active elements like distributed energy resources (DERs) and electric vehicles (EVs) are available massively on the demand side. In such a system, the demand does not have a known pattern, and this amount of flexibility causes difficulties for the system operators to manage their system. Figure 1-10 shows a typical modern distribution system with the main parts. The DERs, such as wind turbines (WTs), photovoltaic panels (PVs), and fuel cells (FCs), besides the flexible loads like EVs and demand responses (DRs), make the distribution systems very flexible and unpredictable. Prediction of the demand,

considering enough reserve and margin, and maintaining acceptable reliability is not accessible as before since the system operators do not know enough about the new customers' behavior. In such a system, the conventional operation and management frameworks cannot work effectively anymore.

In the new structure, a mutual collaboration among the system operators and the customers is essential. The system operator cannot solely manage a distribution system with thousands of active customers (the ones with DERs or EVs or DRs). As a result, a new structure is needed for the distribution systems to reduce the system operators' burden. Figure 1-11 illustrates the complexity of operating in a modern distribution system with massive active customers. Many new challenges affect not only the distribution side but also the transmission side in the new structure.

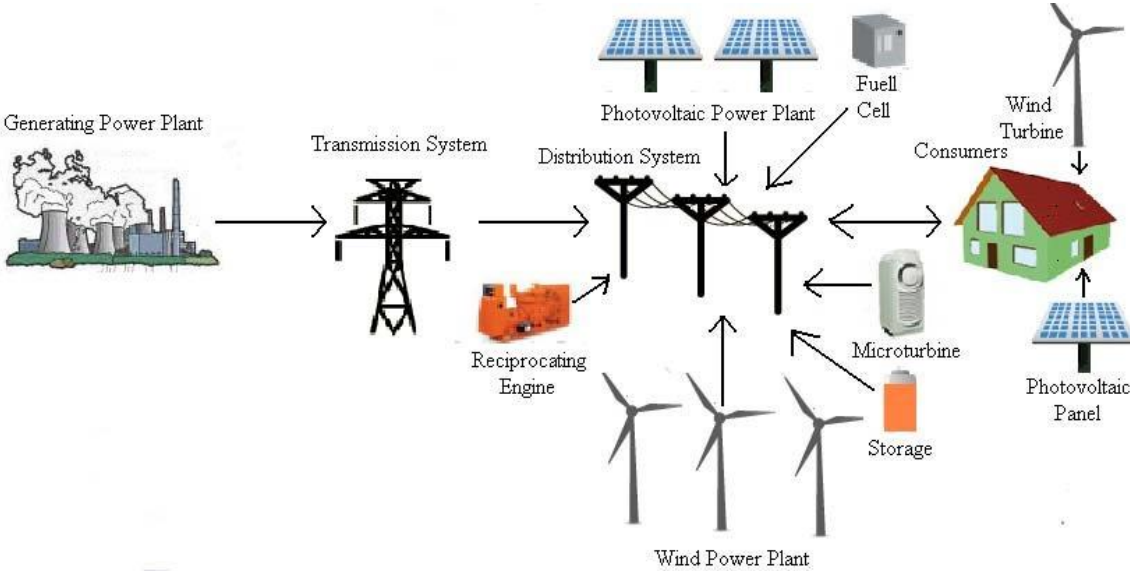


Figure 1-10: A typical modern distribution system with active components [10]

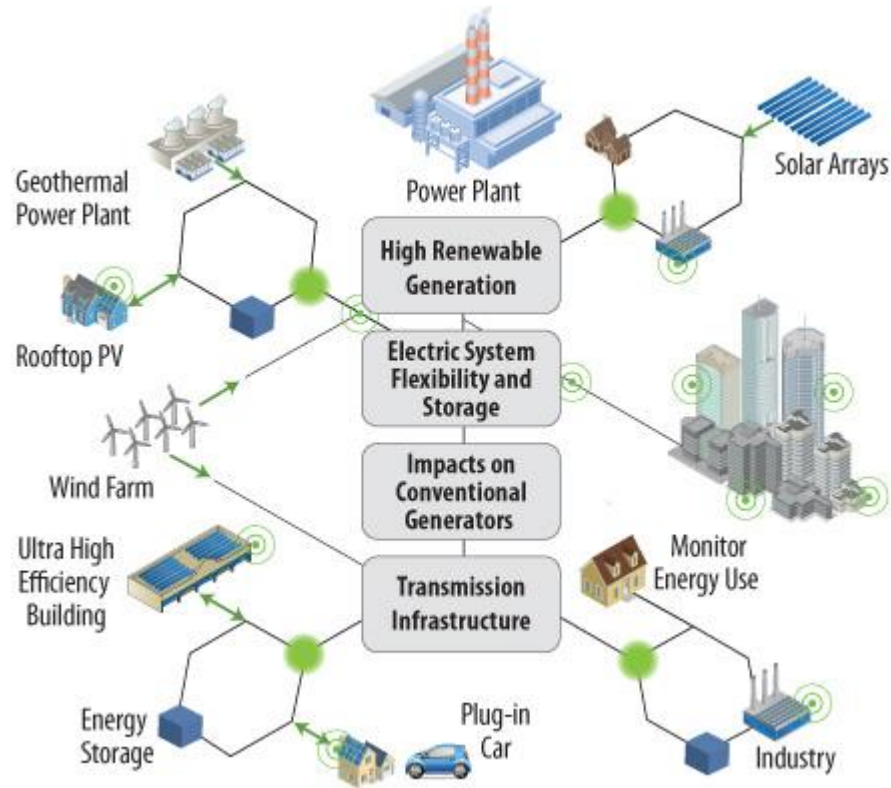


Figure 1-11: A modern distribution system with massive active customers [11]

The new distribution systems have experienced significant changes in the physical and management structure compared to conventional grids. An extensive distribution system is divided into several small microgrids (MGs) that can be managed by local operators. Also, advanced monitoring and control devices are needed in contact with a central controller. All the controllers and monitoring systems are in contact over a reliable telecommunication infrastructure. Any time a system operator or a local operator wants to change the load, generation, or topology of the system, the corresponding commands are sent to these control equipment for execution. Figure 1-12 indicates a modern distribution system with all possible control parties. As is shown in this system, there is an information network in parallel with the electrical network that makes the monitoring and control of different parties possible for the system operator.

From the management point of view, several intermediary entities are available such as local operators and aggregators, traders, etc., that can promote the collaboration between the customers and operators. Also, there is a market mechanism that can handle any negotiation between the entities. The system's operating schedule is determined according to commercial negotiations and technical constraints through a market process. Then, the system operator uses controllable devices and operates the system according to the market's outcome.

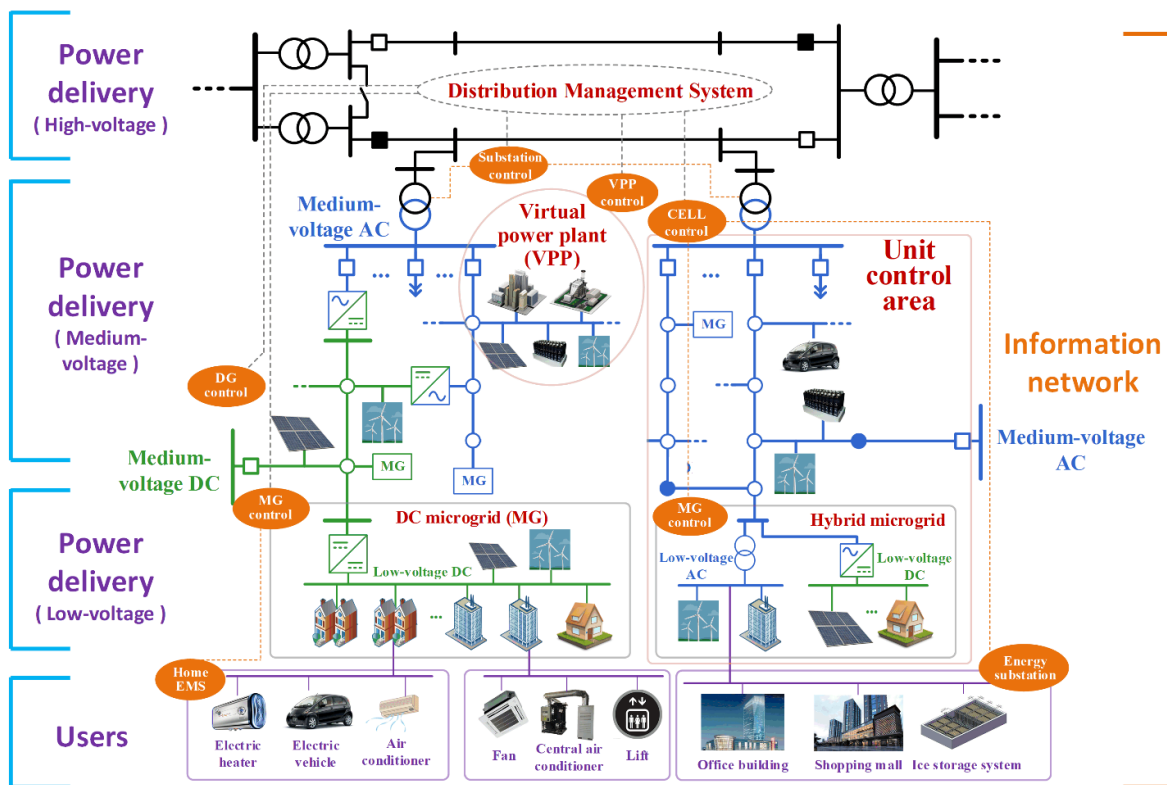


Figure 1-12: A modern distribution system with different control levels [12]

## 1.2. Research motivation

Consider a distribution system with several MGs and a massive number of active elements such as EVs, DERs, and DRs capable loads. As was discussed before, the distribution system operator (DSO) will have challenges managing such a system due to independent actions from

the entities above. One of the severe challenges that can damage the system is overloaded or congested equipment like transformers and branches. It can happen when a large group of consumers demands electricity at once, and the DERs are not willing or able to support it. Even if the DSO has the physical tools (e. g., control devices), it is not a practical way to manipulate the load or generation in the system without an agreement with the owners. The DSO's administrative actions are allowed in a situation when the system's security is treated, and there is no option/time to resolve the issue by the demand side itself. Thus, the DSO should try to take all necessary steps before the operation time to prevent problems. Without a market solution that can manage the active participants, the DSO must maintain too much margin in the equipment to prevent overloading or congestion in the system. However, it is not a cost-effective and secure way to rely only on the reserved capacity of distribution lines in the long-term operation due to the load growth.

An alternative solution is to utilize a new structure that gives the local independent microgrid operators (MGOs) enough privilege to control and manage their system locally. In parallel, it prepares a market environment for the participants to negotiate with the MGOs and provide proper answers for the DSO's demand. In this structure, the DSO only needs to ask the MGOs to adjust their demand leading to overloading/congestion. The MGOs can then provide enough incentive for the active constituents in their territory to motivate them to change their demand/production as the DSO requires. The framework that can support this process which should be iterative and bidirectional. Therefore, an adaptive framework is essential for the secure operation and management of modern distribution systems.

This research aims to provide a framework for all engaged entities (DSO, MGO, EV, DER, aggregators) and propose a holistic market-based model that can facilitate their interactions. The

research scope is the real-time operation, and the main focus is on real-time congestion management (CM).

### **1.3. Literature review**

During recent years, researchers have focused on the modern distribution systems (DSs) or smart grids (SGs) in the planning, operation, and management perspectives. In [13], the authors investigated that the conventional design schemes for the DSs are no longer efficient due to growing of the SGs. Therefore, the DSs should be re-designed in the physical and management infrastructures, accordingly. The advanced telecommunication tools to measure, transfer, and control different parts of the system are needed from the physical point of view. Also, new software and hardware are required to facilitate the interaction between various entities. The new entities such as DSO, MGO, and aggregators (AGGs) should be developed to activate customers' participation within a new market structure from the framework perspective. Due to numerous internet access points in this structure, the vulnerability of the DSs against cyberattacks and sabotages is another prestigious matter that should be taken into account in the modern DS design. Finally, the authors in [13] proposed some typical topologies of a modern DS with massive renewable resources and the capability of interaction with the upper grid. In a modern DS with extensively deployed active elements, the DSO has a main responsibility to manage the system dynamically to prevent or mitigate the possible congestions, especially in real-time operation. The main aim is to keep all electric assets safe against any violation of their capacity. It can be performed directly by an administrative action from the DSO side or indirectly by the demand side's participation. DSO's interferences can negatively affect the market's independency and can cause less active competitions in the market. Therefore, the priority is to use the customers' potential under a market platform to manage the abnormal situation. If the

market's contribution was not enough, then the DSO has to take administrative actions [14]. There are various central control mechanisms that the DSO can utilize to suppress the congestion, administratively. In [15], the authors have proposed a direct mechanism for CM in modern DSs using a three-step strategy. In the first step, the local control devices try to manage the load according to the initial setpoints. If it does not address the problem, the setpoints are optimized to maintain the DERs and DRs to alleviate the congestion in the second step. The DSO uses the last step when the current tools are not enough to relieve the congestion. Therefore, the central controller develops a reconfiguration accompanied with load shedding program to make a more considerable change in the system and release all congested branches. The importance of an adaptive control system in modern DS is irrefutable. The authors in [16] proposed an adaptive control schema for MG control and management. This control system can control the system's DERs, considering the stochastic power generation, frequency issues, and economic dispatch.

Another way that is more desirable in a deregulated environment is to prepare a market mechanism to take advantage of the demand-side potential for CM. We proposed three different frameworks in our previous research projects ([17]-[19]) to engage the customers in the CM process. In [17], we suggested a three-step framework to 1) use the DERs capacity, 2) to check the data traffic status, and 3) to use administrative load shedding and reconfiguration in a daily operation. The data traffic operator (DTO) participation can guarantee that the numerous participants' interactions do not cause trouble for the data transmission channels. The scope of our research in [18] also was a day-ahead CM. In this framework, the AGGs were allowed to collaborate during congestion times. This collaboration can be handled using an iterative game between the DSO and AGGs. The results in this paper showed that the proposed framework can

adequately address the day-ahead congestion. The way the DSO can suppress the congestion in the real-time operation is different from the day-ahead process. In [19], we proposed a framework to use the smart homes' (SH) potential in real-time CM. It can be inferred from this study that if a large number of SHs are in contract with the DSO, most of the congestions caused by loads' fluctuation and DERs' variation can be tackled. This framework has shortcomings such as the absence of the AGGs and MGOs. In [2], the authors have focused on the real-time CM. The participation of elastic costumers that have EV and heat pumps is considered as the solution for real-time congestion. The authors have used an optimal power flow combined with mixed-integer linear programming (MILP) to maintain the system's power balance and settle this service's cost. The results illustrate that if there exists enough EV and heat pumps in the system, a real-time congestion issue can be resolved entirely while the activating service charge is fully covered.

Although using a market-based solution for CM is more effective than an administrative solution, implementing such a solution is not easy. The DSO has challenges to motivate the clients to be a part of the CM program. One of the typical solutions is to use a penalty/reward mechanism to affect the private owners' actions [21]. The DSO can implement this mechanism using a dynamic tariff (DT) or a distribution locational marginal price (DLMP) adjustment method. The authors in [22]-[24] suggested different versions of DT for CM. In [22], a decomposition-based optimization method is used to increase the participation of AGGs during CM. Keeping the power loss and electricity price at the minimum level are the advantages of this method. The proposed DT method makes the CM beneficial for the AGGs. Therefore, it gives more certainty and transparency compared to the other methods. In [23], a distribution system with massive heat pumps, PVs, and EVs with the vehicle to grid function (V2G) is studied. The

authors considered a price regulation such that adding a positive price as a tariff causes the load reduction, and adding a negative price as a subsidy increases consumption at a specific time. The results in this paper illustrate that the tariff and subsidy should be considered simultaneously, especially when the DSO wants to shift a part of the load to another hour. In [24], the authors proposed a control mode with two control loops, one for power flow control and another for voltage control, to modify the electricity price. The interaction of these loops creates sensitivity factors that are needed to have a DT model. Despite the advantages of using the DT for CM, one of the significant shortcomings of this method is to ignore the consumers' location. It means that all the clients in the system are rewarded or penalized similarly, while some have more effects on the congestion than the others. To address this issue, the authors provided a DLMP based price adjustment method in [25] and [26]. Since the DLMP is calculated locally, the location of the customers also affects the final price. According to the proposed framework in those papers, the DSO identifies the customers who should reduce their load to address the congestion. By revising the DLMPs related to those customers, the DSO can motivate them to shift or curtail their demand and mitigate the congestion. According to the definition, DLMP represents the cost of adding one per-unit active consumption power at each bus of the system in a distribution system. The necessary mathematical procedure to calculate the DLMP in unbalanced systems is explained in [27]. According to this model, the DLMP is composed of electricity cost, power loss cost, and congestion cost. The proposed model in [27] is not proper for CM since it is not a dynamic model. Another model is presented in [28], which gives a progressive structure for DLMP. Using such a model, the DSO can engage the customers or their AGGs in the CM process by adjusting the DLMP, dynamically.

One of the main assumptions in [27] and [28] is considering the distribution systems as

balanced systems. Although using a conventional power flow modeling (e.g., newton Raphson [29]) can make the model more straightforward for the distribution systems, it is not a reasonable assumption in the real world. The structure of the distribution systems is radial. Considering the various single-phase loads that the end-users have, the distribution systems' aggregated load is unbalanced [30]. As a result, an unbalanced load flow (ULF) model can make the study more realistic. Different linear and nonlinear methods for ULF have been represented in [31]. The results show that since the distribution systems have too many small loads and branches, the ULF may not converge. It happens mostly when the admittance matrix of the system becomes singular. One idea is to divide a large scale distribution system into several smaller areas and use the ULF for each part, independently. Also, evaluating the linear model for ULF demonstrates that the linear models are not accurate for unbalanced systems. For some long-term studies, the linear model can be useful. But for the operation problems, it is recommended to use an exact model for ULF. The authors in [32] and [33] provided two versions of ULF's linear model. The proposed models are more accurate than the previously investigated model in [31]. But the comparison between the results shows that there is still a noticeable error between the accurate models and linear models.

Since the ULF model affects the DLMP values, the preference is to use a precise model. The researchers have proposed several accurate models for ULF during past years. Despite the technique they used, all of those models can be categorized into two main groups: 1) complex models, 2) d-q models. In [34], a complex model is proposed to solve the ULF problem for a large scale distribution system. In this paper, using the connectivity data, a z-bus for the system was built. Then, the authors used some reasonable constraints to limit the search area and force the algorithm to converge to the real solution faster. This method is useful when the loads are

modeled as constant-impedance (ZIP) elements. This idea presented in [34] is unique because it shows by creating some limitations on the search area, it is possible to make the solution process faster and more reliable.

Some of the optimization software like GAMS<sup>1</sup> does not support complex values. In such cases, a d-q model is valuable. In [35], a ULF model is proposed by the authors according to the d-q decomposition. In this model, all the equations are divided into two sets of parallel equations. The real parts are considered on the d axis, and the imaginary values are considered on the q axis. Both sets of equations are solved in parallel. In our research, we are going to propose a d-q (or Cartesian) model for the unbalanced power flow equations. Each branch in an unbalanced system has three phases of wiring and a neutral network. As a result, there are four sets of complex equations for each bus/branch of the system. A standard method that can reduce the size of the problem is the *Kron* reduction method. *Kron* reduction is a way of eliminating unnecessary data from a large matrix in load flow calculation. Most of the industrial software that can calculate ULF (such as OpenDSS) uses this technique. If the neutral voltage is closed to zero, the *Kron* reduction technique can exclude the neutral equations and reduce the problem's size [36]. Since the neutral systems power loss is essential in this research, it is preferable to work with the exact power flow equations model.

Another essential factor in the CM study is to consider the natural fluctuation of the loads and renewable-based DERs in the system. In an extensive distribution system with numerous loads, the demand side fluctuation is not severe because it is a random variation. As a result, the aggregated load may not change significantly and cause congestion. But the DERs' fluctuation may cause congestion. In [37] and [38], the significance of instability in the generators' output in

---

<sup>1</sup> General Algebraic Modeling Language

a distribution system is investigated. The authors' solution to reduce the impact of these uncertainties is to use a hybrid dispatching energy model. In fact, by engaging the various types of energy resources (wind, solar, fossil), the natural variation can be managed more effectively. The uncertain variables in the system can affect the ULF model, accordingly. In [39], a probabilistic model for ULF is proposed by the authors. This model is beneficial in the impact-based analysis when the primary intention is to analyze the system's renewable resources' impact. However, the complexity of this ULF model brings up serious challenges in optimization studies.

Another challenge that the DSO has in the real-time operation is unreliable data. The uncertain variations in the system, noises in the data, and intentional false data injection are the reasons that create enough necessity to use a dynamic state estimation technique. The *Kalman filtering* (KF) [40] method is suitable for this case. In [41], the authors have used a KF technique to estimate the PV system's production in a distribution system with high PV penetration. This technique helps the system operators estimate the PVs' output if it is not possible to measure and transfer the data associated with all PVs continuously. In [42], another KF technique has been used to control a local load with a local PV system. In this paper, the main idea is to estimate the system condition using a KF technique and set the PV output accordingly. The results show that the proposed method can help the system to stay stable in the under-voltage circumstances.

In this research, the primary goal is to provide a holistic framework consisting of several entities on different levels (DSO, MGO, AGG, and owners). The way that these entities can interact in a regular or congestion circumstance during real-time operation will be studied. Also, adopted mathematical models for all entities will be formulated.

#### 1.4. Main research contributions

Despite extensive research on CM in the modern distribution systems, this area still needs further attention to obtain a realistic decentralized manner for real-time CM. More specifically, in the earlier steps of this research, we proposed a market-based framework to manage day-ahead congestions in [17] and [18]. However, the proposed market schemes in those papers were unable to prevent real-time congestions. As a result, in another study, we proposed a framework to avoid real-time congestion using DRs and SHs. This framework is not holistic, and several entities such as AGGs, DGs, and EVs were not included. In this dissertation, we propose a holistic market framework to prevent real-time congestion in unbalanced distribution systems. A carrot and stick game approach is implemented to engage the private participants in the CM program. Using this game model, the DSO can use the DLMP as a vital signal and affect the players' decisions. The outcome would be a motivation for the participants to cooperate and relieve the congestion. Therefore, the main features of this study (i.e., a market-based approach for realistic decentralized management of real-time congestions in unbalanced distribution systems) are as follows:

- 1) The proposed platform prepares this chance for DSO and MGOs to have interactions. At the same time, the MGOs can negotiate with the AGGs in several rounds. The MGOs can also track the reactions from the AGGs after each round of DLMP revisiting and decide about the next step. As a result, the DSO can take advantage of the demand side to cope with the congestion in a real-time operation.

- 2) Since the complex form of load flow is not compatible with the Lagrange optimization method, a complete cartesian (d-q) unbalanced load flow formulation is developed. The neutral system is not eliminated to have more accurate results. Using this model, it is possible to solve the optimization problem by GAMS or other mathematical-based solvers.

3) A real-time data estimation system is considered to reduce the risk of congestion due to insufficient data or fluctuation in the load's consumption and generation unit's production. This system works according to a basic KF technique. According to the historical data, the idea is to provide an error vector and add that to the received data from the AGGs. The output would be closer to the actual data in the next operation time step.

4) In this framework, the DSO effectively compensates for the CM cost. This cost should be reflected in the DLMPs and should be paid by the consumers. Therefore, the DSO should update the DLMPs according to the CM cost. The proposed DLMP revisiting method in this research is formulated to keep the input-output money transfer clear. This guarantees that all the extra cost that the customers pay is equal to the CM cost. Thus, there is no residual money associated with this mechanism.

## CHAPTER 2

### PROPOSED METHODOLOGY

#### **2.1. Introduction**

This chapter discusses the proposed methodology for the real-time operation in a modern DS. As was discussed earlier, there is an extensive number of active elements in a modern DS. The DSO must control and manage those functional entities to ensure system security during the real-time operation. The consumers' activity in modern DSs can be beneficial for the DSO if an adaptive management strategy is used. The main responsibility of the DSO is to operate the distribution system safely and efficiently. To obtain this goal, DSO has to maintain several studies such as economic dispatch, protection, reliability, adequacy, etc. Dealing with an active demand side besides the mentioned responsibilities increases the DSO burden more than before. It may reduce the quality of DSO performance. This chapter proposes a hierarchical operation and management framework that gives the DSO the ability to manage a modern DS efficiently in real-time operation.

#### **2.2. Problem definition**

##### **2.2.1. The management platform**

There are several ways that the DSO can control the end users. Figure 2-1 illustrates a topology when the DSO directly manages all the entities by itself. This topology is a two-layer platform where only the DSO and the end-users are available in separate layers. Since there are several controllable devices in a modern DS, this topology seems inefficient for implementation. The DSO has to be in contact with massive elements, simultaneously, which reduces the DSO's performance.

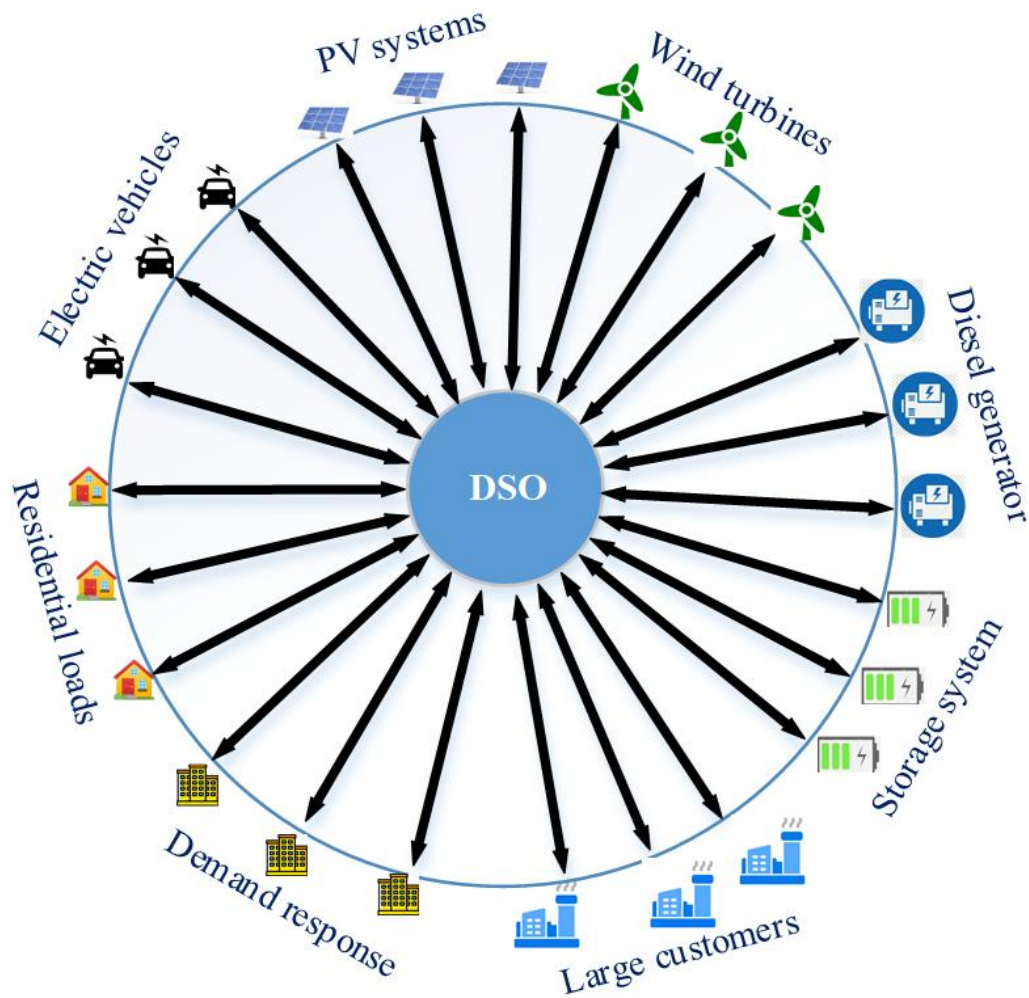


Figure 2-1: A two-layer management platform

One solution to reduce the DSO's burden is to define some aggregators that can integrate the customers' power and act on behalf of them. Figure 2-2 illustrates a three-layer management platform where the DSO only communicates with the aggregators. As a result, the DSO and customers are in contact indirectly. This platform helps the DSO deal with the less direct transaction.

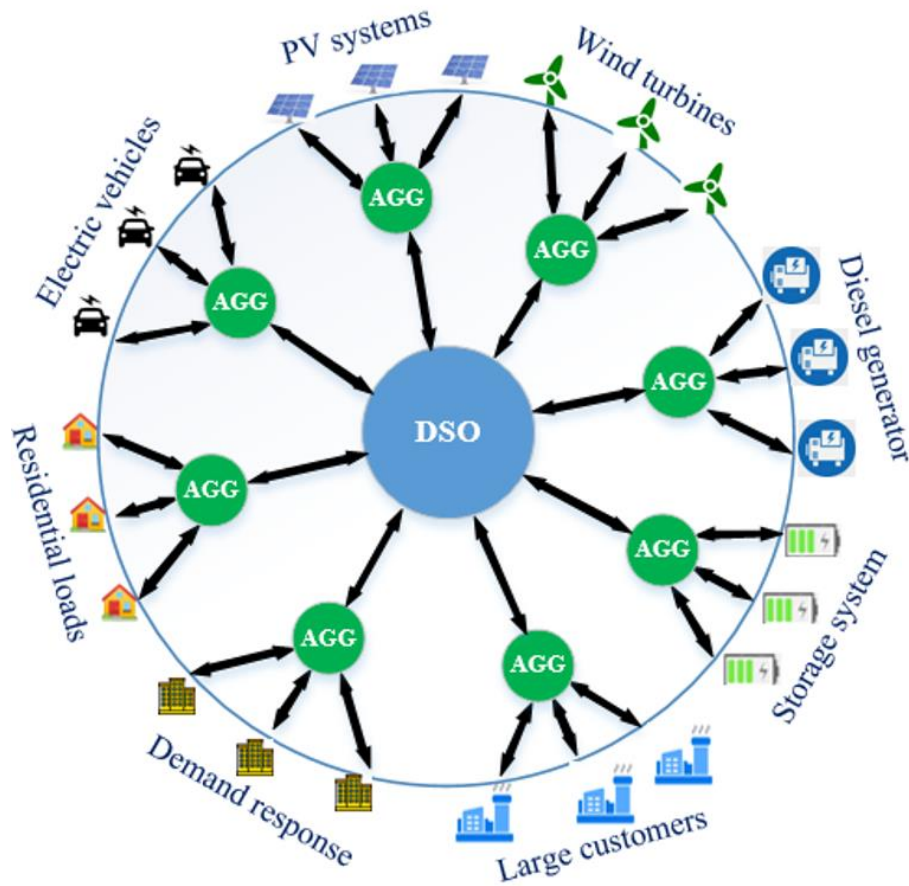


Figure 2-2: A two-layer management platform

Another topology is shown in Figure 2-3, where the MGOs are the new layer and cooperate with the DSO and aggregators, simultaneously. In this structure, the DSO only sends the necessary commands to the MGOs, and the MGOs communicate with the AGGs. The MGOs act as local system operators, and their responsibility is the operation and management of a small part of the system. This topology helps the DSO contact the MGOs directly, which causes less direct transactions than the other topologies. In this research, we use a four-layer topology and define the communication between the layers in detail.

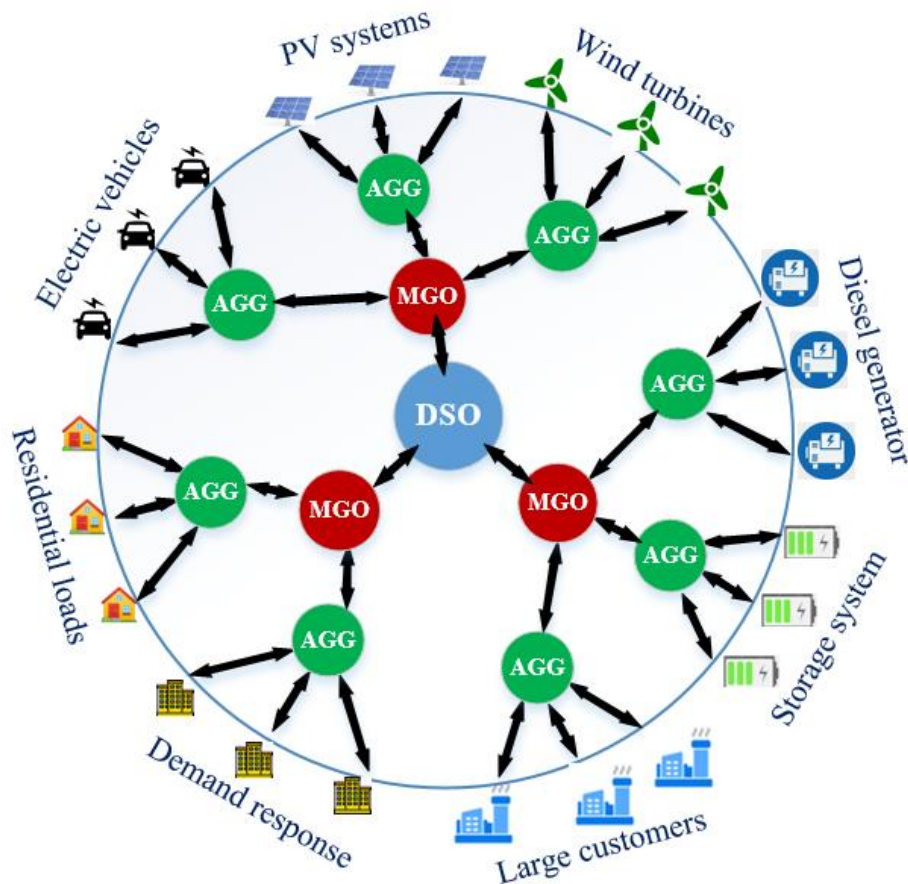


Figure 2-3: A three-layer management platform

### 2.2.2. Entities definition

As discussed, we define two intermediate entities between the DSO and the consumers to facilitate the interactions. As a result, all the entities in the system can be categorized into four hierarchical layers. Figure 2-4 indicates the position of these layers. Arrows show the interaction between different layers. The defined layers are as follows:

#### 1) DSO layer:

The DSO is a part of the distribution company and handles the system's operation and management. DSO is the only member of this layer. Also, the DSO only has interaction with the members of the lower level.

## **2) Micro-grid operators layer:**

According to the framework definition, each part of the grid can be owned and managed by private companies known as MGOs. Depending on the given privilege to an MGO, it can be only a monitoring party or a local DSO. In this study, the MGOs are considered as local DSOs, which means they are responsible for operation and management in their territory. Several MGOs can communicate with a similar DSO from the upper level and several entities from the lower level at the same time. Also, each MGO can supervise several microgrids on the same grid simultaneously.

## **3) Aggregators layer:**

The aggregators (AGGs) are in contract with the end customers and, at the same time, can cooperate with the MGOs. We model the aggregators to reduce the direct contact between the end-users and the MGOs. Using this model, the AGGs can make a deal with the MGOs on behalf of their clients. Generally, three groups of aggregators can be defined in this layer as follows:

- a) Distributed generation aggregators (DGAG)
- b) Electric vehicle aggregator
- c) Demand response aggregator (DRAG)

All the aggregators have a contract with the owners for each service.

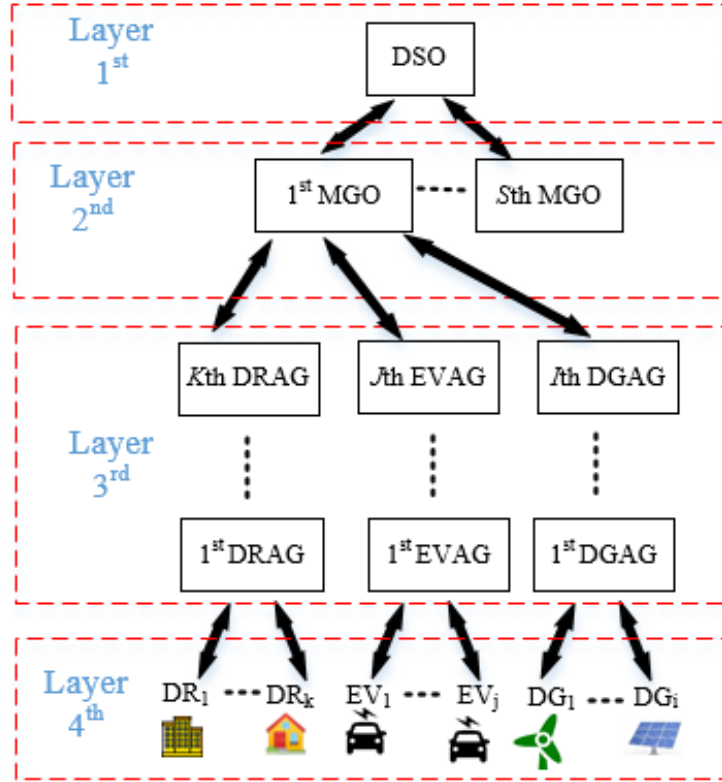


Figure 2-4: Different entities and layers in the proposed platform

### 2.3. Mathematical modeling for aggregators

In this section, the mathematical model for three types of aggregators is defined. The objective function and the constraints are considered according to the real-time operation. The used indices in the formations are as follows:

- $i$ : DG aggregators
- $j$ : EV aggregators
- $k$ : DR aggregators
- $v$ : DG owners
- $w$ : EV owners
- $s$ : micro-grids
- $u$ : DR owner
- $l$ : Curtailment step
- $ph$ : the phase sequence  $\{a,b,c,n\}$

### 2.3.1. EVAG optimization model

The main objective of an EVAG is to minimize the charging cost for its clients. The cost can be minimized by choosing the right time to plug in the vehicles. In addition, the EVAGs can partake in the CM during the congestion times. Equations (2-1) to (2-7) describe the objective function associated with the  $j$ th EVAG where  $P^{EVAG}$ ,  $\rho^{MG}$ ,  $P^{EVBB}$ , and  $E^{EVBB}$  represent the offered power by EVAG, the electricity price, the exchanged power, and the available stored energy regarding the battery bank. In this research, the converters associated with the EVs are considered bidirectional. As a result, the converter can charge or discharge the battery depends on the situation. The integer variable  $X$  is defined to engage with EV owner if it is going to plunge into the grid in the next time step. The customer requests for  $E_w^{EVBB,sch}$  amount of charge and supposes to have it at  $t_{end}$ . Moreover,  $w \in W\{j\}$  means the  $w$ th EV owner has a contract with the  $j$ th EVAG. In this research, it is assumed that each EV owner can only have a contract with one AGG at each time.

$$\min : \sum_{t=t_0}^{24} \sum_{w \in W\{j\}} P_{w,t}^{EVBB} \rho_{s,w,t}^{MG} \quad (2-1)$$

*s.t.*

$$P_{j,t}^{EVAG} = \sum_{w \in W\{j\}} P_{w,t}^{EVBB} \quad (2-2)$$

$$-P_{w,t}^{EVBB} \leq P_w^{EVBB,disch} X_{w,t} \quad (2-3)$$

$$P_{w,t}^{EVBB} \leq P_w^{EVBB,ch} X_{w,t} \quad (2-4)$$

$$E_{w,t}^{EVBB} = E_{w,t-1}^{EVBB} - P_{w,t}^{EVBB} \quad (2-5)$$

$$E_{w,t}^{EVBB} = E_w^{EVBB,sch}, \text{ if } t = t_{end} \quad (2-6)$$

$$X_{w,t} = \begin{cases} 1 & \text{if } t_{st} \leq t \leq t_{end} \\ 0 & \text{otherwise} \end{cases} \quad (2-7)$$

### 2.3.2. DGAG optimization problem

The DGAGs should try to increase their clients' benefit (DG owners) from selling the energy and services to the MGOs during the real-time operation. They should provide the schedule of their clients and submit the aggregated bids to the corresponding MGOs. In this research, we model renewable energy-based DERs with battery banks and smart inverters. Therefore, the produced power can be adjusted by the inverter. Equations (2-8)-(2-14) formulate the objective function and constraints for the  $i$ th DGAG at time  $t$ , which its clients are included in the  $s$ th MG territory. In these equations,  $v \in V\{i\}$  means the  $v$ th DG owner has a contract with the  $i$ th DGAG. This contract gives the privilege to the DGAG to negotiate with the MGO on behalf of the owner. Also,  $P^{DG}$ ,  $P^{DG\text{BB}}$ ,  $P^{DG\text{in}}$ ,  $E^{DG\text{BB}}$ , respectively, represent the total power, the battery bank power, the produced power by DG, the available energy at the next  $\Delta t$  time. The DGAGs should keep batteries partially charged at the end of the day to have a better chance for the first hours of the next day. Thus, (2-14) is included in the model where  $E_0$  the remained energy at the end of the day. According to this equation,  $E_0$  kWh energy must remain in the batteries at the end of the day.

$$\max \sum_{t=t_0}^{24} \sum_{v \in V\{i\}} P_{v,t}^{DG} \rho_{s,v,t}^{MG} \quad (2-8)$$

*s.t.*

$$P_{v,t}^{DG} = P_{v,t}^{DG\text{in}} + P_{v,t}^{DG\text{BB}} \quad (2-9)$$

$$P_{v,t}^{DG\text{BB}} \leq P_v^{DG\text{BB},\text{disch}} \quad (2-10)$$

$$-P_{v,t}^{DG\text{BB}} \leq P_v^{DG\text{BB},\text{ch}} \quad (2-11)$$

$$E_{v,t}^{DG\text{BB}} = E_{v,t-1}^{DG\text{BB}} - P_{v,t}^{DG\text{BB}} \quad (2-12)$$

$$E_v^{DG\text{BB},\text{min}} \leq E_{v,t}^{DG\text{BB}} \leq E_v^{DG\text{BB},\text{max}} \quad (2-13)$$

$$E_{v,24}^{DG\text{BB}} \geq E_0 \quad (2-14)$$

### 2.3.3. DRAG optimal bidding

The DR service is a very beneficial since it can engage the consumers in the system operation process. Many of the customers in the grid have some non-firm loads that can be curtailed or shifted. A client can reduce its load by increasing the temperature of the AC on a warm day. It is an instance of the curtailable loads. In another case, a client can start the laundry at 10 pm instead of 4 pm, and it would be an example of a load which can be shifted. According to a contract between the clients and the AGGs, the DRAGs can integrate all the possible non-firm loads and offer a load reduction at a specific time for receiving particular money from the MGOs. To prepare such a plan, the DRAGs need an optimization problem to maximize the clients' revenue from participating in the DR program and consider the required constraints.

Equations (2-15) and (2-16) formulate the optimization problem for the  $k$ th DRAG where  $P^{cur}$  and  $\rho^{DR}$  stand for the power (kW) and the price for each curtailed step. Also,  $X^{DR}$  is a binary variable, which is one when the corresponding DR step is selected for offering to the MGOs and otherwise is zero. In addition,  $u \in U\{k\}$  represents that the  $u$ th DR owner has a contract with the  $k$ th DR aggregator to reduce the maximum  $E_l^{cur,max}$  energy per day. In this research, the DR service can be offered by a maximum of four steps at different prices.

$$\max \text{rev}_k = \sum_{t=t_0}^T \sum_{u \in U\{k\}} \sum_{l=1}^4 P_{u,l,t}^{cur} X_{u,l,t}^{DR} \rho_{u,l,t}^{DR} \quad (2-15)$$

*s.t.*

$$\sum_{t=t_0}^T \sum_{u \in U\{k\}} \sum_{l=1}^4 P_{u,l,t}^{cur} X_{u,l,t}^{DR} \leq E_l^{cur,max} \quad (2-16)$$

The next step for the DRAGs is to aggregate the DRs and submit an equivalent power and price to the MGOs. The equations (2-17) and (2-18) formulate offered aggregated power and

price to the MGOs. In these equations,  $P_k^{DRAG}$  and  $\rho_k^{DRAG}$  respectively indicate the aggregated DR power and the corresponding price for the offered DR service by the  $k$ th aggregator.

$$P_k^{DRAG} = \sum_{u \in U\{k\}} \sum_{l=1}^4 Pst_{u,l}^{DR} X_{u,l}^{DR} \quad (2-17)$$

$$\rho_k^{DRAG} = \frac{rev_k}{P_k^{DRAG}} \quad (2-18)$$

#### 2.4. Cartesian unbalanced load flow equations

One of the contributions of this study is to develop the decentralized optimization platform during the simulation. In this platform, each MGO solves its optimization problem independently, and then all the MGOs submit their demanded power from the grid to the DSO. This power is valid only for the next time step, and the MGOs should repeat the process continuously for each operation time. Since the MGOs play the role of local DSOs, they should deal with the ULF constraints in the system under their supervision. In this section, a complete cartesian (d-q) ULF model is formulated according to the KVL<sup>1</sup> and KCL<sup>2</sup> laws. These equations will be included in the MGOs' optimization problem as the firm constraints.

Figure 2-5 illustrates a typical bus  $n$  of a system with a local load and a shunt connected impedance. According to the KCL, equations (2-19) to (2-22) represent the power balance equations. In these equations, the variables with  $x$  index stand for the real part, and the variables with  $y$  index stand for the imaginary part of each variable. This calculation can be used for each phase of the system to find the active and reactive power associated with the whole MG.

---

<sup>1</sup> Kirchhoff's Voltage Law

<sup>2</sup> Kirchhoff's Current Law

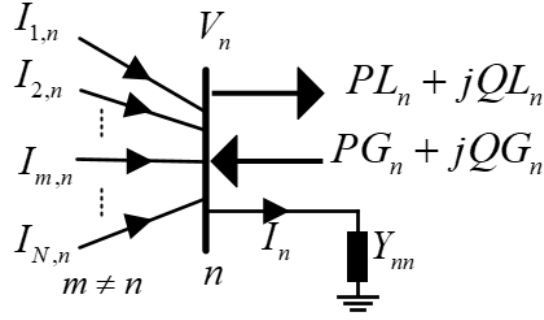


Figure 2-5: A typical bus  $n$  of a system with the input, output power/currents

$$PG_n - PL_n = V_n^x (I_{nn}^x - I_n^x) + V_n^y (I_{nn}^y - I_n^y) \quad (2-19)$$

$$QG_n - QL_n = V_n^y (I_{nn}^x - I_n^x) - V_n^x (I_{nn}^y - I_n^y) \quad (2-20)$$

$$I_{nn} = \sum_{m=1}^N I_{mn} \quad m \neq n \quad (2-21)$$

$$I_n = V_n Y_{nn} \quad (2-22)$$

In these equations,  $PG_n$  and  $QG_n$  stand for active and reactive power generated by the local DGs at the  $n$ th bus. Also,  $PL_n$  and  $QL_n$  represent the active and reactive equivalent local load at bus  $n$ . According to the DRAG decision, the local load can be calculated using (2-23) and (2-24) where  $PL_n^{sch}$ , and  $QL_n^{sch}$  represent the scheduled active and reactive load before engaging the local customer in the CM program. The other variables have been defined in previous sections.

$$PL_n = \left( PL_n^{sch} - \sum_l P_{u,l}^{cur} \right) + PEV_n, u \in n \quad (2-23)$$

$$QL_n = \left( QL_n^{sch} - \sum_l Q_{u,l}^{cur} \right), u \in n \quad (2-24)$$

The power loss can be calculated by adding the injected power into a branch from two end nodes. Figure 2-6 shows the connection between two nodes in a distribution system. The way that the power loss can be calculated per-unit is formulated in (2-25), where “\*” is the conjugate operator.

$$S_{nm}^{Loss} = S_{nm} + S_{mn} = V_n I_{nm}^* + V_m I_{mn}^* \quad (2-25)$$

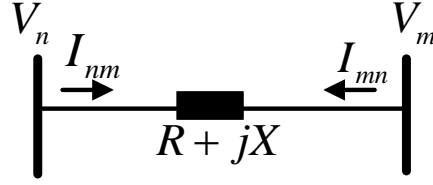


Figure 2-6: A typical branch and its end nodes

If we apply (2-25) to all branches of the system, a closed formulation for total active and reactive power is obtained as (2-26) and (2-27), respectively.

$$P^{loss,ph} = \sum_{n=1}^N \sum_{\substack{m=1 \\ m \neq n}}^N (V_n^{x,ph} I_{nm}^{x,ph} + V_n^{y,ph} I_{nm}^{y,ph}) \quad (2-26)$$

$$Q^{loss,ph} = \sum_{n=1}^N \sum_{\substack{m=1 \\ m \neq n}}^N (V_n^{y,ph} I_{nm}^{x,ph} - V_n^{x,ph} I_{nm}^{y,ph}) \quad (2-27)$$

Knowing that the consumers in the distribution systems have many single-phase loads, the aggregated load is unbalanced. As a result, the summation of three-phase current is not necessarily equal to zero ( $I_a + I_b + I_c \neq 0$ ). According to KCL, the backward current should flow through the neutral wires. Figure 2-7 shows the phases and neutral current for a typical two connected nodes. As is inferred from the figure,  $J_{mn}$  is the backward current and passing through the neutral wires.

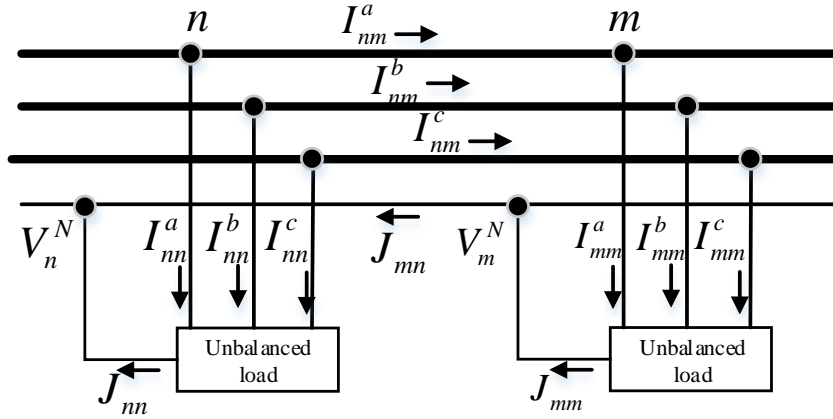


Figure 2-7: A typical two bus with four wires and local loads

Having a current in the neutral system causes power loss. Thus, to consider the power loss associated with the neutral wiring, the equations (2-28) and (2-29) are proposed. According to these equations, the neutral grid's absorbed power is the power loss (the reason is none of the loads are fed by the neutral system).

$$P^{loss,null} = \sum_{n=1}^N [V_n^{x,N} J_{mn}^x + V_n^{y,N} J_{mn}^y] \quad (2-28)$$

$$Q^{loss,null} = \sum_{n=1}^N [V_n^{y,N} J_{mn}^x - V_n^{x,N} J_{mn}^y] \quad (2-29)$$

Equations (2-30)-(2-33) present the KVL and KCL for two connected nodes where  $Z^N$  and  $Z^{ph}$  are the impedance array of the neutral and phase wires, respectively. All other parameters are illustrated in figure 2-7. Since the network is radial, the number of branches is  $N-1$ . As a result, in (2-32), only  $N-1$  variables ( $J_{mn}$ ) are unknown. Therefore, the linear equations in (2-31) have a unique solution.

$$V_n^{Null} = V_m^{Null} - Z_{mn}^N J_{mn}, n \neq m, n \neq slack \quad (2-30)$$

$$V_m^{ph} = V_n^{ph} - Z_{nm}^{ph} I_{nm}, n \neq m, n \neq slack \quad (2-31)$$

$$J_m + \sum_{n=1, n \neq m}^N J_{mn} = 0, n \neq \text{slack} \quad (2-32)$$

$$J_{mn} = I_{mn}^a + I_{mn}^b + I_{mn}^c \quad (2-33)$$

Equations (2-30)-(2-33) are in the complex format. The ULF equations in a cartesian shape are represented as (2-34)-(2-41) where  $R^N$  and  $X^N$  are the resistance and reactance associated with the null system. A 120-degree phase-shifting should be considered to project the values from the phasor domain to the  $x$ - $y$  domain. Figure 2-8 illustrates the projections in a vector space. Thus, (2-33) is represented as (2-40) and (2-41) after projection where  $\varphi^a = 0$ ,  $\varphi^b = \frac{-2\pi}{3}$ , and  $\varphi^c = \frac{2\pi}{3}$ .

$$V_n^{N,x} = V_m^{N,x} - R_{mn}^N J_{mn}^x + X_{mn}^N J_{mn}^y, n \neq \{m, \text{slack}\} \quad (2-34)$$

$$V_n^{N,y} = V_m^{N,y} - R_{mn}^N J_{mn}^y - X_{mn}^N J_{mn}^x, n \neq \{m, \text{slack}\} \quad (2-35)$$

$$V_n^{ph,x} = V_m^{ph,x} + R_{mn}^{ph} I_{mn}^x - X_{mn}^{ph} I_{mn}^y, n \neq \{m, \text{slack}\} \quad (2-36)$$

$$V_n^{ph,y} = V_m^{ph,y} + R_{mn}^{ph} I_{mn}^y + X_{mn}^{ph} I_{mn}^x, n \neq \{m, \text{slack}\} \quad (2-37)$$

$$J_{mn}^x + \sum_{m=1}^N J_{mn}^x = 0, n \neq m \quad (2-38)$$

$$J_{mn}^y + \sum_{m=1}^N J_{mn}^y = 0, n \neq m \quad (2-39)$$

$$\begin{bmatrix} J_{mn}^x \\ J_{mn}^y \end{bmatrix} = \sum_{\substack{m=1 \\ m \neq n}}^N A(\varphi^a) \begin{bmatrix} I_{mn}^{x,a} \\ I_{mn}^{y,a} \end{bmatrix} + A(\varphi^b) \begin{bmatrix} I_{mn}^{x,b} \\ I_{mn}^{y,b} \end{bmatrix} + A(\varphi^c) \begin{bmatrix} I_{mn}^{x,c} \\ I_{mn}^{y,c} \end{bmatrix} \quad (2-40)$$

$$A(\varphi) = \begin{bmatrix} \cos \varphi & -\sin \varphi \\ \sin \varphi & \cos \varphi \end{bmatrix} \quad (2-41)$$

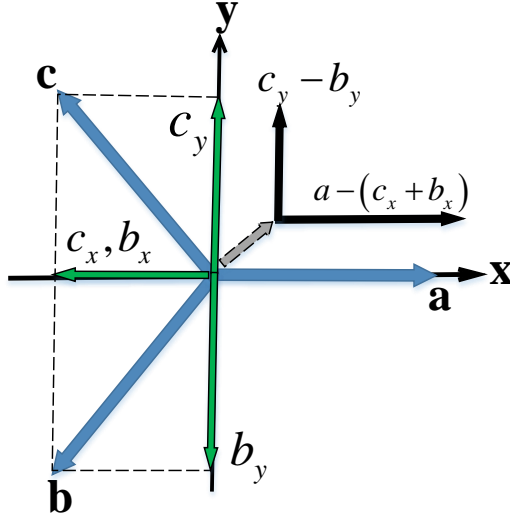


Figure 2-8: Conversion from phasor domain to x-y domain

Equations (2-42)-(2-43) present the complementary constraints associated with the system's voltage and current.  $V^{min}$  and  $V^{max}$  are the values in pu and define the allowable region for the voltage and  $I^{max}$  represents the maximum branches' current.

$$V^{min} \leq \sqrt{V_x^2 + V_y^2} \leq V^{max} \quad (2-42)$$

$$\sqrt{I_x^2 + I_y^2} \leq I^{max} \quad (2-43)$$

## 2.5. MGO optimization formulation

In the proposed framework, the MGOs work as local DSOs. It gives higher privilege and responsibility to the MGOs. The main aim of a typical MGO is to gather all the bids/offers from the AGGs and predict the firm loads for the next time. Then, it solves an optimization problem in its network and, finally, it sends the needed power from the grid to the DSO. Equation (2-44) formulates the objective function for sth MGO. In this equation,  $f_1$  is the total cost of electricity that is purchased from the grid or the DERs, and  $f_2$  is the curtailment cost. If DSO calls an

MGO to reduce its demand due to congestion, both portions should be considered in the optimization problem. Otherwise, only  $f_1$  should be taken into account.

$$\min : \begin{cases} f_1 = P_s^{GR} \rho_s^{GR} \\ f_2 = \sum_{k \in K\{s\}} P_k^{DRAG} \rho_k^{DRAG} \end{cases} \quad (2-44)$$

$$P_s^{GR} = \sum_{ph \in \{a,b,c\}} \sum_{n=1}^N [PL_n^{*,ph} + PEV_n^{ph} - PDG_n^{ph}] + P_s^{loss} \quad (2-45)$$

$$Q_s^{GR} = \sum_{ph} \sum_{n=1}^N [QL_n^{*,ph} - QDG_n^{ph}] + Q_s^{loss} \quad (2-46)$$

In (2-44),  $P_s^{GR}$  represents total active power purchased from the grid by sth MGO with the price of  $\rho_s^{GR}$ . The active and reactive power which are demanded by sth MG can be formulated as (2-42) and (2-43), respectively.  $PL$ ,  $PEV$ ,  $PDG$  and  $P^{loss}$  refer to the active load after DR implementation, EV demand, DG production, and active power loss in each MG, respectively. Also,  $QL$ ,  $QDG$ , and  $Q^{loss}$  stand for reactive demand, reactive power associated with DGs, and reactive loss in each MG, respectively.

Equation (2-47) presents the maximum power which MG can exchange with the grid, where  $P_s^{MG,max}$  and  $P_s^{MG,ord}$  are the transformer capacity and the maximum power which the sth MG can take from the grid to prevent the congestion in the upstream network.  $P_s^{MG,ord}$  is determined by DSO after ULF calculation. In a normal situation,  $P_s^{MG,max} \leq P_s^{MG,ord}$  which means the DSO allows the sth MGO to receive the power from the grid up to its transformer's capacity. But in the congestion condition, if the sth MG is within the congested area, then  $P_s^{MG,max} \geq P_s^{MG,ord}$ .

$$P_s^{MG} \leq \begin{cases} P_s^{MG,max} & \text{in normal condition} \\ P_s^{MG,ord} & \text{in congestion condition} \end{cases} \quad (2-47)$$

In this research, the GAMS software is used to handle the optimization problems (see chapter 3). The selected nonlinear solver (namely “conopt”) solves the problem using the Lagrange method. The overall Lagrangian function (i.e., LaF) for the  $s$ th MGO optimization problem is formulated as (2-48) to (2-71). As can be inferred, (2-48) is the objective function for each MGO. Also, (2-49) to (2-53) represent all constraints, which are explained in (2-45) to (2-47). The ULF constraints (i.e., (2-19) to (2-43)) are an essential part of the MGO optimization problem. These parts are included in the LaF from (2-54) to (2-71) as additional constraints. According to the definition, the DLMP in each node and phase is the Lagrangian multiplication of (2-56) which is denoted by  $\rho_n^{P,ph}$ . This is the rate that the customers at bus  $n$  will be paid or charged.

min :  $LaF =$

$$P_s^{MG} \rho_s^{GR} + \sum_{k \in K\{s\}} P_k^{DRAG} \rho_k^{DRAG} \quad (2-48)$$

$$+ \lambda_s^P \left( P_s^{GR} - \sum_{ph \in \{a,b,c\}} \sum_{n=1}^N [PL_n^{*,ph} + PEV_n^{ph} - PDG_n^{ph}] + P_s^{loss} \right) \quad (2-49)$$

$$+ \lambda_s^Q \left( Q_s^{GR} - \sum_{ph} \sum_{n=1}^N [QL_n^{*,ph} - QDG_n^{ph}] + Q_s^{loss} \right) \quad (2-50)$$

$$+ \lambda_s^{PMG \max} \left( P_s^{MG} - \min \{ P_s^{MG, \max}, P_s^{MG, ord} \} \right) \quad (2-51)$$

$$+ \lambda_n^{Pc} ( PL_n^{*,ph} - [ PL_n^{sch,ph} - \sum_l P_{u,l}^{cur,ph} ] ) \quad (2-52)$$

$$+ \lambda_n^{Qc} ( QL_n^{*,ph} - [ QL_n^{sch,ph} - \sum_{l=1}^4 Q_{u,l}^{cur,ph} ] ) \quad (2-53)$$

$$+\lambda_s^{Pl} \left( \begin{array}{l} P_s^{loss} - \sum_{ph \in \{a,b,c\}} \sum_{n=1}^N \sum_{\substack{m=1 \\ m \neq n}}^N (V_n^{x,ph} I_{nm}^{x,ph} + V_n^{y,ph} I_{nm}^{y,ph}) \\ + \sum_{n=1}^N (V_n^{x,N} J_{nn}^x + V_n^{y,N} J_{nn}^y) \end{array} \right) \quad (2-54)$$

$$+\lambda_s^{Ql} \left( \begin{array}{l} Q_s^{loss} - \sum_{ph \in \{a,b,c\}} \sum_{n=1}^N \sum_{\substack{m=1 \\ m \neq n}}^N (V_n^{y,ph} I_{nm}^{x,ph} - V_n^{x,ph} I_{nm}^{y,ph}) \\ + \sum_{n=1}^N (V_n^{y,N} J_{nn}^x - V_n^{x,N} J_{nn}^y) \end{array} \right) \quad (2-55)$$

$$+\rho_n^{P,ph} \left( \begin{array}{l} PG_n^{ph} - PL_n^{*,ph} - \\ \left[ V_n^{x,ph} (I_{nn}^{x,ph} - I_n^{x,ph}) + V_n^{y,ph} (I_{nn}^{y,ph} - I_n^{y,ph}) \right] \end{array} \right) \quad (2-56)$$

$$+\lambda_n^{Qr,ph} \left( \begin{array}{l} QG_n^{ph} - QL_n^{*,ph} \\ - \left[ V_n^{y,ph} (I_{nn}^{x,ph} - I_n^{x,ph}) - V_n^{x,ph} (I_{nn}^{y,ph} - I_n^{y,ph}) \right] \end{array} \right) \quad (2-57)$$

$$+\lambda_n^x (I_{nn}^{x,ph} + \sum_{m=1}^N I_{mn}^{x,ph}) , n \neq m \quad (2-58)$$

$$+\lambda_n^y (I_{nn}^{y,ph} + \sum_{m=1}^N I_{mn}^{y,ph}) , n \neq m \quad (2-59)$$

$$+\lambda_n^{Ix,ph} (I_n^{x,ph} - V_n^{x,ph} G_{nn}^{ph} - V_n^{y,ph} B_{nn}^{ph}) \quad (2-60)$$

$$+\lambda_n^{Iy,ph} (I_n^{y,ph} - V_n^{x,ph} B_{nn}^{ph} + V_n^{y,ph} G_{nn}^{ph}) \quad (2-61)$$

$$+\lambda_{mn}^{Vx,ph} (V_m^{x,ph} - V_n^{x,ph} + R_{nm}^{ph} I_{nm}^{x,ph} - X_{nm}^{ph} I_{nm}^{y,ph}) , m \neq n \quad (2-62)$$

$$+\lambda_{mn}^{Vy,ph} (V_m^{y,ph} - V_n^{y,ph} + R_{nm}^{ph} I_{nm}^{y,ph} + X_{nm}^{ph} I_{nm}^{x,ph}) , m \neq n \quad (2-63)$$

$$+\lambda_{mn}^{Vx,Nu} (V_n^{N,x} - V_m^{N,x} + R_{mn}^N J_{mn}^x - X_{mn}^N J_{mn}^y) , n \neq m, n \neq slack \quad (2-64)$$

$$+\lambda_{mn}^{Vy,Nu} (V_n^{N,y} - V_m^{N,y} + R_{mn}^N J_{mn}^y + X_{mn}^N J_{mn}^x) , n \neq m, n \neq slack \quad (2-65)$$

$$+\lambda_n^{Jx} (J_{nn}^x + \sum_{m=1}^N J_{mn}^x) , n \neq m \quad (2-66)$$

$$+\lambda_n^{Jy} (J_{mn}^y + \sum_{m=1}^N J_{mn}^y) , n \neq m \quad (2-67)$$

$$+\lambda_n^{V,\min} (V^{\min} - \sqrt{(V_n^{abc,x})^2 + (V_n^{abc,y})^2}) \quad (2-68)$$

$$+\lambda_n^{V,\max} (\sqrt{(V_n^{abc,x})^2 + (V_n^{abc,y})^2} - V^{\max}) \quad (2-69)$$

$$+\lambda_{mn}^{I\max} (\sqrt{(I_{mn}^{abc,x})^2 + (I_{mn}^{abc,y})^2} - I^{\max}) \quad (2-70)$$

$$+\begin{bmatrix} \lambda_n^{Jx} & \lambda_n^{Jy} \end{bmatrix} \begin{pmatrix} \begin{bmatrix} J_{mn}^x \\ J_{mn}^y \end{bmatrix} - \sum_{\substack{m=1 \\ m \neq n}}^N A(\varphi^a) \begin{bmatrix} I_{mn}^{x,a} \\ I_{mn}^{y,a} \end{bmatrix} \\ +A(\varphi^b) \begin{bmatrix} I_{mn}^{x,b} \\ I_{mn}^{y,b} \end{bmatrix} + A(\varphi^c) \begin{bmatrix} I_{mn}^{x,c} \\ I_{mn}^{y,c} \end{bmatrix} \end{pmatrix} \quad (2-71)$$

## 2.6. Proposed real-time CM framework

### 2.6.1. The proposed real-time market framework

In this research, a holistic framework is proposed to facilitate cooperation between different entities in a distributed manner. This framework supports the real-time system operation at the regular and CM situation (see Section 2.2.1). Figure 2-9 illustrates the proposed real-time market framework. In this framework, each owner has a contract with an aggregator, and the aggregators compete under the MGOs' supervision. There are six significant steps in the proposed framework as follows:

**Step1:** In this step, all aggregators solve their optimization problem independently considering the nodal price ( $\rho^{MG}$ ) which is announced by MGOs, and send their offers to corresponding MGOs.

**Step2:** MGOs use the data correction system, which is represented in Figure 2-10, and they estimate a more realistic value for the received data. Then, they use (2-48) to (2-71) to find their

needed power from the grid ( $P^{MG}$ ) and send it to the DSO. The DSO need these data to calculate the ULF and check the steady-state constraints of the system.

**Step3:** The DSO uses (2-19) to (2-43) to solve the ULF. Once the DSO checked the line's capacity, if there is any congestion in the system, the process moves to step 4. Otherwise, the process should proceed with step 6.

**Step 4:** If the DSO identifies any congestion in the system, this step should be taken into account. In this step, DSO uses (2-72) to limit the received power by the MGs ( $P^{MG,ord}$ ) in the congestion zone. The outcome of this part would be the maximum power that each MG can take from the grid according to the CM results.

**Step 5:** A group of MGOs that are called to reduce their demand from the grid should take this step. The main idea is to initiate a DLMP revisiting process (see Section 2.7) to increase the participation of AGGs and reduce the reliance on the upper grid. Each MGO checks its demanded power from the grid with the maximum power that is designated by DSO. There are three possible cases as follows:

1) If the scheduled power is more than the determined value ( $P^{MG,ord} - P^{MG} < 0$ ), then increase the price.

2) If the power is less than the maximum and the difference is acceptable ( $0 \leq P^{MG,ord} - P^{MG} \leq \varepsilon$ ), return to step 3.

3) If the reduced power is higher than a threshold ( $P^{MG,ord} - P^{MG} > \varepsilon$ ), reduce the DLMPs to motivate effective load curtailments. During this process, the MGOs send a signal to the AGGs and motivate them to improve their contribution according to the CM program. It can relieve the congested sections of the system and, in parallel, prevent unnecessary load curtailments.

**Step6:** The DSO implements the final obtained schedule in this step.

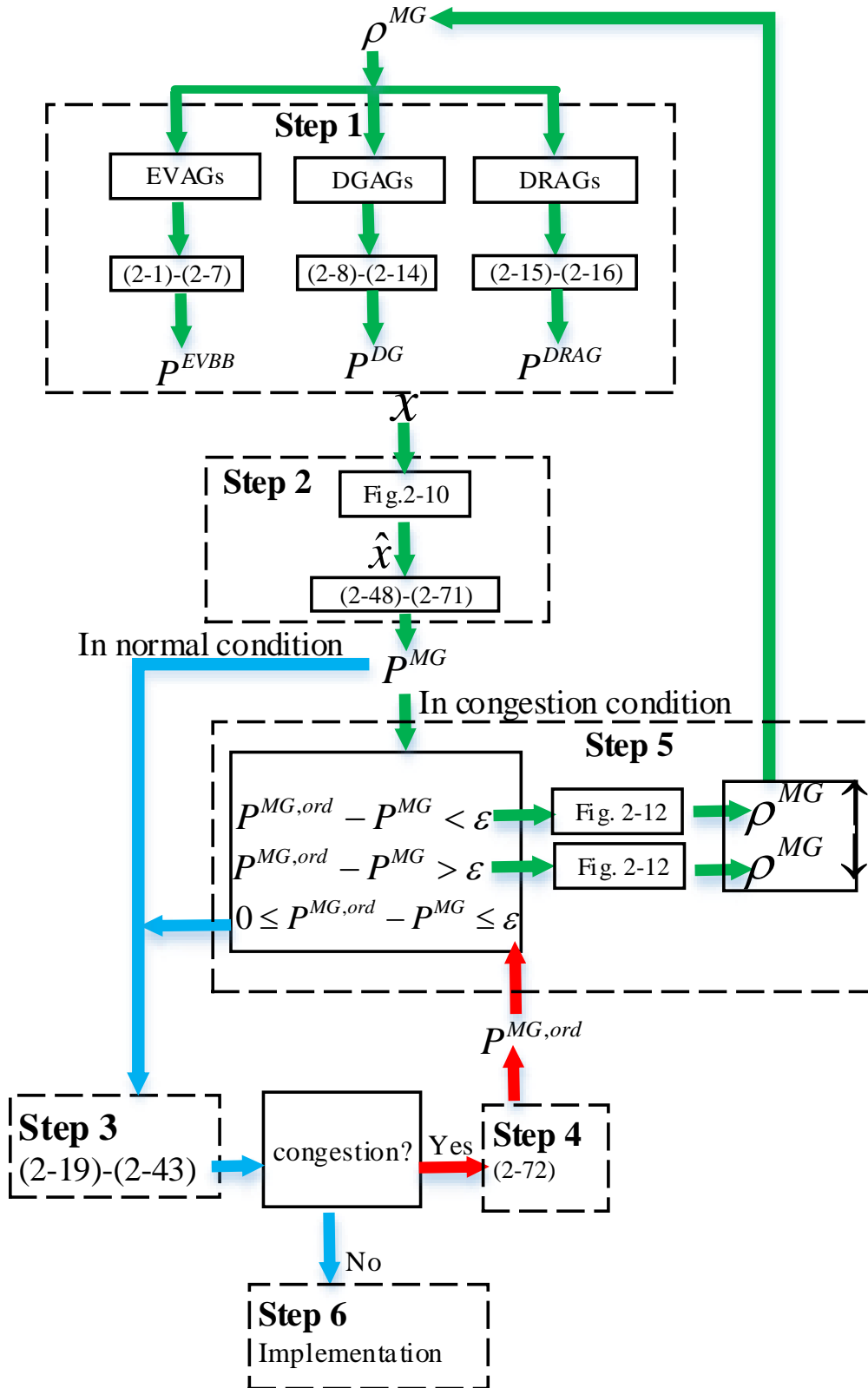


Figure 2-9: The proposed real-time market operation framework

### 2.6.2. The DSO decision making

The DSO should develop a rescheduling plan if there is any congestion after step 3 of the framework. In [18], we proposed an algorithm to identify the entities under the congested branches using the connectivity matrix. Using that algorithm, the DSO provides a list of the MGs that should reduce their demand to suppress the upstream network congestion. The share of the demand reduction for each MG is calculated by DSO, according to (2-72), where  $\Delta P_s$  is the share of  $s$ th MG which initially demands for  $P_s$  kW power from the grid. Also,  $\Delta P_{cong}$  is the total power that should be reduced by all MGs.

$$\Delta P_s = \frac{P_s}{\sum_{s \in D} P_s} \Delta P_{cong} \quad (2-72)$$

### 2.6.3. Real-time data estimating (RDE) system

The MGOs need an RDE system in their operation. The reason is that the MGOs should decide about how to schedule their network according to the numerous data that they receive from the AGGs. The fluctuating nature of the load and renewable DERs makes the situation unpredictable. Therefore, in case the submitted data by the AGGs is not accurate, or some necessary information is missed, such an estimator can be instrumental.

We use a KF scheme for the RDE. Each MGO uses this system to modify the received data from the AGGs before loading them in the calculations. Figure 2-10 illustrates the employed RDE model. In this figure,  $x$ ,  $x^m$  and  $\hat{x}^m$  represent the received data from AGGs, the actual data after the execution, and the modified data after error estimation, respectively. Also,  $e$  and  $\hat{e}$ , respectively, signify the actual error and estimated error in the received data from the AGGs.

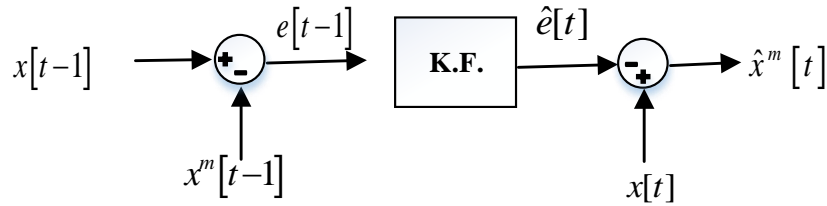


Figure 2-10: The error estimation modeling system

The basic KF block is shown in Figure 2-11. This technique is used to estimate the statistic serial data with a normal distribution. Therefore, the input value to the KF block should be a variable with a normal distribution function. In this research, the MGOs should deal with two sorts of data in the real-time operation process: power and price. Since the power and price information are not statistical variables, we cannot send them directly to a KF block. As a result, the prediction error is used as the input variable to the KF block in figure 2-10. If there is no intentional false data in the system, the prediction error should be a random variable that follows the normal distribution with zero means. This is a proper signal for estimation using a KF method.

The main steps in the KF algorithm are formulated in (2-73) to (2-77) [40]. The first step is to predict the next sample using the current sample, which is formulated in (2-73). In this equation,  $\alpha$  is a constant gain that can be adjusted (we consider  $\alpha=1$  in this study). In the next step, the minimum  $MSE^1$  of the signal is determined using (2-74), and then the Kalman gain can be calculated as (2-75). The third step is to estimate the signal using Kalman gain in (2-76). The last step of this algorithm is to update the minimum  $MSE$  for the next round of calculations. The output of the KF block in figure 2-10 ( $\hat{e}$ ) is the output of (2-73). Therefore, we only need the first step of the KF algorithm to predict the error, and all other steps should be taken to keep the

---

<sup>1</sup> Minimum square error (MSE)

parameters up to date for the next round of calculations.

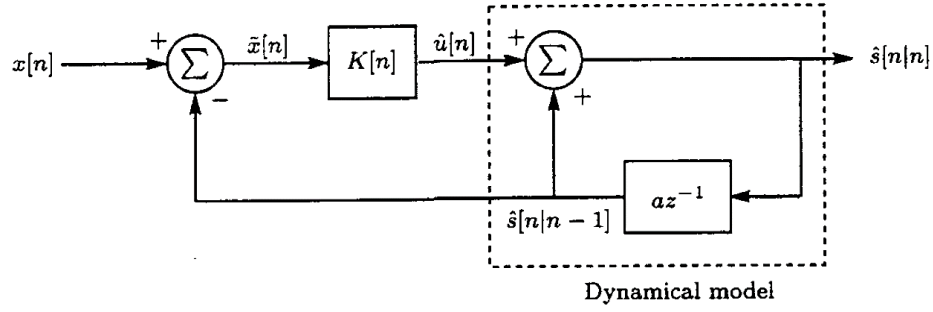


Figure 2-11: A discrete Kalman filtering block [40]

$$\hat{x}[n|n-1] = \alpha \hat{x}[n-1|n-1] \quad (2-73)$$

$$M[n|n-1] = \beta = \alpha^2 M[n-1|n-1] + \sigma^2 \quad (2-74)$$

$$K[n] = \frac{M[n|n-1]}{\sigma^2 + M[n|n-1]} \quad (2-75)$$

$$\hat{x}[n|n] = \hat{x}[n|n-1] + K[n](x[n] - \hat{x}[n|n-1]) \quad (2-76)$$

$$M[n|n] = (1 - K[n])M[n|n-1] \quad (2-77)$$

## 2.7. DLMP revisiting mechanism

The DLMP in this framework is considered to cover the entire electricity costs and, at the same time, to create enough motivation for the aggregators to participate in the CM process.

Figure 2-12 shows the elements of DLMP in the process of money transfer in the market for CM.

The DSO's and MGOs' rates are not considered in this part. As is shown, the initial electricity price is the wholesale market rate ( $\rho^{WM}$ ), and the rest of the elements are added to reflect the power loss cost and congestion cost in the system.

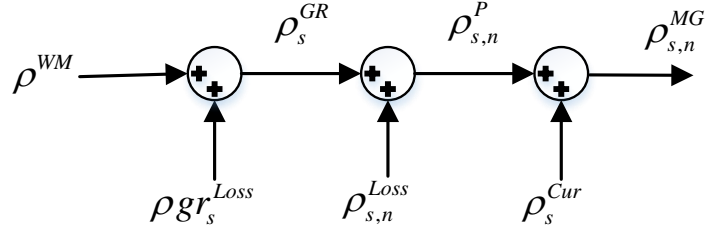


Figure 2-12: Electricity rate calculation process

The values  $\rho_{gr_s}^{Loss}$  and  $\rho_{s,n}^{Loss}$  represent the price associated with power loss in the SO's network and MGO's system, respectively. Also,  $\rho_{gr_s}^{Cur}$  is the equivalent curtailment rate and is calculated as (2-78).

$$\rho_s^{Cur} = \frac{\sum_{k \in K\{s\}} P_k^{DRAG} \rho_k^{DRAG}}{P_s^{GR}} \quad (2-78)$$

Figure 2-13 illustrates the input and output cash flow related to each MG. The revenues and costs are defined using (2-79) to (2-83). In this framework, all the received money by the microgrid financial center (MGFC) is equal to output money, and there is no residual currency within the process. Furthermore,  $R^{EV}$  and  $R^L$  are the cash amounts collected by the MGO remove from the corresponding EVs and other loads, respectively. Also,  $C^{GR}$ ,  $C^{DG}$  and  $C^{DR}$  are the cash amounts that MGO should pay to the SO, DGs, and curtailed load agents, respectively.



Figure 2-13: Cash flow process

$$R^{EV} = \sum_n \sum_{ph} PEV_n^{ph} \rho_{s,n}^{MG} \quad (2-79)$$

$$R^L = \sum_n \sum_{ph} \left( PL_n^{sch,ph} - \sum_l P_{u,l}^{cur,ph} \right) \rho_{s,n}^{MG} \quad (2-80)$$

$$C^{GR} = P_s^{GR} \rho_s^{GR} \quad (2-81)$$

$$C^{DG} = \sum_n \sum_{ph} PDG_n^{ph} \rho_{s,n}^{MG} \quad (2-82)$$

$$C^{DR} = \sum_{k \in K\{s\}} P_k^{DRAG} \rho_k^{DRAG} \quad (2-83)$$

## 2.8. Distributed ULF calculation process

As was mentioned, MGO acts as a local DSO. Therefore, the ULF for any part of the system should be calculated by the DSO or one of the MGOs. In this research, we define the MGs according to the voltage level. After the main substation and before the distribution transformers, all the equipment should be managed by the DSO directly. After each distribution transformer, all the equipment/networks are considered an MG, which is managed by the corresponding MGO. Figure 2-14 shows a typical distribution system with a substation, two industrial loads, and four distribution transformers. The blue network is the high voltage (12.4 kV), and the operation and management of this part are on DSO. The black parts are the low voltage networks (0.2 kV), where the MGOs are responsible for these parts of the system.

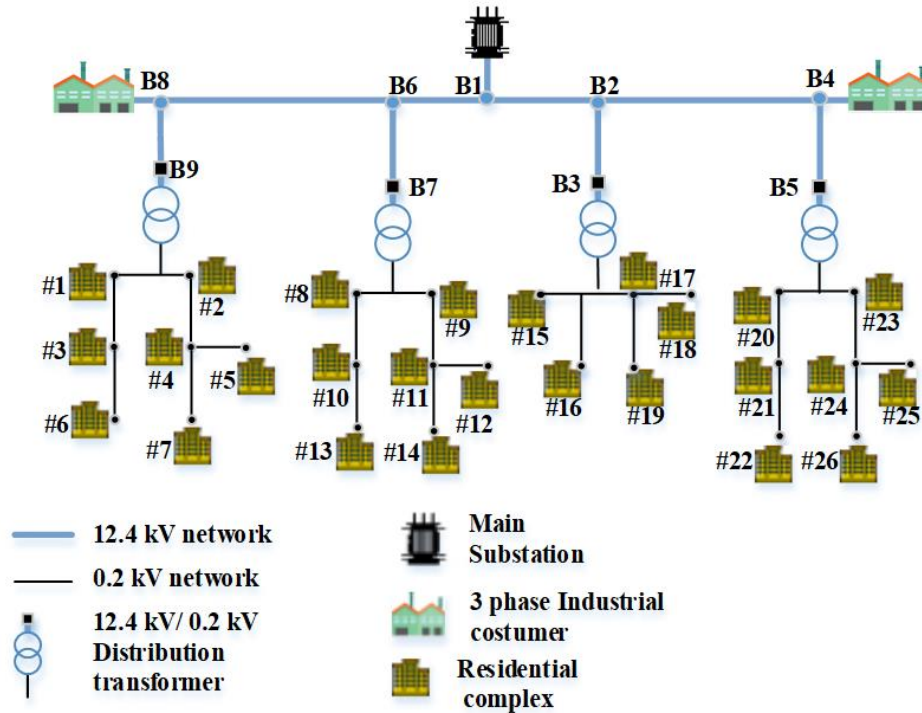


Figure 2-14: A typical distribution system

Figure 2-15 illustrates how to divide the system in Figure 2-14 into several low-voltage independent MGs and a high-voltage system. As shown, there are four low-voltage systems and a high voltage system after decomposing. To find the voltage and current regarding all parts of the system, the ULF should be calculated for all systems in Figure 2-15 independently and parallel. The voltage at the main substation is known, and we can consider this bus as the slack bus. But the voltages at the beginning of the MGs are unknown. Therefore, we need a backward-forward mechanism to calculate the ULF. The idea is to track the voltages at the MGOs interconnection buses (two sides of distribution transformers). The high-voltage values are determined during the DSO's ULF calculation, while the low-voltage values are used in the MGOs' ULF calculation. We should repeat the calculation process until the per-unit of the voltage at both sides of the distribution transformers are almost equal. The process is as follows:

**Step1:** First, the voltage at all MGs' slack bus is considered one per-unit with the angle of zero radians, and the ULF is calculated for all MGs.

**Step2:** In this step, each MGs' input power is determined using the slack bus voltages and calculated currents from *step 2*. These powers are considered as the MGs' aggregated loads in the DSO's network.

**Step3:** The ULF is calculated for the DSO's network, and the value of the voltage is determined for each MG's connection bus. These voltages are the new values for the MGs' slack buses.

**Step4:** In this step, if there is no noticeable difference between the new values of the MGs' slack voltages (from *step 3*) and the values that have been used in *step 1*, the ULF is accomplished. Otherwise, we return to *step 1* using the new values of the MGs' slack voltages.

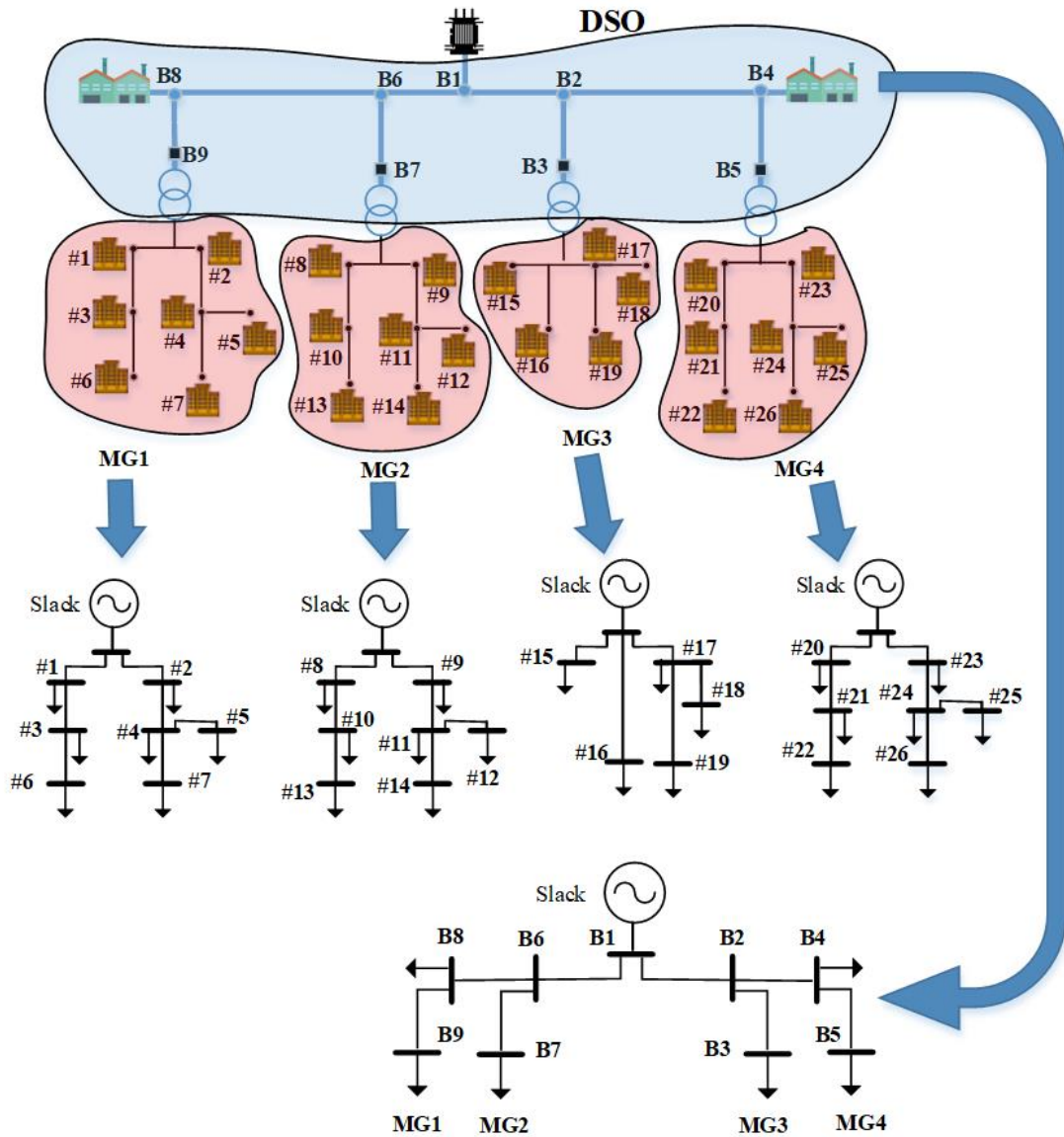


Figure 2-15: Dividing a distribution system into several low-voltage parts and a high-voltage

## CHAPTER 3

### GAMS-MATLAB CONFIGURATIONS

#### 3.1. Software tools

This research uses the MATLAB software linked with the General Algebraic Modeling Language (GAMS) to study the proposed framework against two IEEE test systems. MATLAB's flexibility, combined with the GAMS's strength in handling complicated optimization problems, makes a powerful platform that can optimize large-scale cases in an acceptable time. Figure 3-1 illustrates the deployed configuration of the GAMS-MATLAB interaction. As is shown, the GAMS optimization models are used as MATLAB's built-in functions. This platform provides the ability to call GAMS scripts from MATLAB multiple times during an optimization process.

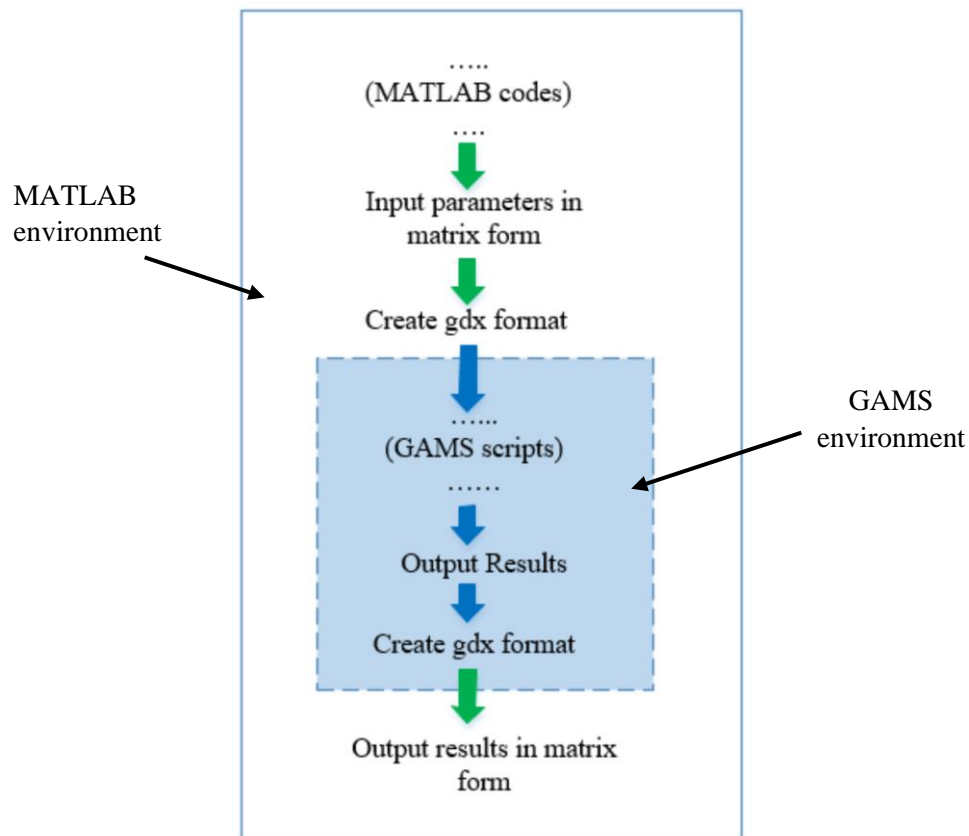


Figure 3-1: The interaction between MATLAB and GAMS

### **3.2. Steps to solve an optimization problem using GAMS-MATLAB**

There are four significant steps to create the platform in figure 3-1 as follows:

1. First, the GAMS installation path should be defined in the MATLAB path library
2. In the second step, the input variables that the GAMS needs for optimization should be defined in the MATLAB. The variables should be in the “\*.gdx” format, which can be supported by GAMS.
3. The third step is to execute the GAMS scripts from the MATLAB side. This step can be done using the “gams” command.
4. The last step is to extract the GAMS’s outputs and bring them into the MATLAB in the matrix or array format.

#### **3.2.1. Define GAMS in MATLAB’s path library**

As the first step in connecting GAMS and MATLAB, we should define the GAMS installation directory as one of MATLAB’s saved paths. Figure 3-2 demonstrates the way to complete this step. As is shown, we should click on the “set path” option in MATLAB home and add the GAMS directory using the “Add” button. Without this step, the related GAMS commands do not work in MATLAB.

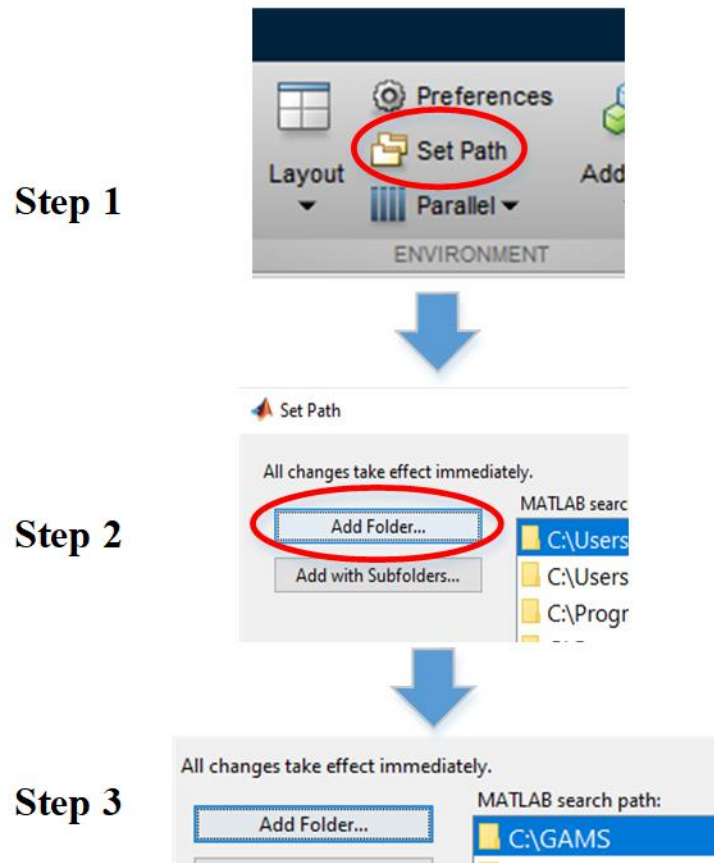


Figure 3-2: Adding GAMS directory to the MATLAB paths list

### 3.2.2. Generate input parameters in “gdx” format

To have a flexible model, we should provide GAMS optimization models in a general form, which means all the parameters and sets should be defined as GAMS inputs. It helps us use a single GAMS model for several cases by preparing the necessary inputs from the MATLAB side and calling the GAMS model.

#### 3.2.2.1. Generated gdx files in MATLAB

The template to define the sets and tables in gdx format is different. We use the following command to define the sets in gdx format. These commands should be run on the MATLAB side.

*[the set name in MATLAB].name='[the used set name in gams]'*

```
[the set name in MATLAB].uels={'[value 1]','[value 2]',...};  
wgdx(['the.gdx file name'], [the set name in MATLAB]);
```

As an example, the following MATLAB commands show how to define the time set for a GAMS model. The set's name in GAMS optimization is "t," and we assign the values {1,2} to it. After running these commands, the MATLAB generates a.gdx file named "t\_file.gdx."

```
t_set.name='t';  
t_set.uels={'1','2'};  
wgdx('t_file ', t_set)
```

The matrix form data (e. g., tables) should be inserted as input parameters into the GAMS. Below is a general MATLAB command to define an array in.gdx format.

```
iwgdx(['the.gdx file name'], '[MATLAB Array1]', '[MATLAB Array2]',...)
```

Using this format, we can store multiple arrays with different dimensions in a single.gdx file.

For example, the R and X matrixes are saved into a.gdx file named "Impedance" as follows.

```
R= [ 0  0.015; 0.015  0];  
X= [ 0  0.1; 0.1  0];  
iwgdx('Impedance','R','X')
```

### 3.2.2.2. Read.gdx files from GAMS

After generating the inputs for a GAMS model, we need specific commands to load the parameters and sets into the GAMS model. The following format should be added to a GAMS optimization model to read the generated.gdx files.

Loading a.gdx file related to sets:

```
$GDXIN [gdx file with full drectory]  
$LOAD [set name]  
$GDXIN
```

Example for GAMS commands:

```
$GDXIN C:\User\Desktop\ t_file.gdx  
$LOAD t  
$GDXIN
```

Reading.gdx file associated with arrays:

```
$GDXIN [gdx file with full drectory]
```

```
$LOADIDX [arrays' names]
```

```
$GDXIN
```

Example for GAMS commands:

```
$GDXIN C:\User\Desktop\Impedance.gdx  
$LOADIDX R X  
$GDXIN
```

### 3.2.3. Saving the output GAMS results in.gdx format

We need to send back the GAMS outputs to the MATLAB for the next calculations. Since the.gdx format is the standard form of communication, additional commands are needed in the GAMS model to provide a.gdx file for the outputs. By adding the following command to the GAMS model, we can save the preferred results in.gdx format.

```
execute_UnloadIdx '[gdx file name with full directory]' [GAMS result to be saved]
```

Below is an example of GAMS commands to save the magnitude of voltage after an unbalanced load flow calculation. The.gdx output file is named “MagV.gdx”. Vd and Vq are the GAMS optimization variables for real and imaginary parts of the voltage.

```
Parameter V(n) ;  
V(n)=sqrt(V_d.l(n)*V_d.l(n)+ V_q.l(n)*V_q.l(n));  
execute_UnloadIdx 'C:\User\Desktop\ MagV' V
```

### 3.2.4. Executing a GAMS model from MATLAB

After providing all the necessary commands for communication, the GAMS model should be run from MATLAB side. We use the “gams” command as a MATLAB script to runt the GAMS model as follows:

```
gams('[gams file name]')
```

Here is an example of running a GAMS file named “loadflow.gms” from MATLAB:

```
gams('loadflow');
```

### 3.2.5. Extracting results form generated gdx files

The instruction in section 3.2.3 provides this ability to have the results of a GAMS optimization in gdx format. If we need to load the GAMS results to MATLAB, the following commands should be used.

```
irgdx '[generated gdx file by GAMS]'
```

Here is an example:

```
irgdx 'MagV.gdx';
```

### 3.3. An example of unbalanced load flow with GAMS-MATLAB programming

A two-bus unbalanced test system is shown in figure 3-3. There are a slack bus and a load bus in this system. All the values regarding the impedances and loads are in per-unit.

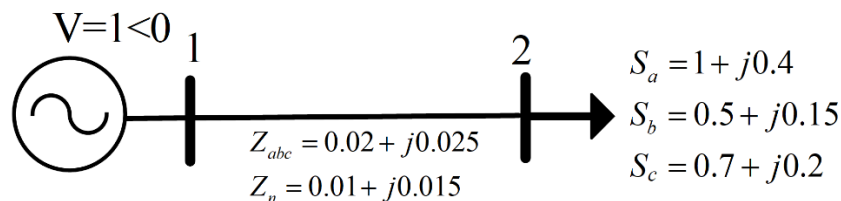


Figure 3-3: A two-bus unbalanced test system

The main intention is to solve the ULF for this system with GAMS-MATLAB programming. The input parameters should first be defined in MATLAB scripts as follows. As is shown,  $n$  and  $ph$  are the needed sets to show the buses and phases, respectively. All other parameters, such as impedances and loads, are stored in a gdx file named “InputData”. The rest of the commands are used to run the case and extract the magnitude of the voltages from the GAMS outputs.

```

6 - n.name='n';
7 - n.uels={'1','2'};
8 - ph.name='ph';
9 - ph.uels={'1','2','3','4'};
10 - R= [ 0 0.02;0.02 0];
11 - Rn=[ 0 0.01; 0.01 0];
12 - X= [ 0 0.025;0.025 0];
13 - Xn=[ 0 0.015;0.015 0];
14 % a b c n
15 - SP=[ 0 0 0 0
16 1 0.5 0.7 0 ];
17 % a b c n
18 - SQ=[ 0 0 0 0
19 0.4 0.15 0.2 0 ];
20
21 % All arrays
22 - iwgdxd('InputData','R','Rn','X','Xn','SP','SQ')
23 % sets
24 - wgdxd('n',n)
25 - wgdxd('ph',ph)
26 - gams('loadflow')
27 - irgdxd 'V.gdx'
28 - v

```

The following commands show the model in the GAMS side, where the input gdx files are read from a known directory. Then the ULF commands are defined as the GAMS equations. The current ULF model is a nonlinear problem; therefore, one of the nonlinear GAMS solvers should be chosen to solve it.

GAMS commands for defining sets, parameters, and variables:

```

SETS
n bus numbers
ph phase sequence
;
$GDXIN C:\Users\Desktop\n
$LOAD n
$GDXIN
;
$GDXIN C:\Users\Desktop\ph
$LOAD ph
$GDXIN
;
alias (n,m)
;
parameters
R(n,m)
Rn(n,m)
X(n,m)
Xn(n,m)
SP(n,PH)
SQ(n,PH)
;
$GDXIN C:\Users\Desktop\InputD
$LOADIDX R Rn X Xn SP SQ
$GDXIN
;
variables
V_x(ph,n)
V_y(ph,n)
I_x(ph,n,m)
I_y(ph,n,m)
In_x(ph,n)
In_y(ph,n)
J_x(n,m)
J_y(n,m)
Ploss
Qloss
;

```

### GAMS commands for modeling ULF equation:

```

eq1(ph).. V_x(ph,'1')=e=1.05$(ord(ph) ne 4)+0$(ord(ph)=4);
eq01(ph).. V_y(ph,'1')=e=0;
Ploss1.. Ploss=e= sum((n,m,ph)$((ord(ph) ne 4)and(ord(n) ne ord(m))),V_x(ph,n)*I_x(ph,n,m)+V_y(ph,n)*I_y(ph,n,m)
+sum(n,V_x('4',n)*J_x(n,n)+V_y('4',n)*J_y(n,n));
Qloss1.. Qloss=e= sum((n,m,ph)$((ord(ph) ne 4)and(ord(n) ne ord(m))),V_y(ph,n)*I_x(ph,n,m)-V_x(ph,n)*I_y(ph,n,m)
+sum(n,V_y('4',n)*J_x(n,n)-V_x('4',n)*J_y(n,n));
eq2(n,ph)$((ord(ph) ne 4)and(ord(n)>1)).. -SP(n,ph)-(V_x(ph,n)*I_x(ph,n,n)+V_y(ph,n)*I_y(ph,n,n))=e=0;
eq3(n,ph)$((ord(ph) ne 4)and(ord(n)>1)).. -SQ(n,ph)-(V_y(ph,n)*I_x(ph,n,n)-V_x(ph,n)*I_y(ph,n,n))=e=0;
eq4(ph,n).. I_x(ph,n,n)=e=-sum(m$(ord(n) ne ord(m)),I_x(ph,m,n));
eq5(ph,n).. I_y(ph,n,n)=e=-sum(m$(ord(n) ne ord(m)),I_y(ph,m,n));
eq6(ph,n,m).. V_x(ph,m)=e=V_x(ph,n)-(R(n,m)*I_x(ph,n,m)-X(n,m)*I_y(ph,n,m));
eq7(ph,n,m).. V_y(ph,m)=e=V_y(ph,n)-(R(n,m)*I_y(ph,n,m)+X(n,m)*I_x(ph,n,m));
eq8(n,m).. V_x('4',n)=e=V_x('4',m)-(Rn(m,n)*J_x(m,n)-Xn(m,n)*J_y(m,n));
eq9(n,m).. V_y('4',n)=e=V_y('4',m)-(Rn(m,n)*J_y(m,n)+Xn(m,n)*J_x(m,n));
eq10(n).. sum(m,J_x(n,m))=e=0;
eq11(n).. sum(m,J_y(n,m))=e=0;
eq12(n).. -J_x(n,n)=e=sum(m$(ord(m) ne ord(n)),I_x('1',m,n)-I_x('2',m,n)*0.5+0.866*I_y('2',m,n)-0.5*I_x('3',m,n)-0.866*I_y('3',m,n) );
eq13(n).. -J_y(n,n)=e=sum(m$(ord(m) ne ord(n)),I_y('1',m,n)-I_x('2',m,n)*0.866-0.5*I_y('2',m,n)+0.866*I_x('3',m,n)-0.5*I_y('3',m,n) );

```

### GAMS commands to solve the model and create.gdx file for voltage magnitude:

```

model ULF /all/
option optca=1e-10,optcr=1e-10,nlp=CONOPT;
solve ULF minimizing Ploss using nlp
;
parameter V(ph,n)
;
V(ph,n)=sqrt(V_x.l(ph,n)*V_x.l(ph,n)+ V_y.l(ph,n)*V_y.l(ph,n));
execute_unloadIdx 'C:\Users\Desktop\V' V

```

After running the MATLAB script, the results for the voltage's magnitude would be as follows where the first column is the voltage magnitude for bus#1, and the second column is the voltage magnitude at bus#2. Due to the unbalanced load, the voltage magnitude at bus#2 is not similar for three phases. Also, the magnitude of the voltage for the neutral system at the second bus is not zero, which means there is a backward current in the neutral wires.

V =

1.0000	0.9689
1.0000	0.9860
1.0000	0.9805
0	0.0085

## CHAPTER 4

### CASE STUDIES AND INPUT DATA

#### 4.1. Input data

Since there are renewable energy resources in the system, the data associated with wind velocity and solar radiation for the next 24 hours are needed. The utilized data for the numerical study are related to a similar neighborhood to have more realistic results. Thus, all the data regarding wind speed, solar radiation, and load profile is associated with the *Southern Illinois* neighborhood. Figure 4-1 shows solar radiation, wind velocity, and ambient temperature on May-1<sup>st</sup>-2019 [44] for the *Southern Illinois* neighborhood. The data are available for every 15 minutes interval, which is proper for the real-time operation study. As is shown, the wind speed is higher at the initial hours and drops during the day. Also, the solar radiation in the middle of the day (around noon) has a noticeable value compared to the other hours.

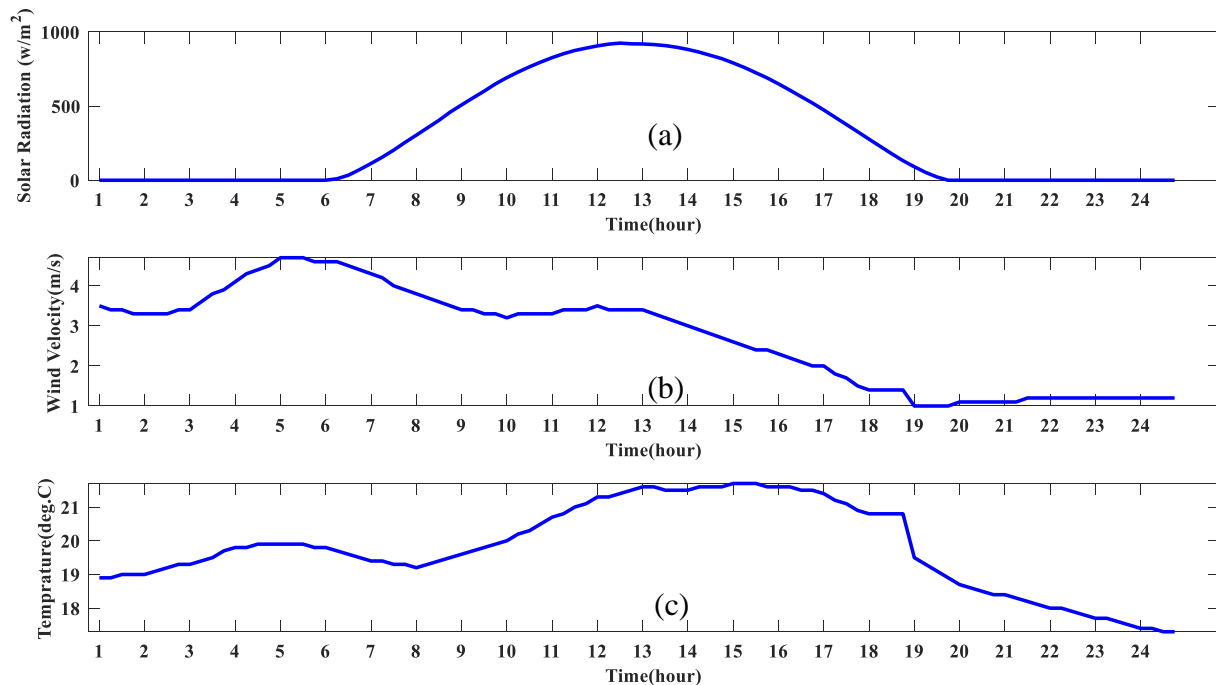


Figure 4-1: (a)-Daily solar radiation, (b)-wind velocity, (c)-ambient temperature [44]

Since the IEEE test systems only have the spot load value (i.e., the peak value), we need to use a load pattern to create a proper load profile for the whole 24 hours. Figure 4-2 illustrates the extracted load pattern from [45]. The pattern is created by the load profile associated with *Ameren Illinois Rate Zone III (AmerenIP)*, *RESDDL-IP*. By multiplying this profile with the IEEE test systems' spot load, we can obtain a load profile for the next 24 hours.

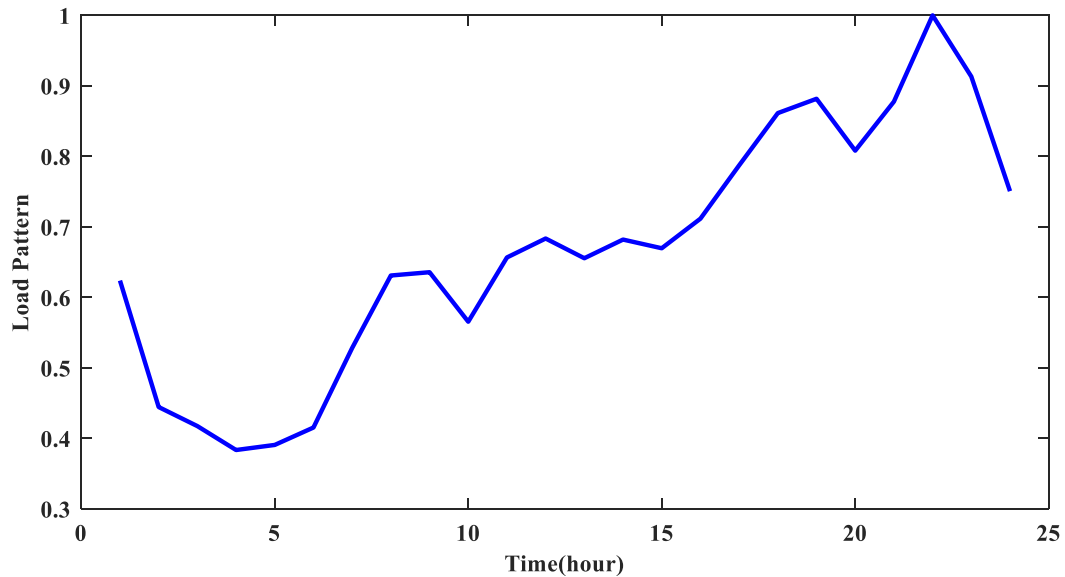


Figure 4-2: Hourly load pattern

Another input data that is needed for the simulation is the electricity price on the wholesale side. Figure 4-3 shows the hourly wholesale electricity price [46]. According to the power markets' structure, these rates are determined by competition in the wholesale markets among large generation companies as sellers and utilities plus large customers as buyers. In this research, we assume that the electricity price at the beginning of the distribution system (after the substation) is equal to the wholesale price. The current data is hourly prices; therefore, we assume a similar wholesale price for every 15 minutes of an hour real-time operation. As is explained in section 2.7, this price is the major part of DLMPs.

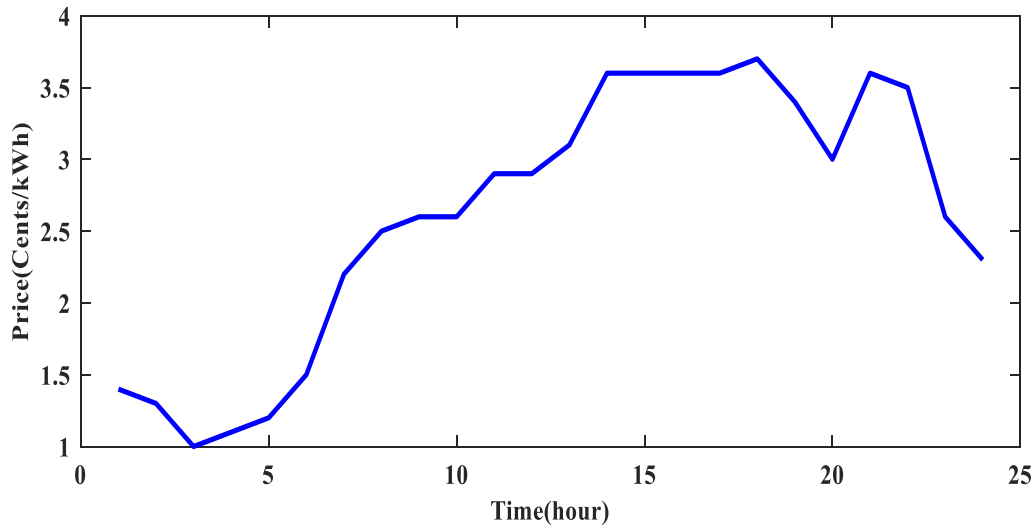


Figure 4-3: The wholesale electricity price [46]

## 4.2. DER, EV, and DR designations

In a modern distribution system, there are several DERs, EVs, and DRs. Therefore, to transform the conventional IEEE test systems into a modern system, we need to upgrade the test systems by integrating some active entities. Below is the specification of the functional elements that are used to upgrade the IEEE test systems. These elements are chosen from the real market to have more realistic results.

### 4.2.1.1. Wind turbines:

Three types of wind turbines are used in the test systems. The main characteristics of the turbines are as follows:

**Type 1:** manufactured by *Fortis* [47], rated power of 6 kW, and diameter of 5.3 m

Manufacturer	Type	Rated power	Diameter	Swept area	Power density 1	Power density 2
 Fortis	Montana-Q 6 kW	6,00 kW	5,3 m	21,6 m <sup>2</sup>	277,8 kW/m <sup>2</sup>	3,6 m <sup>2</sup> /kW

**Type 2:** manufactured by *Aeolos* [48], rated power of 10 kW, and diameter of 5.5 m

Manufacturer	Type	Rated power	Diameter	Swept area	Power density 1	Power density 2
 Aeolos	Aeolos-V 10kW	10,00 kW	5,5 m	23,8 m <sup>2</sup>	420,2 kW/m <sup>2</sup>	2,4 m <sup>2</sup> /kW

**Type 3:** Manufactured by *Britwind* [49], rated power of 15 kW, and diameter of 10.4 m.

Manufacturer	Type	Rated power	Diameter	Swept area	Power density 1	Power density 2
 Britwind	H15 Class II	15,00 kW	10,4 m	85,0 m <sup>2</sup>	176,5 kW/m <sup>2</sup>	5,7 m <sup>2</sup> /kW

#### 4.2.1.2. PV modules:

Three types of PV arrays are used in this study. The final capacity of a PVDG is related to the PV module's type and the allocation area. Here are the main specifications of the used PV arrays:

**Type 1:** manufactured by *Kyocera* manufacturer [50] with the rated power of 135W and the efficiency of 12.9%.

**Type 2:** Manufactured by *Solaria* manufacturer [51] with the rated power of 360 and the efficiency of 20%.

**Type 3:** Manufactured by *Sunpower* manufacturer [52] with the rated power of 400 and the efficiency of 22.3%.

#### 4.2.1.3. Inverters:

Since the PV systems produce electricity at DC voltage, we need inverters to convert it to AC and connect a PV system to the grid. Also, the WT systems cannot produce electricity by a constant frequency and voltage amplitude. As a result, a rectifier besides an inverter is needed to connect a WT to the grid. The inverters associated with the PV modules and WTs are selected from the *Xantrex* manufacturer [53]. The inverters' rated power and efficiency are chosen according to the aggregated DER capacity. For example, the range 1500 w has an efficiency of 92% [53].

#### 4.2.1.4. EV models:

Table 4-1 shows the data associated with three different EV types that are modeled in this research. According to table 4-1, the first EV type can be charged up to 16 kWh by a maximum of 4.5 kW/hour charging/discharging ramp. The owners of this type are willing to plug their EVs into the grid from 1 AM to 7 AM. The aggregators should schedule how to fully charge the vehicles during this interval, knowing that the initial charge is %25 for this group of EVs. The second and third EV types have the maximum capacity of 10 kWh and 25 kWh with a ramp of 4 kW/h and 2.75 kW/h, respectively. Their desired charging time is from 10 AM to 2 PM and 3 PM to 8 PM, respectively. The initial charge is considered %30 and %35 for EV type 1 and EV type 2.

Table 4-1: Types of Modeled EVs \*

Types	$E^{max}$	$E^{min}$	$P_{EVBB}^{ch}$	$P_{EVBB}^{disch}$	$t_{st}$	$t_{end}$	$SOC_0$
1	16	4	4.5	4.5	1	7	%25
2	10	3.6	4	4	10	14	%30
3	25	6.6	2.75	2.5	15	20	%35

\* All the nomenclatures are defined in section 2.3.1

#### 4.2.1.5. Demand Response contracts:

The demand response programs are an essential part of a modern distribution system analysis. According to the DR contracts, the customers agree to reduce their demand at a specific time for an agreed price. The DR loads can be curtailable (the operator can curtail a part of the load) or shiftable (the operator can shift a part of the load). An example of a curtailable load is the air conditioner systems where the customer set the AC temperature to a higher value during the summer to reduce electricity consumption. The dishwasher is an instance of a shiftable load where it can be shifted during the day but cannot be excluded totally. Table 4-2 shows the three

types of available curtailable DR contracts in the system. The first type of agreement allows the DRAGs to reduce 10% of customers' hourly loads from 1 AM to 11 AM. Simultaneously, the daily curtailed energy should not exceed 5% of the overall daily consumption. According to this contract, the customer receives 0.5 cents per kWh for this service. The same explanation can be expressed for the other mentioned DR contracts in table 4-2. Table 4-3 represents the available shiftable DR contracts. The first type of arrangement allows the DRAGs to reduce 10% of the scheduled load from 10 AM to 12 PM (two hours). Instead, that part of the load should be supplied sometime from 1 PM to 10 PM. This service's rate is 0.1 cents per kWh of the shifted load. The other types of contracts have the same explanation.

Table 4-2: Demand Response contracts

	Curtail time	Curtail amount per hour	Total daily curtailment	Price (cents/kwh)
Type 1	1 AM to 11 AM	10%	5%	0.5
Type 2	2 PM to 10 PM	15%	8%	0.7
Type 3	6 AM to 12 PM	20%	5%	0.8

Table 4-3: Shiftable DR contracts

	Initial Scheduled	substitute time	duration	reduction	Price (cents/kwh)
Type 1	10 AM to 12 PM	1 PM to 10 PM	2 hours	10%	0.1
Type 2	1 PM to 4 PM	4 PM to 12 PM	3 hours	15%	0.3
Type 3	6 AM to 9 AM	1 PM to 8 PM	3 hours	20%	0.5

### 4.3. IEEE case studies

#### 4.3.1. Modified IEEE 13-bus unbalanced test system

The IEEE 13-bus unbalanced test system is the first case study that is used for numerical studies in this research. The raw data associated with the original test system is represented in

[43]. Figure 4-4 illustrates the modified single diagram with all assets. As can be inferred, four MGs are defined in the system. MG#3 is shown in detail to realize the wiring in this unbalanced test system. All the loads in this model are considered as constant power factor for simplification. Table 4-4 shows the system's load per phase and bus at peak time. The real-time load profile for the IEEE-13 bus test system can be generated using this table and the load pattern in figure 4-2.

Table 4-4: Spot load Data associated with IEEE 13-bus test system [43]

Bus	phase a		phase b		phase c	
	kW	kVar	kW	kVar	kW	kVar
634	160	110	120	90	120	90
645	0	0	170	125	0	0
646	0	0	230	132	0	0
652	128	86	0	0	0	0
671	385	220	385	220	385	220
675	485	190	68	60	290	212
692	0	0	0	0	170	151
611	0	0	0	0	170	80
Total	1158	606	973	627	1135	753
<b>All three phases: 3266 kW + 1986 kVar</b>						

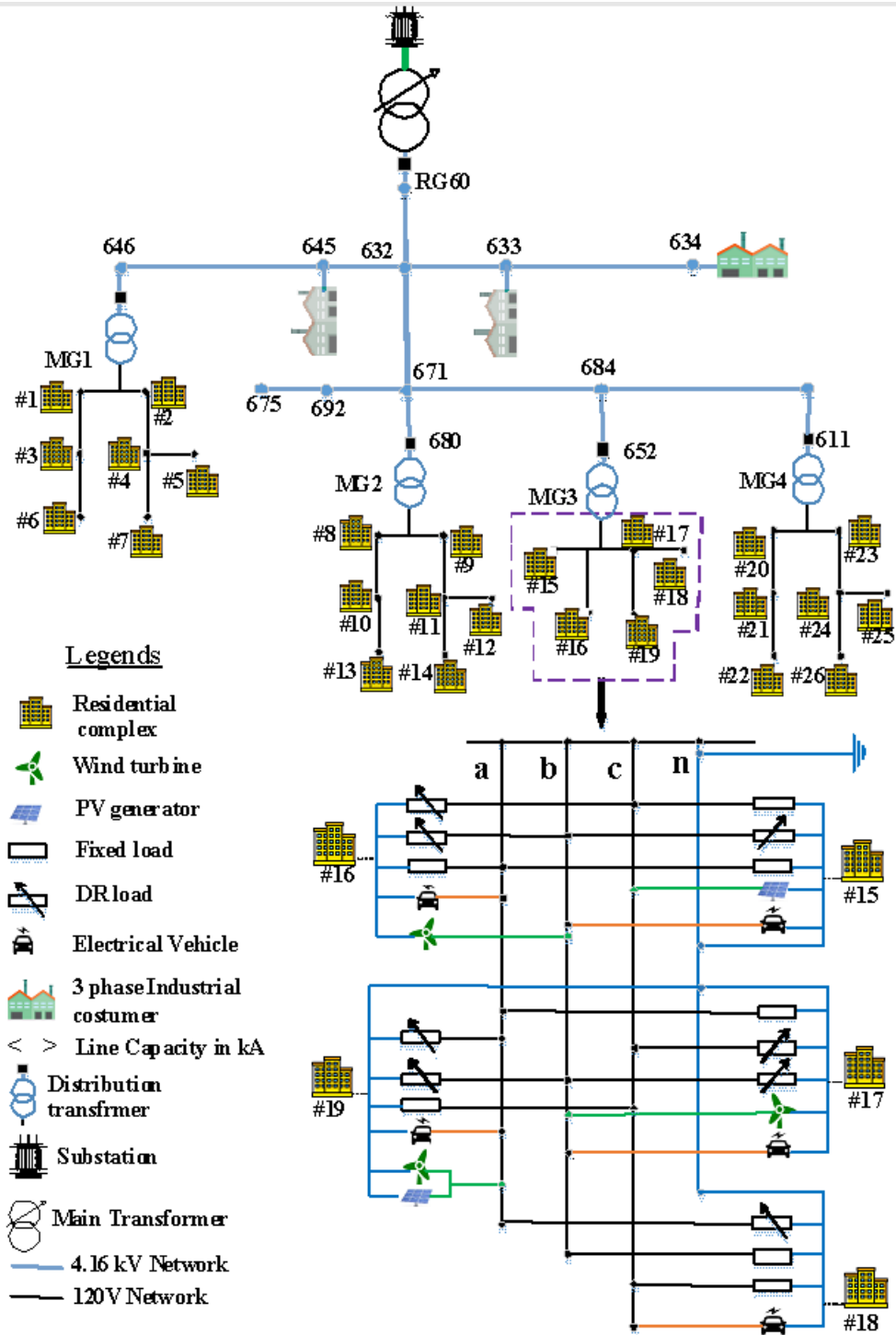


Figure 4-4: Modified IEEE 13-bus test system

To increase this system's flexibility as a modern distribution system, 1072 EVs, 307 PVs, and 276 WT's are added to the MGs. Moreover, 629 residential customers out of 2691 are considered

with a DR contract with one of the system’s DRAGs. Table 4-5 represents the details regarding the MGs components.

Table 4-5: MGs components in the modified case

		<b>MG #1</b>	<b>MG #2</b>	<b>MG #3</b>	<b>MG #4</b>	<b>Total</b>
<b>EVs</b>	No.	301	285	206	280	1072
	kWh-Battery	1507	1546	1013	1425	5491
<b>PVs</b>	No.	43	75	72	117	307
	kW	995.7	1678.5	1413	1995	6082
	kWh-Battery	1991	3357	2527	4081	11956
<b>WTs</b>	No.	101	76	48	51	276
	kW	2323	1679	942	855	5799
	kWh-Battery	4647	3357	1684	1749	11437
<b>Customers with DR contract</b>	No.	107	196	195	131	629
	kWh	642	980	781	917	3319
<b>Total customers</b>	No.	580	835	715	562	2691
	kWh	3478	4173	2861	3932	14444

#### 4.3.2. Modified IEEE 123-bus unbalanced test system

Figure 4-5 illustrates the single diagram for IEEE 123-bus unbalanced test system [43].

According to the initial raw data, this system’s peak load is 1425 kW for phase A, 931 kW for phase B, and 1169 kW for phase C. The details regarding the spot load for this system are presented in table 4-6. All the loads are modeled as the constant power factor model with a Y connection for simplification. As is shown in Figure 4-5, 30 MGs are added to this system to form a modern distribution system. These MGs have 8712 PV systems, 9113 EVs, 2936 WTs, and 13703 DR contracts. The detailed data regarding the MGs’ components are available in table 4-7.

Moreover, we define a DGAG, an EVAG, and a DRAG for each of the MGs. The customers within an MG’s territory only can have a contract with the local AGGs. As a result, the collaboration among the AGGs in different MGs is not considered in this study.

Table 4-6: Spot load data associated with IEEE 123-bus test system [43]

Bus	phase a		phase b		phase c	
	kW	kVar	kW	kVar	kW	kVar
1	40	20	0	0	0	0
2	0	0	20	10	0	0
4	0	0	0	0	40	20
5	0	0	0	0	20	10
6	0	0	0	0	40	20
7	20	10	0	0	0	0
9	40	20	0	0	0	0
10	20	10	0	0	0	0
11	40	20	0	0	0	0
12	0	0	20	10	0	0
16	0	0	0	0	40	20
17	0	0	0	0	20	10
19	40	20	0	0	0	0
20	40	20	0	0	0	0
22	0	0	40	20	0	0
24	0	0	0	0	40	20
28	40	20	0	0	0	0
29	40	20	0	0	0	0
30	0	0	0	0	40	20
31	0	0	0	0	20	10
32	0	0	0	0	20	10
33	40	20	0	0	0	0
34	0	0	0	0	40	20
35	40	20	0	0	0	0
37	40	20	0	0	0	0
38	0	0	20	10	0	0
39	0	0	20	10	0	0
41	0	0	0	0	20	10
42	20	10	0	0	0	0
43	0	0	40	20	0	0
45	20	10	0	0	0	0
46	20	10	0	0	0	0
47	35	25	35	25	35	25
48	70	50	70	50	70	50
49	35	25	70	50	35	20
50	0	0	0	0	40	20
51	20	10	0	0	0	0
52	40	20	0	0	0	0

Bus	phase a		phase b		phase c	
	kW	kVar	kW	kVar	kW	kVar
53	40	20	0	0	0	0
55	20	10	0	0	0	0
56	0	0	20	10	0	0
58	0	0	20	10	0	0
59	0	0	20	10	0	0
60	20	10	0	0	0	0
62	0	0	0	0	40	20
63	40	20	0	0	0	0
64	0	0	75	35	0	0
65	35	25	35	25	70	50
66	0	0	0	0	75	35
68	20	10	0	0	0	0
69	40	20	0	0	0	0
70	20	10	0	0	0	0
71	40	20	0	0	0	0
73	0	0	0	0	40	20
74	0	0	0	0	40	20
75	0	0	0	0	40	20
76	105	80	70	50	70	50
77	0	0	40	20	0	0
79	40	20	0	0	0	0
80	0	0	40	20	0	0
82	40	20	0	0	0	0
83	0	0	0	0	20	10
84	0	0	0	0	20	10
85	0	0	0	0	40	20
86	0	0	20	10	0	0
87	0	0	40	20	0	0
88	40	20	0	0	0	0
90	0	0	40	20	0	0
92	0	0	0	0	40	20
94	40	20	0	0	0	0
95	0	0	20	10	0	0
96	0	0	20	10	0	0
98	40	20	0	0	0	0
99	0	0	40	20	0	0
100	0	0	0	0	40	20
102	0	0	0	0	20	10
103	0	0	0	0	40	20

Bus	phase a		phase b		phase c	
	kW	kVar	kW	kVar	kW	kVar
104	0	0	0	0	40	20
106	0	0	40	20	0	0
107	0	0	40	20	0	0
109	40	20	0	0	0	0
111	20	10	0	0	0	0
112	20	10	0	0	0	0
113	40	20	0	0	0	0
114	20	10	0	0	0	0
Total	20	10	0	0	0	0

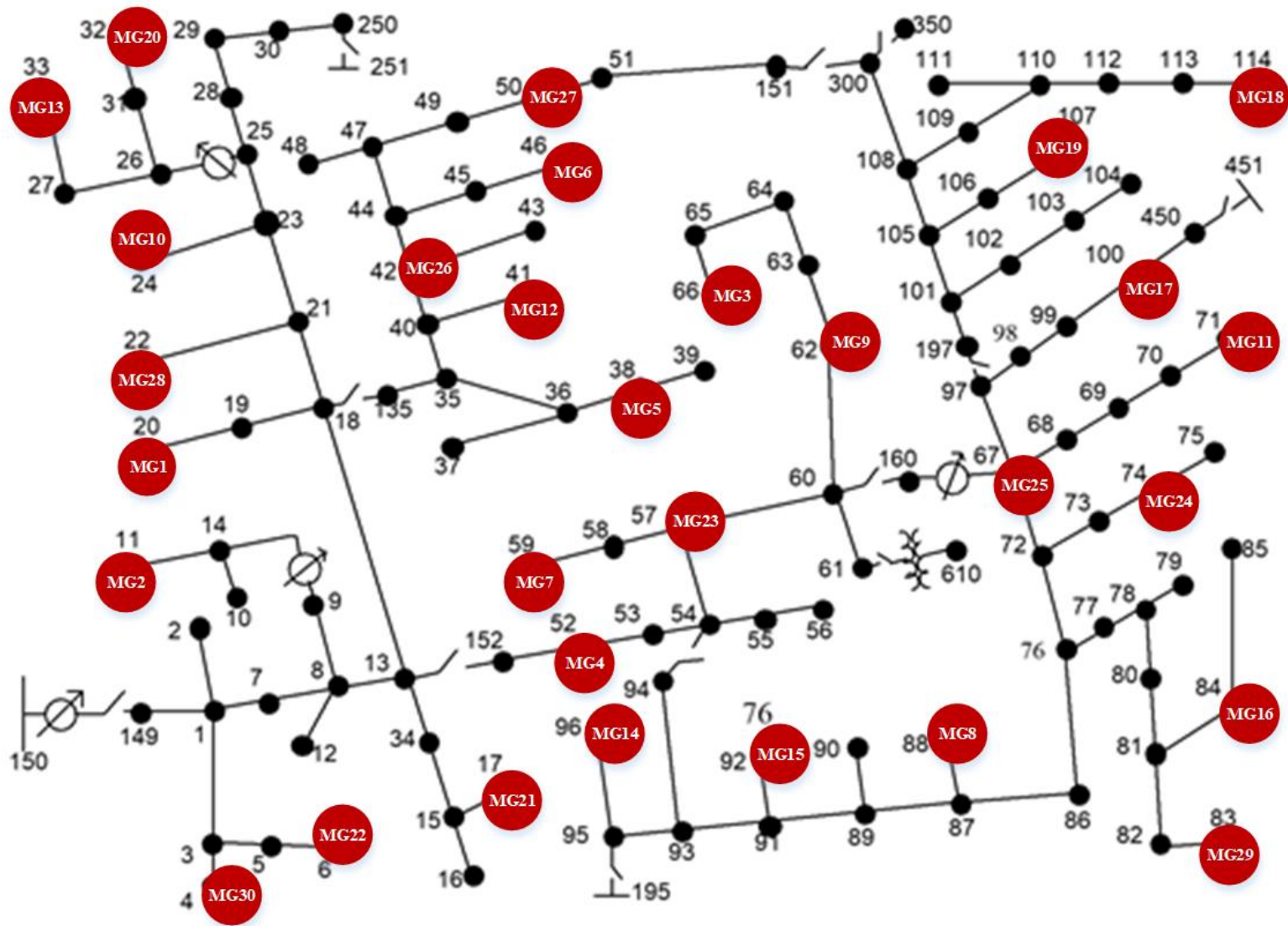


Figure 4-5: The single diagram for the IEEE 123-bus test system

Table 4-7: MGs' components in the modified 123-bus test system

	Bus	No. PV			No. EV			No. WT			No. DR contract		
		Type1	Type2	Type3	Type1	Type2	Type3	Type1	Type2	Type3	Type1	Type2	Type3
MG #1	20	76	77	92	145	122	76	27	13	59	132	153	185
MG #2	11	109	65	96	71	102	54	25	49	53	165	133	151
MG #3	66	52	78	127	121	149	125	13	27	14	196	155	164
MG #4	52	93	94	82	74	72	74	25	40	28	194	140	195
MG #5	38	81	103	128	62	61	94	12	47	28	146	142	144
MG #6	46	66	96	97	111	61	119	35	15	44	124	118	106
MG #7	59	68	138	54	95	56	86	48	16	40	176	126	187
MG #8	88	92	102	68	96	90	124	42	37	49	176	102	163
MG #9	62	59	144	122	116	95	89	14	34	28	174	192	136
MG #10	24	110	114	97	127	87	118	14	55	20	174	165	200
MG #11	71	97	146	65	85	126	120	49	50	14	111	193	122
MG #12	41	120	74	84	116	113	94	55	47	49	168	116	165
MG #13	33	120	118	111	92	127	52	37	13	20	146	192	160
MG #14	96	114	79	69	134	143	83	15	14	29	121	179	139
MG #15	92	53	117	124	133	147	92	51	14	38	110	158	114
MG #16	84	57	120	74	76	69	77	27	50	21	182	144	103
MG #17	100	82	57	142	111	64	70	25	57	42	118	126	142
MG #18	118	103	75	77	108	120	132	47	44	34	116	175	118
MG #19	107	115	72	127	104	59	93	11	17	18	167	123	173
MG #20	32	91	117	69	137	103	139	12	46	49	189	106	137
MG #21	17	132	134	79	76	103	89	43	16	15	152	177	184
MG #22	6	122	84	59	82	136	127	40	16	25	170	167	173
MG #23	23	147	128	108	62	98	90	36	42	22	115	172	157
MG #24	74	103	118	118	144	89	131	46	26	37	195	164	118
MG #25	67	83	51	105	115	117	126	45	43	15	154	142	196
MG #26	42	61	110	93	98	124	88	49	47	30	168	139	127
MG #27	50	111	89	114	114	102	72	24	39	15	104	182	192

	Bus	No. PV			No. EV			No. WT			No. DR contract		
		Type1	Type2	Type3	Type1	Type2	Type3	Type1	Type2	Type3	Type1	Type2	Type3
MG #28	22	128	142	115	104	85	129	45	47	16	181	132	122
MG #29	83	92	50	118	115	65	145	38	22	49	175	181	137
MG #30	4	59	96	114	104	109	83	30	47	25	112	179	109

## CHAPTER 5

### NUMERICAL RESULTS

#### **5.1. Introduction**

In this chapter, the described GAMS-MATLAB combination is used as the optimization tool to apply the proposed framework on the two IEEE unbalanced test systems in a real-time operation. The specifications of the case studies were expressed in Chapter 4. We analyze the test systems in two scenarios under certain and uncertain data situations. In the first scenario, it is assumed that all the submitted bids/offers by the aggregators and MGOs occur without any variations. It means if a DGAG sends a bid to generate 100 kW in the next 15 minutes, it generates precisely 100 kW. In the uncertain scenario, we consider an error vector with zero mean and variance of 10% in all the aggregators' submitted data. The intent is to take into account the natural errors in predicting, reading, and transferring the data or some common failures during the real-time operation. Intentional sabotage, such as hacking and false data injection, are not considered in this study. Therefore, the error vector is white noise and does not have a specific direction or trend. A fixed-rate of 0.1 cents/kWh is defined as a penalty for any mismatches in the delivered power by MGs comparing to their scheduled demand. It makes an incentive to the MGOs to mitigate any uncertainty in their system.

#### **5.2. Case study #1: IEEE 13-bus**

The analysis is performed by MATLAB 2019a academic version, and the academic version of General Algebraic Modeling System (GAMS), License Number of G180502:1210AO-WIN with the nonlinear solver of CONOPT, and mixed-integer solver of BARON [54]. The main specification of the utilized computer for this study is as follows:

## System

Processor: Intel(R) Core(TM) i7-7700 CPU @ 3.60GHz 3.60 GHz  
Installed memory (RAM): 16.0 GB (15.9 GB usable)  
System type: 64-bit Operating System, x64-based processor

Figure 5-1 shows the GAMS solvers configuration for NLP<sup>1</sup> and MINLP<sup>2</sup> optimizations. As is evident, BARON and CONOPT are the solvers that have been selected for MINLP and NLP problems, respectively.

Solver	License	CNS	DNLP	EMP	LP	MCP	MINLP	MIP	MIQCP	MPEC	NLP	QCP	RMINLP	RMIP	RMIQCI
ALPHAECP	Demo						*		*						
AMPL	Full	-	-	-	-	-	-	-	-	-	-	-	-	-	-
ANTIGONE	Demo	*	*				*		*		*	*	*		*
BARON	Full	*	*	*			X	*	*		*	*	*	*	*
BDMLP	Full			*				*						*	
BENCH	Full	-	-	-	-	-	-	-	-	-	-	-	-	-	-
BONMIN	Full						*		*						
BONMINH	Demo						*		*						
CBC	Full			*				*						*	
CONOPT	Full	*	*	*							X	*	*	*	*
CONOPT4	Full	*	*	*							*	*	*	*	*
CONVERT	Full	-	-	-	-	-	-	-	-	-	-	-	-	-	-
COUENNE	Full	*	*				*		*		*	*	*		*
CPLEX	Full			*				*	*		*		*	*	*

Figure 5-1: GAMS solvers configuration

### 5.2.1. Real-time simulation without considering uncertainty

In this scenario, the proposed real-time operation framework is utilized without considering uncertainty in the data. The operation schedule is determined every 15 minutes, according to the

<sup>1</sup> Non linear programming (NLP)

<sup>2</sup> Mixed integer non linear programming (MINLP)

framework presented in Section 2.6.1. To have a better perspective, we present nine operation points out of 96 (every 15 minutes for 24 hours) associated with the time zone from  $t=8$  am to  $t=10$  am. The timing schedule for every operation step is considered as follows:

- 1- All aggregators send their data to the MGOs at least 20 minutes before the operation time.
- 2- The MGOs submit their demand to the DSO at least 15 minutes before the operation time.
- 3- The DSO calculates the power flow and calls the operators under the congested areas to reduce their demand. This process is performed 10 minutes before the operation time.
- 4- The MGOs negotiate with the aggregators, finalize their demand, and send their new demand to the DSO at least five minutes before the operation time.
- 5- The DSO manages the system according to the final schedule.

After analyzing the modified IEEE 13-bus test system, two congestions are experienced in the system from 8 am to 10 am as follows:

**I) Congestion in the branch B1-B6:**

As can be inferred from figure 5-2 (a), this branch is congested at  $t=8:45$ . According to DSO's calculation, this branch needs 150 kW, 115 kW, and 98 kW of power reduction in phases  $a$ ,  $b$ , and  $c$ , respectively, to be relived. As a result, DSO calls MG#1 and MG#2 to maintain the total 363 kW load reduction according to the values mentioned above. As is displayed in Figure 5-3, MG#1 and MG#2 are located down the congested branch; therefore, only these MGs can change the loading of branch B1-B6. That is the reason the DSO only calls MG#1 and MG#2 for this congestion alleviation. DSO calculates the share of the demand reduction for each MG according to (2-72). Using (2-72), MG#1 should reduce its demand by 70 kW, 150 kW, and 45 kW from phases  $a$ ,  $b$ , and  $c$ , respectively. The load reduction share for MG#2 is 80 kW, 65 kW, and 53 kW for phases  $a$ ,  $b$  and  $c$ , respectively.

## II) Congestion in branch B1-B2:

This branch is congested at  $t=9:30$  am (see Figure 5-2 (b)). By taking a look at the system in Figure 5-3, it can be perceived that the DSO should ask the operators of MG#3 and MG#4 to reduce their load since only these MGs are located down the congested branch. According to the DSO's calculation, by 140 kW reduction from MG#3 and 246 kW reduction from MG#4 (the total of 386 kW), the congestion will be eliminated.

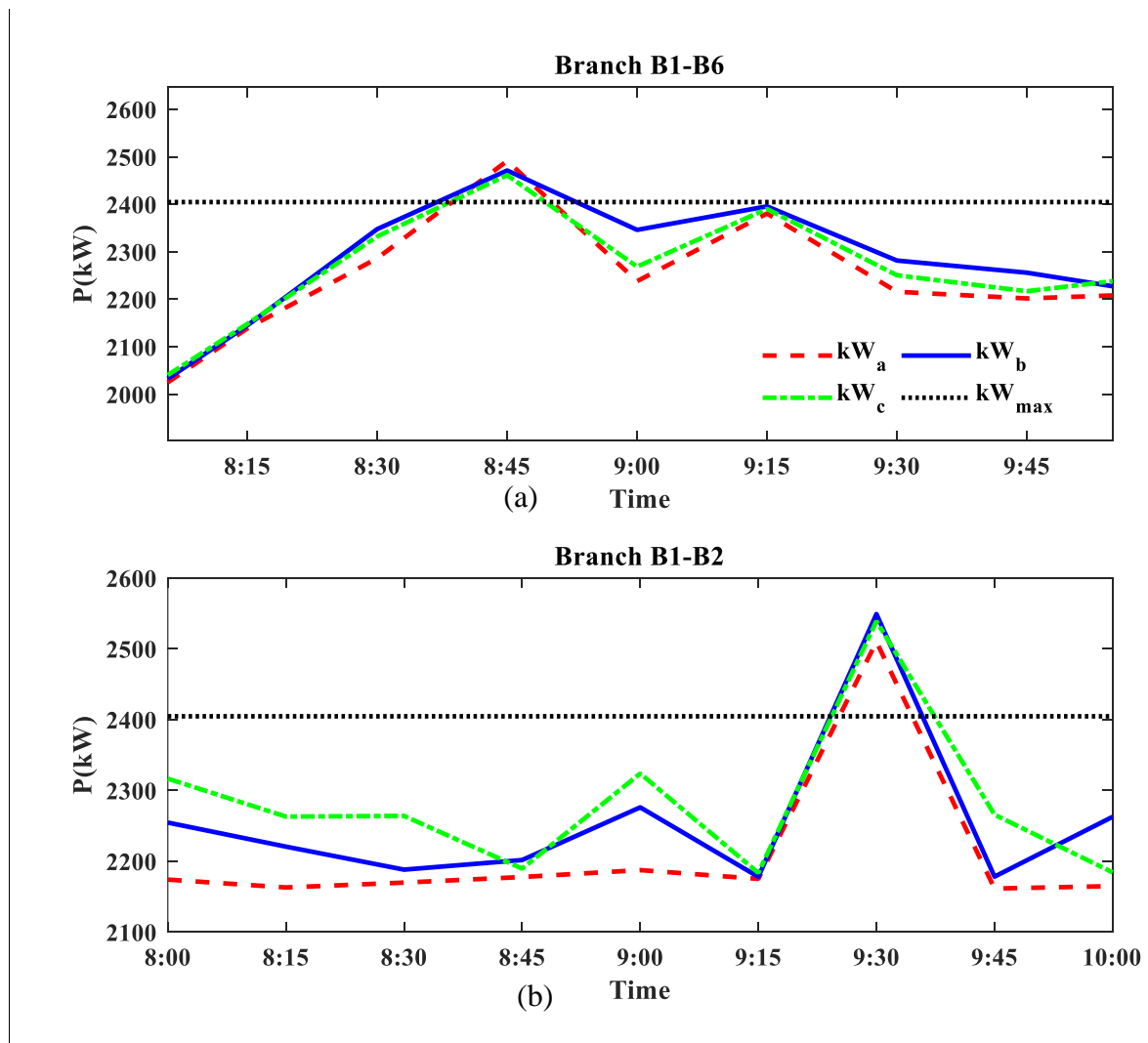


Figure 5-2: (a)- The loading of branch B1-B6, (b)- the loading of branch B1-B2

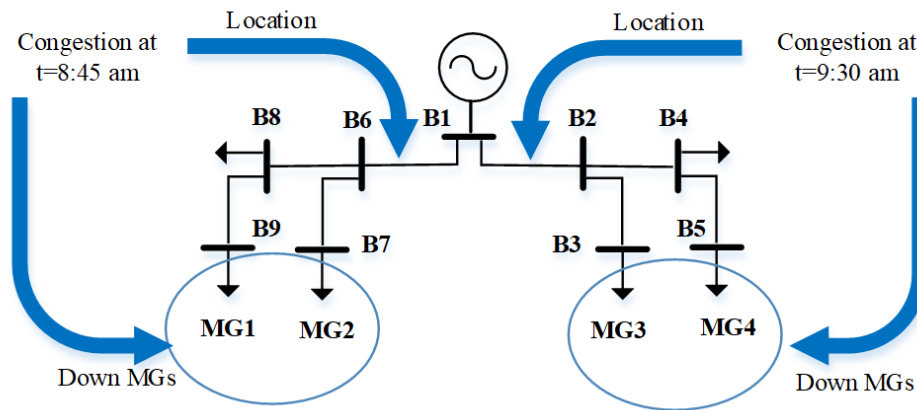


Figure 5-3: The congested branches and down MGs

After identifying the congestion and the engaged MGs in the congestion management process, the MGOs use the proposed DLMP revisiting method in Section 2.7 and decrease their overall demand from the grid based on the DSO’s order. According to this method, the priority is to encourage the DGAGs to increase their production at the congestion times and supply more local loads. The second priority is to ask the EVAGs to choose other times for charging their clients instead of the congestion times. As the last priority, the MGOs use the available DR contracts with the DRAGs to address the DSO’s order. Table 5-1 shows the simulation results for this scenario. As is established, the MGOs could address the DSO’s orders for power reduction.

Table 5-1: The MGOs response to the DSO’s demand reduction orders

MGs	congestion time	ordered power reduction				accrued power reduction			
		phase a	phase b	phase c	total	phase a	phase b	phase c	total
MG#1	8:45	70	50	45	165	74	50	50	174
MG#2	8:45	80	65	53	198	84	71	55	210
MG#3	9:30	35	65	50	150	41	55	57	153
MG#4	9:30	71	80	85	236	75	83	91	249

Figure 5-4 depicts the MGs’ power purchased from the grid during the simulation. The MG#1 and MG#2 have changed their schedule at t=8:45 because of the congestion at branch B1-B6. MG#3 and MG#4 have also experienced a noticeable reduction at t=9:30 due to the congestion at

branch B1-B6. The necessary activities for congestion management change the schedule for future times as well. It is because the aggregators solve their optimization problem for a full 24 hours. As a result, any change at the closest operation time may change the future times accordingly. As an example, if an EVAG in MG#1 reduces its demand at 8:45, that aggregator should increase the demand at another time to compensate for the reduction. It changes the load and production profiles for the next hours.

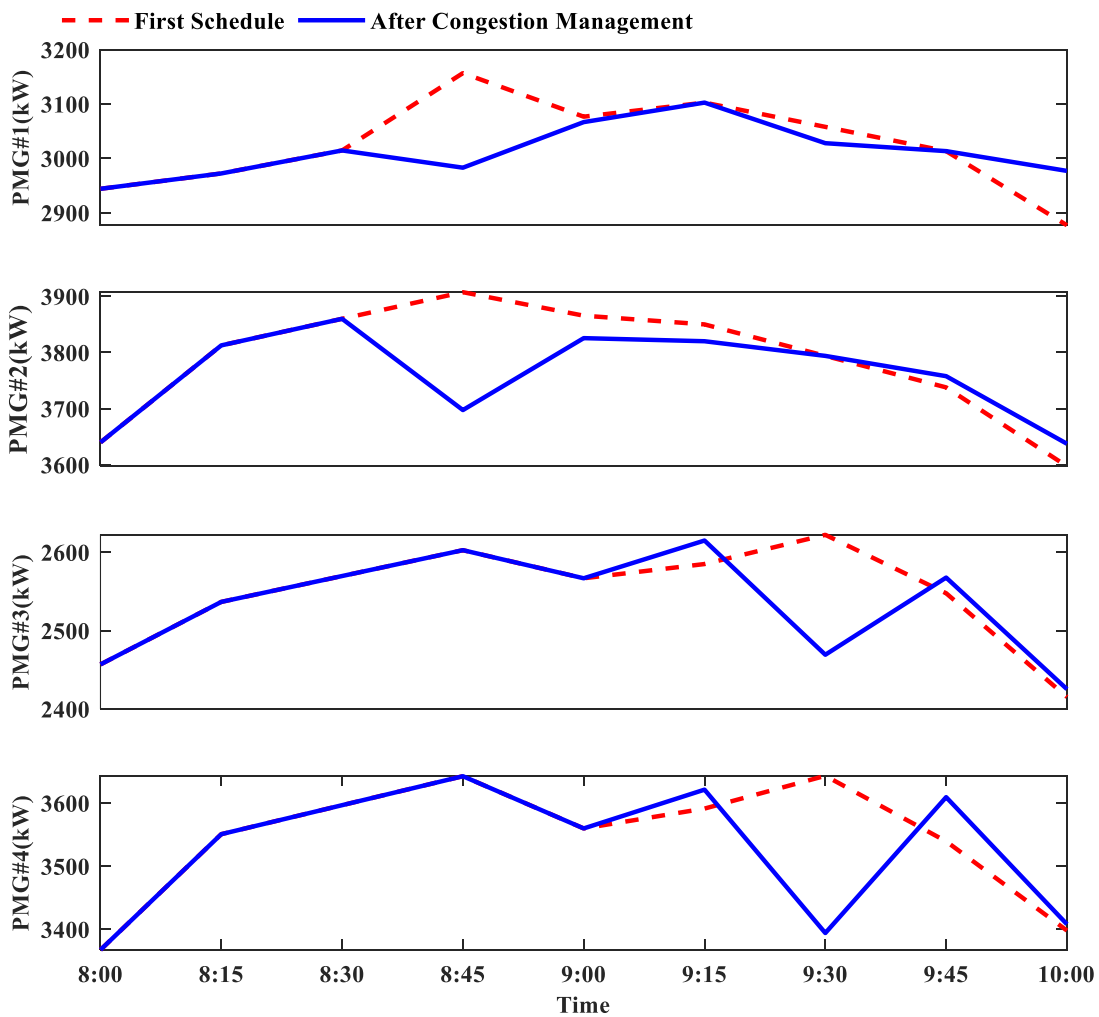


Figure 5-4: MGs power purchased from the grid during time

Figure 5-5 illustrates the amount of exchanged money for all aggregators and MGs during the simulation period. After rescheduling, the revenue of DGs and DRs are increased. The MGOs

raise the electricity price (DLMP) at the congestion times to create congestion management motivation. The DGAGs use their storage system to inject more power at congestion times. Therefore, the overall revenue for the DGAG is increased. Also, a part of congestion is addressed by DR's contribution (i.e., load curtailment). As a result, these aggregators are rewarded by the MGOs for their cooperation. Moreover, the EVs shift their demand as much as possible due to the DLMP enhancement. It changes their overall cost, accordingly.

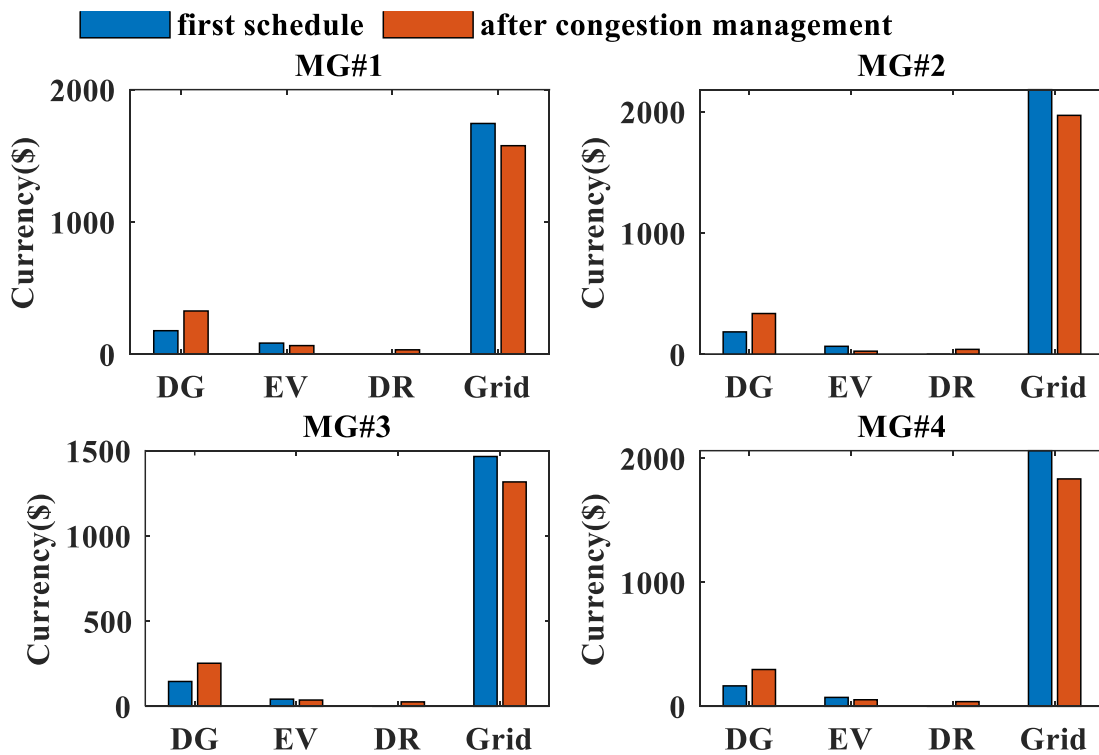


Figure 5-5: MGs Currency components for the whole interval

Figure 5-6 outlines the average electricity price for each MG during the simulated interval. It is evident that although the wholesale price is similar for all the MGs in the system, the real-time price is different. Referring to figure 2-12, multiple rates increase the wholesale price to cover power loss and congestion management costs. Therefore, there is a gap between the wholesale

price and real-time DLMP at the MGs. At  $t=8:45$ , the price at MG#1 and MG#2 is increased, instantaneously. It is because these MGs are engaged in the congestion management process at this time. The same situation happens for MG#3 and MG#4 at  $t=9:30$ . These fluctuations in the DLMP due to the congestion management will push the EVAGs to shift their demand to another time at a lower price. At the same time, it motivates the DGs to sell more energy by sharing their storage system at the congestion time, where the MGOs increase the price.

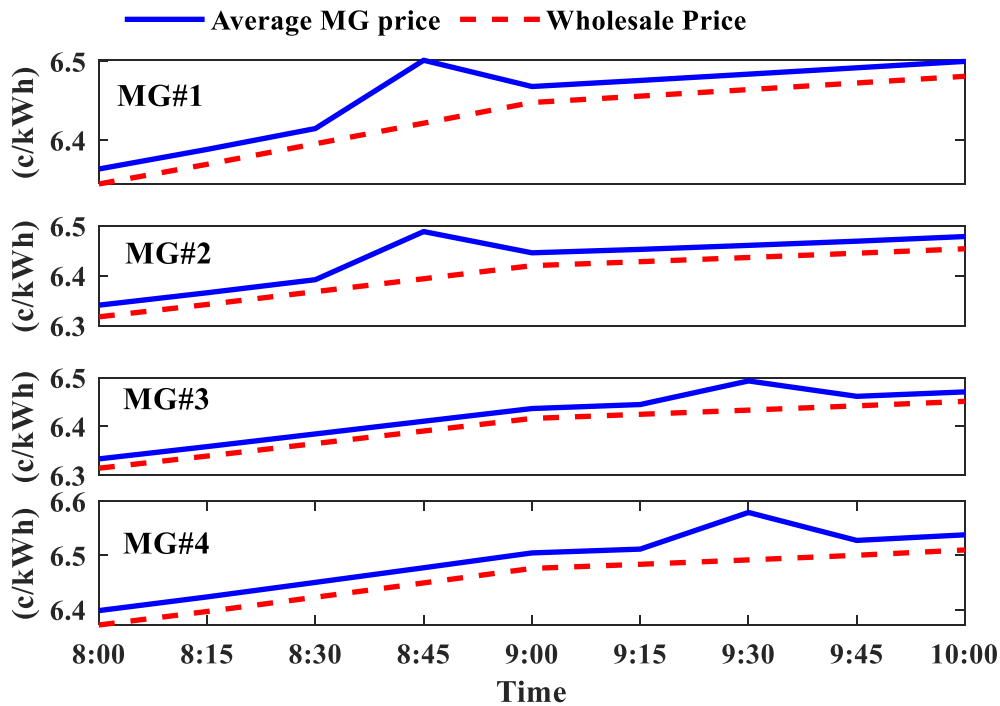


Figure 5-6: Wholesale price and updated MG price

According to the DLMP model, the electricity price is determined locally. As a result, the participants in an MG may experience different prices. Figures 5-7 illustrates the DLMP in all MGs at  $t=8:45$  and  $t=9:30$ , where there are detected congestions in the system. The DLMP for MG#1 and MG#2 is higher at  $t=8:45$  because of the congestion at branch B1-B6. The congestion at branch B1-B2 causes an increase in DLMP for MG#3 and MG#4 at  $t=9:30$ . Therefore, if any

congestion occurs, the DLMP in all the corresponding MGs will be enhanced in the entire buses.

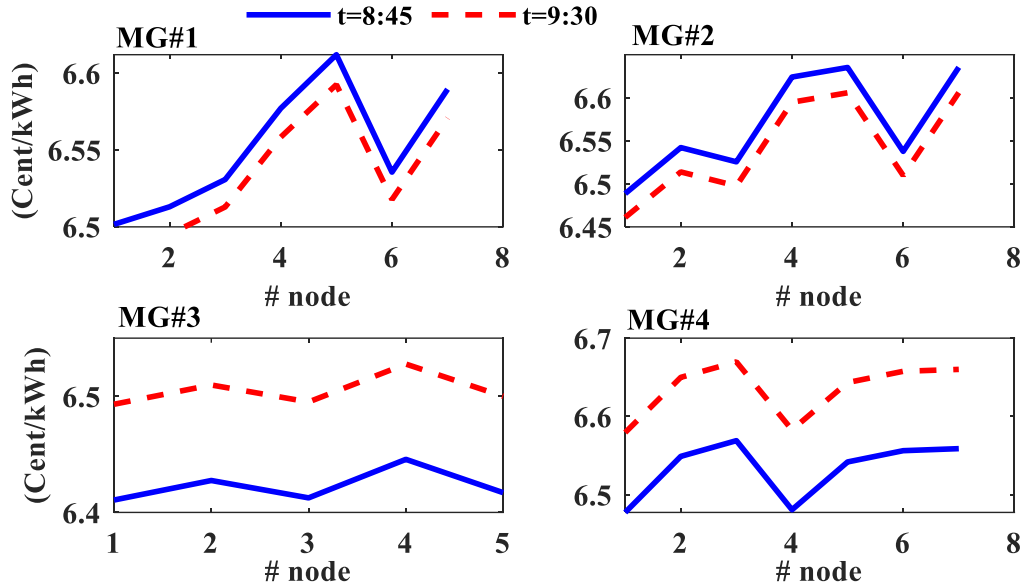


Figure 5-7: DLMP in MGs at the detected congestion times

### 5.2.2. Considering uncertainty in transferred data

In this scenario, an error vector is added to take into account the common errors in reading or transferring data (refer to Section 5.1). The simulation results are shown for  $t=12$  pm to  $t=2$  pm. Figure 5-8 depicts the loading for the branches B1-B2 and B1-B6 in this scenario with and without using the data estimation system which is proposed in Section 2.6.3. As is indicated, the branch B1-B6 is marked as a congested branch at  $t=13:15$  without using the data correction system, while the solid blue curve in Figure 5-8 (a) demonstrates that there is no congestion according to the correct information. This miss-detection convinces the DSO to ask the down MGs for an unnecessary load reduction. After using the real-time estimator, the calculation shows no congestion at  $t=13:15$ .

Branch B1-B2 is identified as a congestion case at  $t=13.30$  if the MGOs do not use the RDE system in their calculation. As a result, the random errors in the data can cause miss-detected congestions. Initially, the discovered congestion at branch B1-B2 causes 88 kW load reduction,

while after using the estimator, this value reduces to 6 kW. Dealing with 6 kW load reduction is very easier than 88 kW. Therefore, the proposed RDE can prevent unnecessary congestion management cases (e.g., Figure 5-8 (a)) or can reduce the level of congestion (e.g., Figure 5-8 (a)).

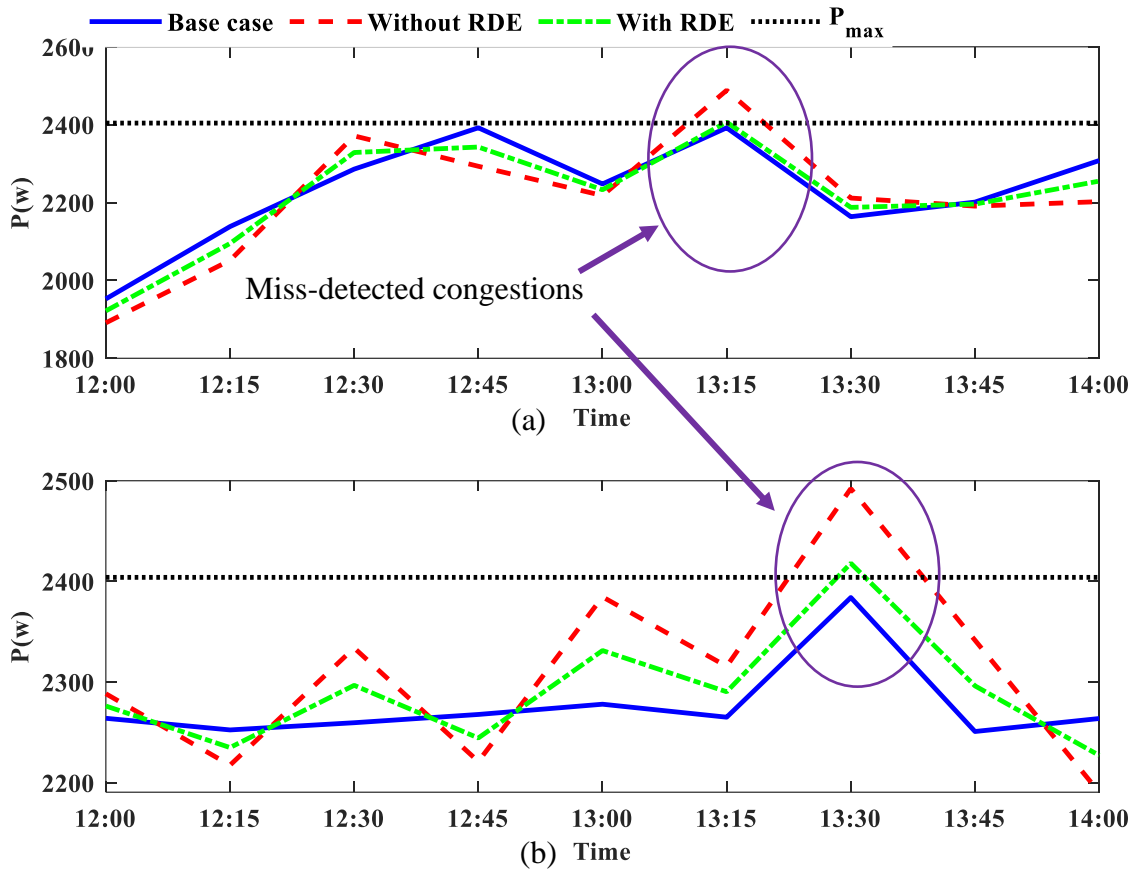


Figure 5-8: (a)-Loading for branch B1-B6, (b)- loading for branch B1-B2 in 3 scenarios

### 5.3. Case study #2: IEEE 123-bus

#### 5.3.1. Real-time simulation without considering uncertainty

The modified IEEE 123-bus test system was presented in Section 4.3.2. All 30 available microgrids in this system should cooperate with the DSO and the aggregators within their territory. After simulating this system for an entire 24 hours according to the proposed framework, 11 congestion cases are detected by the DSO. These congestion cases happen in five

different branches at different times. Figure 5-9 illustrate the congested branches and their downstream MGs. The orange MGs are the ones that are called by DSO for congestion management during the day. The blue MGs are not engaged in any of the congestion management processes. As is shown in Figure 5-9, branch 21-23 is congested at  $t=1$  pm,  $t=4$  pm, and  $t=9$  pm. The DSO's calculation determines that this branch's loading should be reduced by 121 kW, 203 kW, and 61 kW at  $t=1$  pm,  $t=4$  pm, and  $t=9$  pm, respectively. According to the single diagram, MG#10, MG#13, and MG#20 are supplied by branch 21-23. As a result, the DSO calls the corresponding MGOs to reduce their demand in the aforementioned MGs. The interaction between the MGOs and their aggregators should lead to a demand reduction equal to or greater than the DSO's determined value. The other detected congestions are specified in Figure 5-9. The DSO identifies three congested branches at  $t=1$  pm, four congestion cases at  $t=4$  pm, and four congested branches at  $t=9$  pm. Also, 15 MGs are affected by the congestion management process during the day.

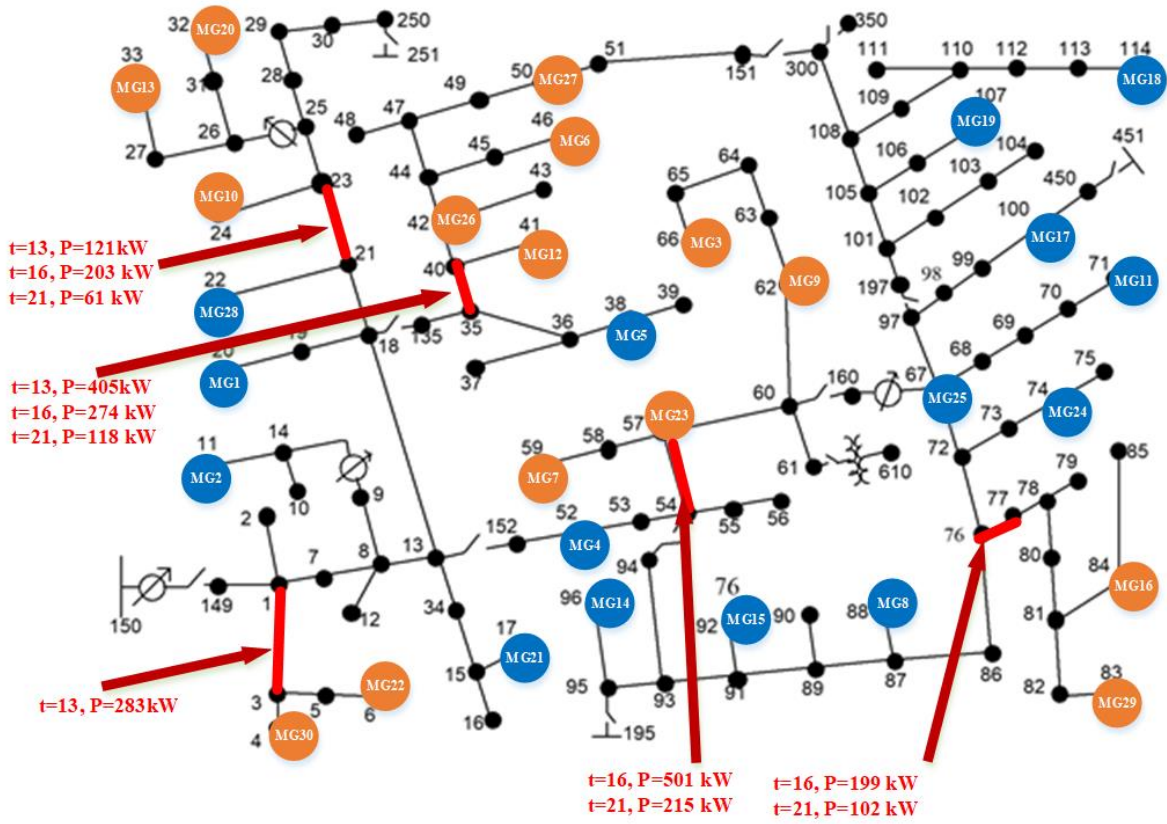


Figure 5-9: Congested branches with called MGs

Table 5-2 displays the power reduction due to congestion management. The DSO needs 121 kW power reduction from MG#10, MG#13, and MG#20 to relieve the branch 21-23 at t=13. After calling the corresponding MGOs, they could maintain a 128 kW power reduction which is enough to eliminate the congestion. The same explanation can be expressed for other congestion cases. As is evident, the final power reduction is greater for all congestion cases than the DSO's ordered value. It means all of the congestion issues are addressed by MGOs participation.

Table 5- 2: The managed congestions during 24 hours of real-time operation

Congestion time	Congested Branch	Called MGs	DSO's ordered Power Reduction	Final Power Reduction
t=13	21-23	#10, #13, #20	121	128
	35-40	#26, #12, #6, #27	405	415
	1-3	#30, #22	283	297
t=16	21-23	#10, #13, #20	203	207
	35-40	#26, #12, #6, #27	274	281
	54-57	#3, #7, #9, #23	501	515
	76-77	#16, #29	199	202
t=21	21-23	#10, #13, #20	61	65
	35-40	#26, #12, #6, #27	118	126
	54-57	#3, #7, #9, #23	215	218
	76-77	#16, #29	102	108

Figure 5-10 illustrates the total purchasing power from the wholesale market which is delivered by the main substation. As is shown in this figure, the scheduled power is reduced at  $t=1$  pm,  $t=4$  pm, and  $t=9$  pm due to the real-time congestion management (RCM). It can be inferred from this figure and Table 5-2 that an 840 kW reduction is maintained to relieve the congestions of branches 21-23, 35-40, and 1-3 due to the congestion at  $t=1$  pm. According to the proposed framework, the MGOs change the electricity price to motivate the aggregators to reduce the overall demand. It means that the MGOs do not have a direct control over the demand. As a result, the amount of reduction is not exactly equal to the DSO's determined value. For this reason, the reduction value at  $t=1$  pm is 840 kW, while the DSO asks for 809 kW (see table 5-2). Also, the total reduction for the other congestion times is 1205 kW at  $t= 4$  pm and 517 kW at  $t=9$  pm.

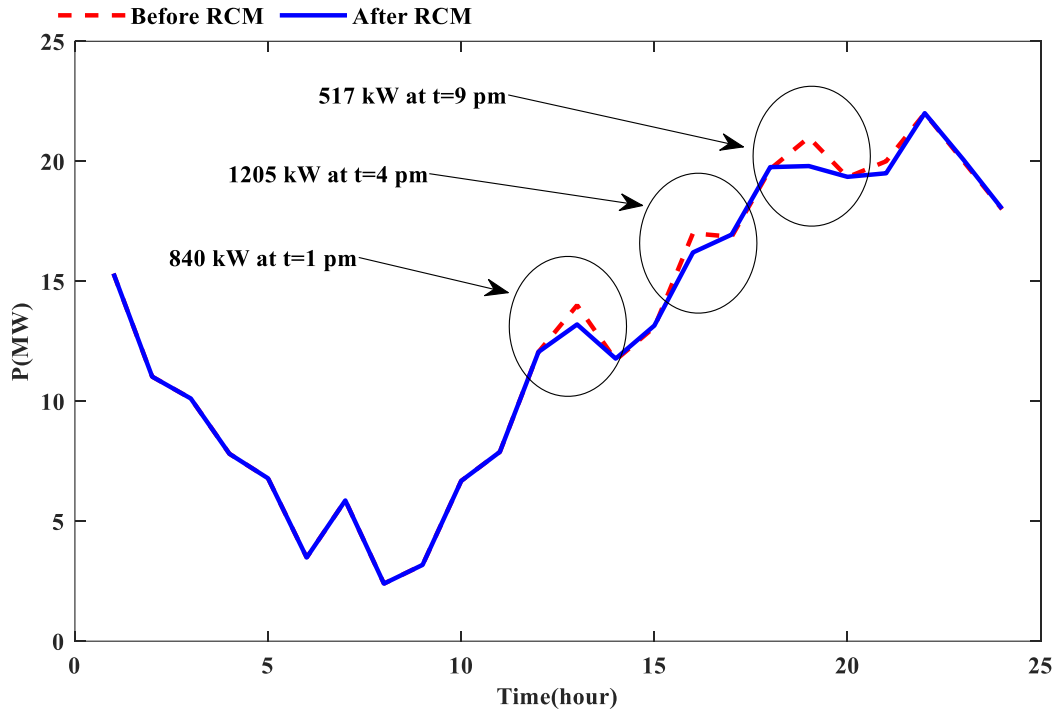


Figure 5-10: Total purchasing power before and after real-time congestion management

The demand associated with an MG is the aggregated load minus the generated power ( $P_D = P_L - P_G$ ). As a result, to reduce the demand associated with an MG, the DGAGs should increase their injected power, and the EVAGs and DRAGs should reduce their demand at the congestion time. Figure 5-11 (a) shows the total generated power by all DGADs before and after the congestion management. The values are calculated from the summation of output power from the wind turbines and the PV systems in the MGs. As is shown, at  $t=1$  pm (subfigure (1)), the DGAGs have an active participation in the congestion management. The aggregated power production by the DGAGs is increased at this time. It can supply more local loads and reduce the passing power from the congested branches. The participation of the DGAGs is reduced at  $t=4$  pm (subfigure (2)) due to solar intensity and wind velocity at this time (see Figure 4-1). Also, at  $t=9$  pm, the DGAGs do not have any congestion management activity because there is not sufficient solar radiation and wind speed to support the DGs. Also, due to the previous actions,

the DGs do not have enough storage to be a part of congestion management at this time.

Figure 5-11(b) illustrates the participation of the EVAGs and DRAGs during the day for MG#10. At  $t=4$  pm (subfigure (3)), the load is reduced due to the involvement of EVAGs and DRAGs in congestion management. Also, sub-plot (4) shows the reduction in the load after congestion management at  $t=9$  pm. As is shown at  $t=1$  pm, there is no activity from the demand side. It is because the DGAGs fully address the detected congestions at  $t=1$  pm, and there is no need for engaging the EVAGs and DRAGs in the congestion management. According to the framework, the first priority for MGO#10 in congestion management is to encourage the DGAGs to generate more power; the second priority is to motivate the EVAGs to use another time for charging their clients, and the last priority is to use the DRAGs ability to curtail a part of the load.

Figure 5-11(c) depicts the aggregated demand for MG#10. As can be realized from this figure, the aggregated demand is reduced at the congestion times. We have zoomed on the areas associated with the congestion times for more clarity. The overall demand related to MG#10 is reduced at  $t=1$  pm (sub-plot (5)),  $t=4$  pm (sub-plot (6)), and  $t=9$  pm (sub-plot (7)). Another result extracted from Figure 5-11(c) is the overall demand is a negative value at  $t=8$  am and  $t=9$  am. It means MG#10 acts as a power supply at these times.

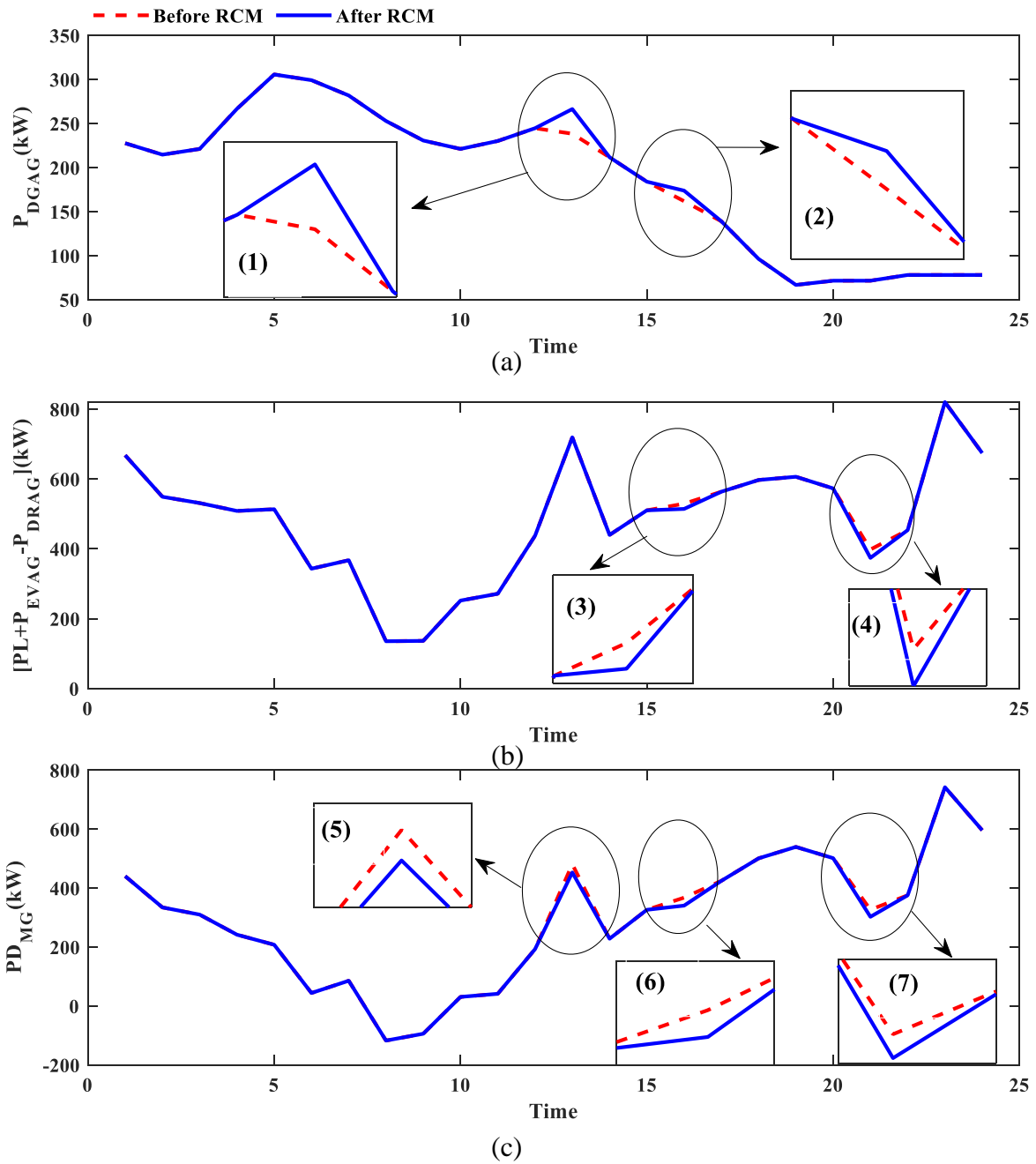


Figure 5-11: The MG#10 (a) DGAGs production, (b) aggregated load, (c) overall demand

The average hourly electricity price is shown in Figure 5-12. This price is the overall money that the consumers pay divided by the total purchasing power from DGAGs and the wholesale market. According to the pricing model in Section 2.7, the wholesale market is increased by several rates to cover the system's power loss cost and congestion cost. Therefore, the average electricity price is greater than the wholesale price at all times. Also, as is specified in sub-plots (1), (2), and (3), the electricity price has an additional supplement after the congestion management. The reason is that the MGOs have to increase the DLMPs to manage the congestion, and it causes a higher electricity rate at the congestion times. This increment is not very significant because only the electricity price within the called MGs is increased at each congestion time. As a result, the majority of the customers do not have to pay an additional cost for congestion management.

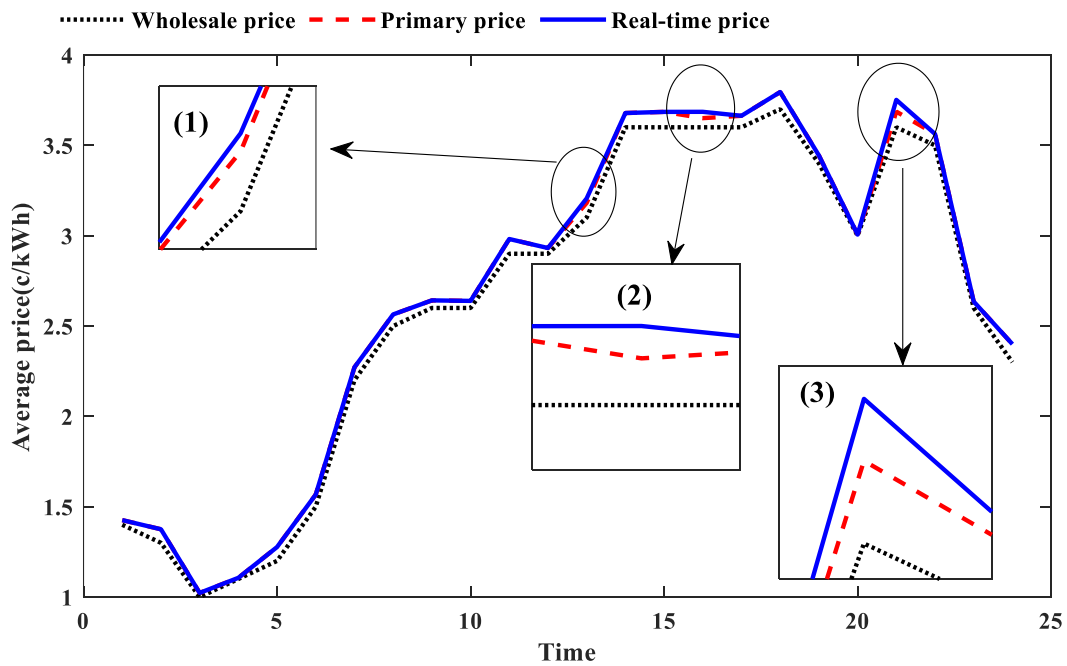


Figure 5-12: Average electricity price of the system

### **5.3.2. Considering uncertainty in transferred data**

In this case, a 10% error is considered in the submitted data by the aggregators. Figure 5-13 shows the congested branches in this scenario. The red branches are the actual congestions, and the orange branches are the wrong detections. As can be found out from the figure, if the MGOs use the received data from the aggregators without any pre-processing, it will add three new branches into the congested branches list. Table 5-3 shows the details regarding the congestion cases in this scenario. The miss-detected congestion cases are highlighted in Table 5-3.

According to these results, without using the RDE, 18 wrong congestion cases are detected by the DSO. These wrong detections will engage many MGOs in congestion management and will increase the electricity cost accordingly. The last two columns of table 5-3 display the identified congestion cases after using the RDE by the MGOs. As is shown, the DSO only detect four wrong congestion cases if the MGOs use the RDE in their calculations. These results show how RDE can reduce unnecessary reactions to congestion.

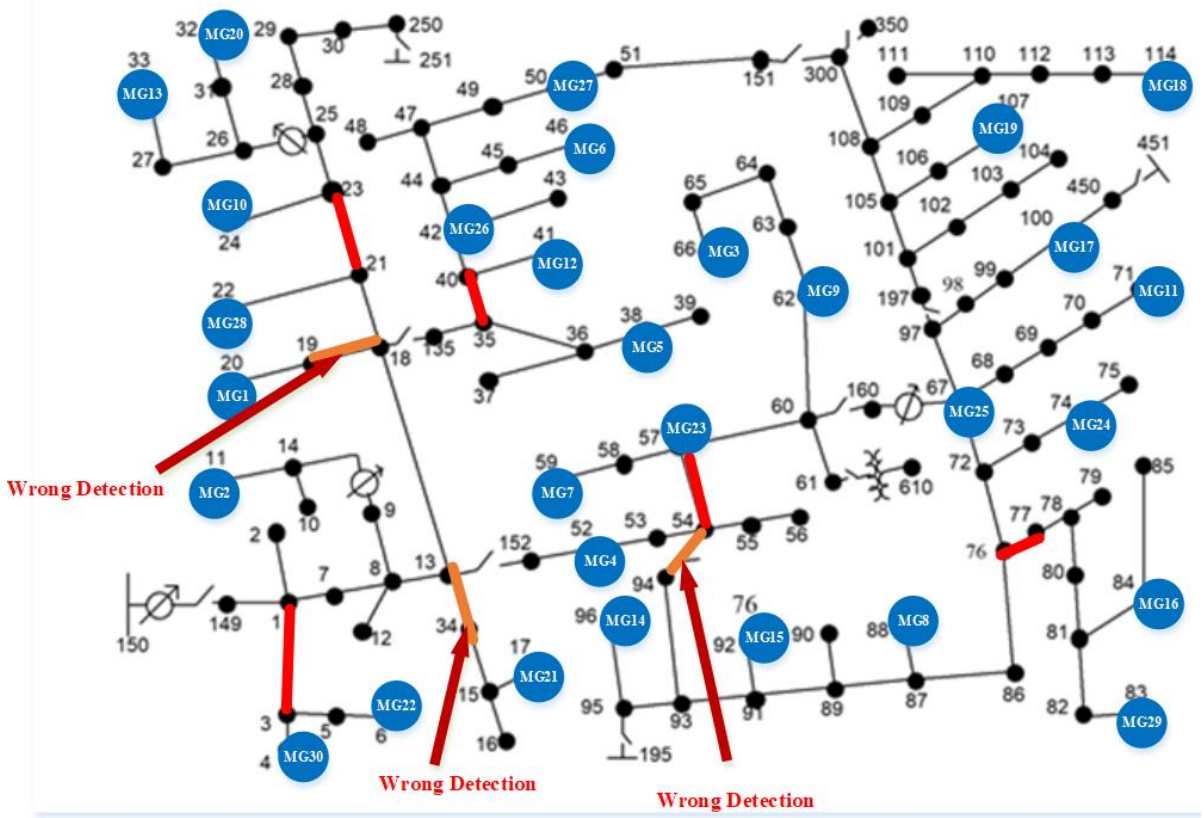


Figure 5-13 : All congested branches along with three wrong detections

Table 5-3: Total detected congestions

congestion time	Without RDE		With RDE	
	Congested Branch	Called MGs	Congested Branch	Called MGs
t=13	21-23	#10, #13, #20	21-23	#10, #13, #20
	35-40	#26, #12, #6, #27	35-40	#26, #12, #6, #27
	1-3	#30, #22	1-3	#30, #22
	13-34	#21	*	*
t=15	21-23	#10, #13, #20	21-23	#10, #13, #20
	35-40	#26, #12, #6, #27	35-40	#26, #12, #6, #27
	54-57	#3, #7, #9, #23	54-57	#3, #7, #9, #23
	76-77	#16, #29	76-77	#16, #29
	13-34	#21	*	*
	18-19	#1	*	*
t=20	21-23	#10, #13, #20	*	*
	35-40	#26, #12, #6, #27		
	54-57	#3, #7, #9, #23	54-57	#3, #7, #9, #23
	76-77	#16, #29	76-77	#16, #29
	13-34	#21	*	*
	54-94	#14, #15, #8	*	*
	18-19	#1	*	*
t=21	21-23	#10, #13, #20	21-23	#10, #13, #20
	35-40	#26, #12, #6, #27	35-40	#26, #12, #6, #27
	54-57	#3, #7, #9, #23	54-57	#3, #7, #9, #23
	76-77	#16, #29	76-77	#16, #29
	13-34	#21	*	*
	54-94	#14, #15, #8	*	*
t=22	18-19	#1	*	*
	21-23	#10, #13, #20	*	*
	35-40	#26, #12, #6, #27	*	*
	54-57	#3, #7, #9, #23	54-57	#3, #7, #9, #23
	76-77	#16, #29	76-77	#16, #29
	54-94	#14, #15, #8	*	*
	Number of wrong detections	18		4

Figure 5-14 focuses on the loading at branch 21-23 with and without using RDE. The blue stars in the figure specify the congestion times. Any time that the power passing through this branch exceeds the maximum value (the black dot curve in figure 5-14), there is congestion in this line. There are five congestion times associated with branch 21-23 at  $t=1$  pm,  $t=4$  pm,  $t=8$  pm,  $t=9$  pm, and  $t=10$  pm without using RDE. According to the results from Table 5-2, this branch is not congested at  $t=8$  pm and  $t=10$  pm. Therefore, without any pre-processing, the DSO calls the operators of MG#10, MG #13, and MG #20 for a load reduction at  $t=8$  pm,  $t= 10$  pm, and the other congestion times. It causes an unnecessary reaction from the MGOs above. But using the RDE, the miss-detected congestion cases are filtered, and the DSO identifies the true congestions.

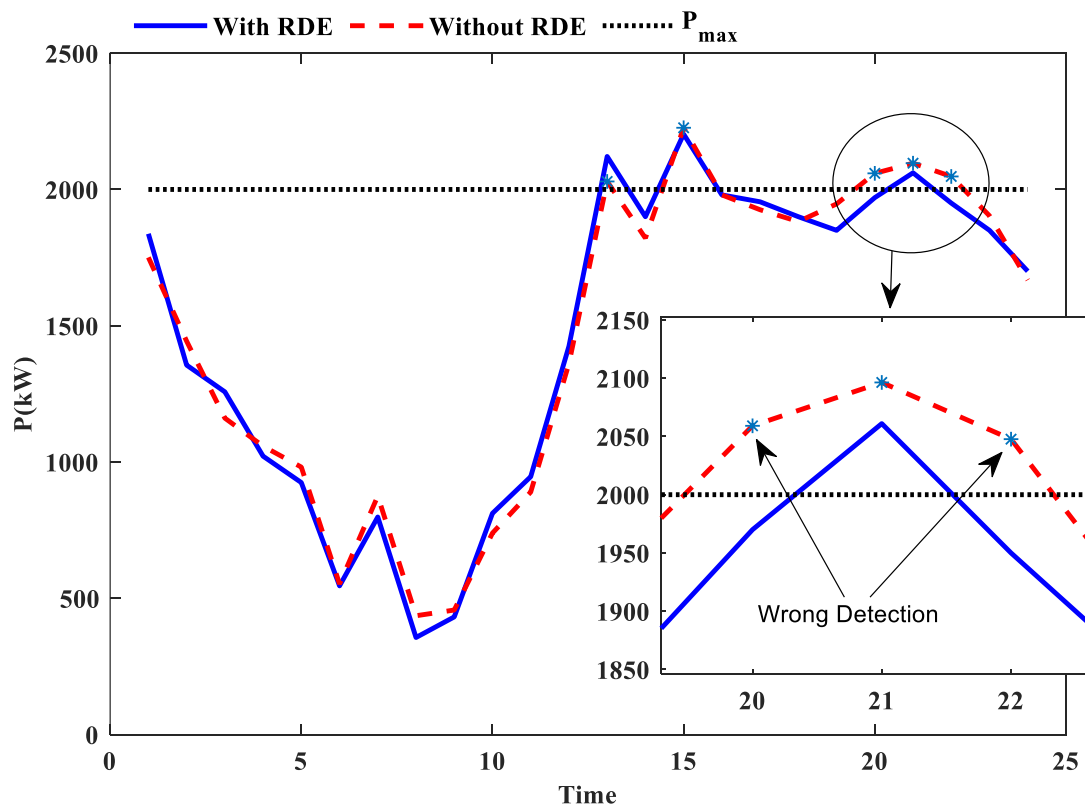


Figure 5-14: Loading of branch 21-23

## CHAPTER 6

### CONCLUSION AND FUTURE WORK

#### 6.1. Conclusion

In this research, a real-time operation and management framework is proposed, which is adaptive for modern distribution systems with massive active elements. The proposed hierarchical framework is able to manage the congestion in the real-time process by taking advantage of the demand side potential. The background of the subject with the relevant work are discussed in the first chapter. The second chapter discusses the proposed framework in detail with all the utilized mathematical models. The role of intermediary entities such as aggregators and microgrid operators are also discussed in the second chapter. Moreover, the steps that the DSO should take for congestion management are expressed in the second chapter. To have a powerful tool for optimization, a GAMS-MATLAB composition is utilized, which is presented in the third chapter. All the settings and significant commands that are needed to have a collaborative GAMS-MATLAB structure are highlighted in the third chapter. In the fourth chapter, the input data and technical specifications associated with two modified IEEE test systems are represented. Finally, the numerical study for case studies in the certain and uncertain situation is discussed in the fifth chapter.

The numerical results demonstrate that the proposed framework can fully address real-time congestions. After detecting congestions, the DSO engages the relevant MGOs downstream the congested areas and gives them an order to tackle the congestions. The proposed hierarchical structure facilitates the interaction between the MGOs and the aggregators, especially in the congestion times. The results show that by increasing the DLMP at the congestion times, the DGAGs increase their generation and supply more local loads. Simultaneously, the EVAGs try

to charge their clients at other times with lower prices. It will reduce the expected load associated with the EVs. Finally, the MGOs use the available DR contracts and address the remaining congestions (if any) with the help of the DRAGs. Table 6-1 expresses the overall results associated with both case studies.

Table 6-1: The overall needed load reduction and the maintained load reduction

Case study	Congestion time	Total needed load reduction (kw)	Maintained load reduction (kw)
IEEE 13-bus	8:45 am	363	384
	9:30 am	384	402
IEEE-123 bus	1:00 pm	809	840
	3:00 pm	1177	1205
	9:00 pm	497	517

The results validate the effectiveness of the proposed market framework in congestion prevention when there is uncertainty with the delivered data to the MGOs. According to the results in Sections 5.2.2, the DSO’s calculations show congestion at branch B1-B2 of the IEEE 13-bus test system by mistake due to the uncertain data. It causes the MGOs an 88 kW load reduction while using the RDE this value reduces to 6 kW. Also, the proposed RDE can prevent miss-detected congestion at branch B1-B6 at  $t=1:15$  pm.

The results associated with the IEEE 123-bus test system demonstrate that the DSO detects 18 wrong congestion cases for a 24 hours operation. The proposed RDE reduces the miss-detected congestions to four cases. Therefore, even if the RDE could not entirely address the miss-detected congestions, it can still prevent the majority of them.

## 6.2. Future studies

In the future step of this research, we will upgrade the proposed market scheme to prevent the real-time congestions caused by organized false data injections of hackers. Figure 6-1 illustrates

the proposed scheme for this situation. According to this scheme, a hacker can access some part of the aggregators' data and falsify it by injecting an error vector.

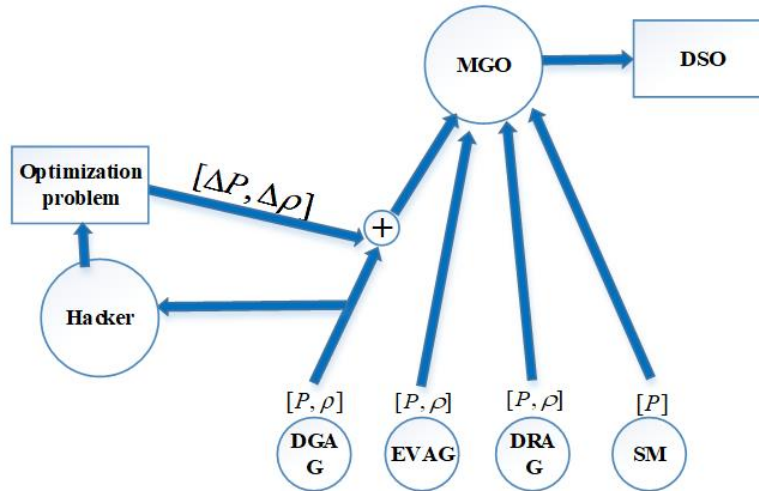


Figure 6-1: The main scheme of hacking the data

The MGOs need an estimator that can estimate data in which the false data could be identified. According to (2-76), if the MGOs use a K.F technique for estimation, the estimated error would be as (6-1). A significant increase in  $Er$  shows abnormal false data in the system. It could be because of a suddenly load/generation variation, outage or a cyberattack.

$$Er = \hat{x}[n|n] - x[n] = \hat{x}[n|n](1 - K[n]) + x[n](K[n] - 1) \quad (6-1)$$

The proposed detection system in (6-1) is not reliable if the hacker uses the same model to minimize the hack's visibility. A general model for a hacker is formulated as (6-2), where  $X = [p^{EVAG}, p^{DGAG}, p^{DRAG}, p^{L0}]$  is the submitted data by the aggregators. In this model, the hacker tries to manipulate the data to maximize one of the aggregator's benefit in the market.

$$\max = \left\{ \begin{array}{l} \sum_n \rho_{n,i}^{DGAG} P_{n,i}^{DGAG} \quad \text{If hacker has a deal with } i\text{th DGAG} \\ -\sum_n \rho_{n,j}^{EVAG} P_{n,j}^{EVAG} \quad \text{If hacker has a deal with } j\text{th EVAG} \\ \sum_n \rho_{n,k}^{DRAG} P_{n,k}^{DRAG} \quad \text{If hacker has a deal with } k\text{th DRAG} \end{array} \right\} \quad (6-2)$$

s.t.

$$\min\{g(X^H, X)\}$$

$$\text{var}(X^H - X) < \sigma_{\max}$$

The  $g(X^H, X)$  is the visibility of the hack and is formulated as (6-3). The hacker can hide false data from the DSO by minimizing this function and bypassing the bad data detection algorithm.

$$g(x^h[n], x[n]) = (K[n]-1)(x^h[n] - x[n]) \quad (6-3)$$

Therefore, conventional models such as K.F are not capable of detecting the hidden injected data. In the future studies, an advanced model for false data detection is proposed to detect the incorrect data even if the hacker uses an optimization model to optimally target the system with a stealthy attack.

## REFERENCES

- [1] S. A. A. Kazmi, M. K. Shahzad, A. Z. Khan, and D. R. Shin, "Smart Distribution Networks: A Review of Modern Distribution Concepts from a Planning Perspective," *Energies*, vol. 10, no. 4, pp. 501-548, Apr. 2017.
- [2] A. N. M. M. Haque, M. Nijhuis, G. Ye, P. H. Nguyen, F. W. Bliiek, and J. G. Slootweg, "Integrating Direct and Indirect Load Control for Congestion Management in LV Networks," *IEEE Trans. Smart Grid*, vol. 10, no. 1, pp. 741–751, Jan. 2019.
- [3] A. Kulmala, M. Alonso, S. Repo, H. Amaris, A. Moreno, J. Mehmedalic, Z. A. Jassim, "Hierarchical and distributed control concept for distribution network congestion management," *IET Generation, Transmission & Distribution*, vol. 11, no. 3, pp. 665–675, Apr. 2019.
- [4] M. A. Rustam, B. Khan, S. M. Ali, M. B. Qureshi, C. A. Mehmood, M. U. S. Khan, and R. Nawaz, "An Adaptive Distributed Averaging Integral Control Scheme for Micro-Grids With Renewable Intermittency and Varying Operating Cost," *IEEE Access*, vol. 8, pp. 455 – 464, (Early Access) <https://ieeexplore.ieee.org/document/8936905>
- [5] W. P. Gorzegno and P. V. Guido, "Load Rejection Capability for Large Steam Generators," in *IEEE Transactions on Power Apparatus and Systems*, vol. PAS-102, no. 3, pp. 548-557, March 1983.
- [6] <https://pdfslide.net/documents/98280298-electrical-distribution-system-topics-1pdf.html>
- [7] <https://www.nordpoolgroup.com>
- [8] <https://www.nordicenergyregulators.org>
- [9] [https://uk.practicallaw.thomsonreuters.com/w-019-3060?transitionType=Default&contextData=\(sc.Default\)&firstPage=true](https://uk.practicallaw.thomsonreuters.com/w-019-3060?transitionType=Default&contextData=(sc.Default)&firstPage=true)
- [10] <https://www.nigeriaelectricityhub.com/download/distributed-generation-definition-benefits-and-issues>
- [11] <https://newscenter.lbl.gov/2016/01/14/berkeley-lab-launches-new-projects-for-grid-modernization>
- [12] <https://electricala2z.com/electrical-power/smart-grid-distribution-system>
- [13] S. A. A. Kazmi, M. K. Shahzad, A. Z. Khan, and D. R. Shin, "Smart Distribution Networks: A Review of Modern Distribution Concepts from a Planning Perspective," *Energies*, vol. 10, no. 4, pp. 501-548, Apr. 2017.
- [14] A. N. M. M. Haque, M. Nijhuis, G. Ye, P. H. Nguyen, F. W. Bliiek, and J. G. Slootweg, "Integrating Direct and Indirect Load Control for Congestion Management in LV Networks," *IEEE Trans. Smart Grid*, vol. 10, no. 1, pp. 741–751, Jan. 2019.
- [15] A. Kulmala, M. Alonso, S. Repo, H. Amaris, A. Moreno, J. Mehmedalic, Z. A. Jassim, "Hierarchical and distributed control concept for distribution network congestion management," *IET Generation, Transmission & Distribution*, vol. 11, no. 3, pp. 665–675, Apr. 2019.

- [16] M. A. Rustam, B. Khan, S. M. Ali, M. B. Qureshi, C. A. Mehmood, M. U. S. Khan, and R. Nawaz, "An Adaptive Distributed Averaging Integral Control Scheme for Micro-Grids With Renewable Intermittency and Varying Operating Cost," *IEEE Access*, vol. 8, pp. 455 – 464, (Early Access) <https://ieeexplore.ieee.org/document/8936905>
- [17] M. Ansari, A. Asrari, J. Khazaei, and P. Fajri, "A market framework for holistic congestion management in unbalanced distribution systems," *IEEE PES General Meeting (PESGM)*, Atlanta, GA, 2019, pp. 1-5.
- [18] A. Asrari, M. Ansari, J. Khazaei, and P. Fajri, "A Market Framework for Decentralized Congestion Management in Smart Distribution Grids Considering Collaboration Among Electric Vehicle Aggregators," *IEEE Transactions on Smart Grid*, vol. 11, no. 2, pp. 1147 - 1158 Mar. 2020.
- [19] A. Asrari, M. Ansari and K. C. Bibek, "Real-time Congestion Prevention in Modern Distribution Power Systems via Demand Response of Smart Homes," *North American Power Symposium (NAPS)*, Wichita, KS, USA, 2019, pp. 1-6.
- [20] S. Huang, and Q. Wu, "Real-Time Congestion Management in Distribution Networks by Flexible Demand Swap," *IEEE Trans. Smart Grid*, vol. 9, no. 5, pp. 4346–4355, Sep. 2018.
- [21] M. H. Moradi, A. R. Reisi, and S. M. Hosseinian "An Optimal Collaborative Congestion Management Based on Implementing DR," *IEEE Trans. Smart Grid*, vol. 9, no. 5, pp. 5323–5334, Sep. 2018.
- [22] S. Huang, Q. Wu, H. Zhao, and C. Li, "Distributed Optimization-Based Dynamic Tariff for Congestion Management in Distribution Networks," *IEEE Trans. Smart Grid*, vol. 10, no. 1, pp. 184–192, Jan. 2019.
- [23] S. Huang, and Q. Wu, "Dynamic Tariff-Subsidy Method for PV and V2G Congestion Management in Distribution Networks," *IEEE Trans. Smart Grid*, vol. 10, no. 5, pp. 5851–5860, Sep. 2019.
- [24] S. Huang, Q. Wu, M. Shahidehpour, and Z. Liu, "Dynamic Power Tariff for Congestion Management in Distribution Networks," *IEEE Trans. Smart Grid*, vol. 10, no. 2, pp. 2148–2157, Sep. 2019.
- [25] L. Bai, J. Wang, C. Wang, C. Chen, and F. Li, "Distribution Locational Marginal Pricing (DLMP) for Congestion Management and Voltage Support," *IEEE Trans. on Power Systems*, vol. 33, no. 4, pp. 4061-4073, Jul. 2018.
- [26] J. Zhao, Y. Wang, G. Song, P. Li, C. Wang, and J. Wu, "Congestion Management Method of Low-Voltage Active Distribution Networks Based on Distribution Locational Marginal Price," *IEEE Access*, vol. 7, pp. 32240–32255, Mar. 2019
- [27] S. Hanif, K. Zhang, C. M. Hackl, M. Barati, H. B. Gooi, and T. Hamacher, "Decomposition and Equilibrium Achieving Distribution Locational Marginal Prices Using Trust-Region Method," *IEEE Trans. Smart Grid*, vol. 10, no. 3, pp. 3269–3281, May 2019.
- [28] Z. Liu, Q. Wu, S. S. Oren, S. Huang, R. Li, and L. Cheng, "Distribution Locational Marginal Pricing for Optimal Electric Vehicle Charging Through Chance Constrained

- Mixed-Integer Programming,” *IEEE Trans. Smart Grid*, vol. 9, no. 2, pp. 644–654, Mar 2018.
- [29] L. Kunjumammed, S. Kuenzel, B. Pal, “Simulation of Power System with Renewables 1st Edition,” Copyright: © Academic Press 2020, eBook ISBN:9780128112540, Oct. 2019.
- [30] Y. Liao, Y. Weng, G. Liu, Z. Zhao, C.W. Tan, R. Rajagopal, “Unbalanced multi-phase distribution grid topology estimation and bus phase identification,” *IET Smart Grid*, vol. 2, no. 4, pp. 557-570, Dec. 2019.
- [31] A. Bernstein, C. Wang, E. Dall’Anese, J. Y. L. Boudec, C. Zhao, “Load Flow in Multiphase Distribution Networks: Existence, Uniqueness, Non-Singularity and Linear Models,” *IEEE Trans. Power Syst.*, vol. 33, no. 6, pp. 5832–5843, Nov. 2018.
- [32] Alejandro Garces, “A Linear Three-Phase Load Flow for Power Distribution Systems,” *IEEE Trans. Power Syst.*, vol. 31, no. 1, pp. 827–828, Jan. 2016.
- [33] Y. Wang, N. Zhang, H. Li, J. Yang, and C. Kang, “Linear three-phase power flow for unbalanced active distribution networks with PV nodes,” *CSEE Journal of Power and Energy Systems*, vol. 3, no. 3, pp. 321–324, Sep. 2017.
- [34] M. Bazrafshan, and N. Gatsis, “Convergence of the Z-Bus Method for Three-Phase Distribution Load-Flow with ZIP Loads,” *IEEE Trans. Power Syst.*, vol. 33, no. 1, pp. 153–165, Jan. 2018.
- [35] S. A. Saleh, “The Formulation of a Power Flow Using d–q Reference Frame Components—Part II: Unbalanced 3 $\phi$  Systems,” *IEEE Trans. Ind Appl*, vol. 54, no. 2, pp. 1092–1107, Mar. / Apr. 2019.
- [36] S. Avdaković, J. Kacprzyk, “Lecture Notes in Networks and Systems Advanced Technologies, Systems, and Applications III” *Proceedings of the International Symposium on Innovative and Interdisciplinary Applications of Advanced Technologies (IAT)*, vol. 1, pp. 70-85, ISSN 2367-3370, © Springer Nature Switzerland AG 2019.
- [37] V. K. Prajapati, and V. Mahajan, “Congestion management of power system with uncertain renewable resources and plug-in electrical vehicle,” *IET Generation, Transmission & Distribution*, vol. 13, no. 6, pp. 927–938, May 2019.
- [38] S. W. Alnaser, and L. F. Ochoa, “Hybrid controller of energy storage and renewable DG for congestion management,” in *IEEE Power and Energy Society General Meeting, 2012, San Diego, CA*.
- [39] Y. Fu, H. Liu, X. Su, Y. Mi, and S. Tian, “Probabilistic direct load flow algorithm for unbalanced distribution networks considering uncertainties of PV and load,” *IET Renewable Power Generation*, vol. 13, no. 11, pp. 1968–1980, Aug. 2019.
- [40] Steven M. Kay “Fundamentals of Statistical Signal Processing: Estimation Theory” Prentice Hall PTR , 1993, ch. 13, sec. 13.4, pp. 431-442.
- [41] S. S. Alam, A. R. Florita, B. M. Hodge, “Distributed PV generation estimation using multi-rate and event-driven Kalman kriging filter,” *IET Smart Grid*, vol. 3, no. 4, pp. 2515-2947, Aug. 2020

- [42] P. Shah, B. Singh, “Kalman Filtering Technique for Rooftop-PV System Under Abnormal Grid Conditions,” IEEE Transactions on Sustainable Energy, vol. 11, no. 1, pp. 282-293, Jan. 2020
- [43] IEEE PES AMPS DSAS Test Feeder Working Group [Online] <https://site.ieee.org/pes-testfeeders/resources/>
- [44] The solar radiation data [Online] Available: <https://maps.nrel.gov/nsrdb-viewer/?aL=UdPEX9%255Bv%255D%3Dt%26f69KzE%255Bv%255D%3Dt%26f69KzE%255Bd%255D%3D1&bL=clight&cE=0&IR=0&mC=45.9511496866914%2C-92.2412109375&zL=5>
- [45] The used data for extracting load pattern [Online] Available: <http://apps.ameren.com/ILChoice/Default.aspx>
- [46] The wholesale price data [Online] Available: <https://hourlypricing.comed.com/live-prices/?date=20190610>
- [47] The used wind turbine model data [Online] <https://en.wind-turbine-models.com/turbines/2144-fortis-montana-q-6-kw>
- [48] The used wind turbine model data [Online] <https://en.wind-turbine-models.com/turbines/1854-aeolos-aeolos-v-10kw>
- [49] The used wind turbine model data [Online] <https://en.wind-turbine-models.com/turbines/1694-britwind-h15-class-ii>
- [50] Kyocera website. [Online]. Available: <http://www.kyocerasolar.eu/>.
- [51] Sunpower website. [Online]. Available: <https://us.sunpower.com/products/solar-panels>
- [52] Solaria website Available [Online] <https://www.solaria.com/powerxt-300-solar-panels>
- [53] Xantrex website. [Online]. Available: <http://www.xantrex.com/>.
- [54] GAMS Solver Manuals [Online]. Available: [https://www.gams.com/latest/docs/S\\_MAIN.html](https://www.gams.com/latest/docs/S_MAIN.html).

## VITA

Graduate School

Southern Illinois University

Meisam Ansari

Ansari.meisam@gmail.com

Power And Water University Of Technology, Tehran, Iran, 2010

Master of Science, Electrical Power Engineering, May 2021

Special Honors and Awards:

Doctoral fellowship for fall 2020 and spring 2021

Dissertation Paper Title:

REAL-TIME CONGESTION MANAGEMENT IN MODERN DISTRIBUTION SYSTEMS

Major Professor: Dr. Arash Asrari

Publications:

### **Conference Papers:**

1. **M. Ansari**, A. Asrari, J. Khazaei and P. Fajri, "A Market Framework for Holistic Congestion Management in Unbalanced Distribution Systems," *IEEE Power & Energy Society General Meeting (PESGM)*, Atlanta, GA, USA, **2019**, pp. 1-5, doi: 10.1109/PESGM40551.2019.8973789.
2. **M. Ansari** and A. Asrari, "Reaction to Detected Cyberattacks in Smart Distribution Systems," *IEEE Power & Energy Society Innovative Smart Grid Technologies Conference (ISGT)*, Washington, DC, USA, **2020**, pp. 1-5, doi: 10.1109/ISGT45199.2020.9087771.
3. **M. Ansari**, Mo. Ansari and A. Asrari, "A Framework for Simultaneous Management of Greenhouse Gas Emission and Substation Transformer Congestion via Cooperative Microgrids," *North American Power Symposium (NAPS)*, Wichita, KS, USA, **2019**, pp. 1-6, doi: 10.1109/NAPS46351.2019.9000372.
4. **M. Ansari**, Mo. Ansari, J. Valinejad and A. Asrari, "Optimal Daily Operation in Smart Grids Using Decentralized Bi-level Optimization Considering Unbalanced Optimal Power Flow," *IEEE Texas Power and Energy Conference (TPEC)*, College Station, TX, USA, **2020**, pp. 1-6, doi: 10.1109/TPEC48276.2020.9042532.
5. A. Asrari, **M. Ansari**, J. Khazaei and V. Cecchi, "Real-time Blackout Prevention in Response to Decentralized Cyberattacks on a Smart Grid," *2020 IEEE Texas Power and Energy Conference (TPEC)*, College Station, TX, USA, **2020**, pp. 1-5, doi: 10.1109/TPEC48276.2020.9042567.

6. A. Asrari, **M. Ansari** and K. C. Bibek, "Real-time Congestion Prevention in Modern Distribution Power Systems via Demand Response of Smart Homes," *North American Power Symposium (NAPS)*, Wichita, KS, USA, **2019**, pp. 1-6, doi: 10.1109/NAPS46351.2019.9000380.
7. P. Okunade, **M. Ansari**, A. Asrari and J. Khazaei, "Application of Optimization for Daily Scheduling of Renewable Distributed Generations Considering Market Profits in Distribution Networks," *North American Power Symposium (NAPS)*, Fargo, ND, **2018**, pp. 1-6, doi: 10.1109/NAPS.2018.8600654

**Journal Papers:**

8. A. Asrari, **M. Ansari**, J. Khazaei, P. Fajri, M. H. Amini and B. Ramos, "The Impacts of a Decision Making Framework on Distribution Network Reconfiguration," in *IEEE Transactions on Sustainable Energy*, vol. 12, no. 1, pp. 634-645, Jan. **2021**, doi: 10.1109/TSTE.2020.3014518.
9. A. Asrari, **M. Ansari**, J. Khazaei and P. Fajri, "A Market Framework for Decentralized Congestion Management in Smart Distribution Grids Considering Collaboration Among Electric Vehicle Aggregators," in *IEEE Transactions on Smart Grid*, vol. 11, no. 2, pp. 1147-1158, Mar. **2020**, doi: 10.1109/TSG.2019.2932695.
10. A. Asrari, M. Mustafa, **M. Ansari** and J. Khazaei, "Impedance Analysis of Virtual Synchronous Generator-Based Vector Controlled Converters for Weak AC Grid Integration," in *IEEE Transactions on Sustainable Energy*, vol. 10, no. 3, pp. 1481-1490, Jul. **2019**, doi: 10.1109/TSTE.2019.2892670.